COARSE-GRAINED MEAN-FIELD SIMULATIONS OF SURFACTANT MICELLES: STATIC AND DYNAMIC EQUILIBRIUM PROPERTIES

Fabián Alonso García Daza

Coarse-Grained Mean-Field Simulations of Surfactant Micelles: Static and Dynamic Equilibrium Properties

Fabián Alonso García Daza

DOCTORAL THESIS

supervised by Dr. Allan Donald Mackie

Departament d'Enginyeria Química

Escola Tècnica Superior d'Enginyeria Química

UNIVERSITAT ROVIRA i VIRGILI

Tarragona
2016

UNIVERSITAT ROVIRA I VIRGILI
COARSE-GRAINED MEAN-FIELD SIMULATIONS OF SURFACTANT MICELLES: STATIC AND DYNAMIC EQUILIBRIUM PROPERTIES
Fabián Alonso García Daza

UNIVERSITAT
ROVIRA i VIRGILI

Departament d'Enginyeria Química

Av. Països Catalans, 26
43007 Tarragona
Tel. +34 977 55 96 74
Fax. +34 977 55 96 67

I STATE that the present study, entitled "Coarse-Grained Mean-Field Simulations of Surfactant Micelles: Static and Dynamic Equilibrium Properties", presented by Fabián Alonso García Daza for the award of the degree of Doctor, has been carried out under my supervision at the Department of Chemical Engineering of this university.

Tarragona, July 2016

Doctoral Thesis Supervisor

Dr. Allan Donald Mackie

UNIVERSITAT ROVIRA I VIRGILI
COARSE-GRAINED MEAN-FIELD SIMULATIONS OF SURFACTANT MICELLES: STATIC AND DYNAMIC EQUILIBRIUM PROPERTIES
Fabián Alonso García Daza

Acknowledgements

Este trabajo no hubiera sido posible sin el apoyo fundamental e incondicional de mi director, el Dr. Allan Mackie; quien con su paciencia, disponibilidad para siempre atender mis inquietudes y sobre todo por su interés en promover la discusión alrededor de este proyecto han motivado la consecución de esta tesis, a él gracias por permitirme aprender y trabajar bajo su dirección. También quiero agradecer a Teresa Mármol en quien siempre encontré un maravilloso soporte, asimismo, agradezco a mis compañeros de despacho, profesores y aquellas personas que hicieron grata mi permanencia en la universidad y en la ciudad.

Un profundo agradecimiento a mi esposa, Tammy Goretty, por estar desde el principio hasta el final de este capítulo, su irrestricto amor y compañía han sido el pilar de este trabajo. Adicionalmente agradezco a mis papás José e Hilda, mi hermano Sergio, mis abuelos y demás familiares por siempre estar a mi lado a pesar de la distancia.
Finalmente, quiero dedicar este trabajo a la memoria de mi papá-abuelo José Daza; sin él, estas palabras nunca pudieron haber sido escritas.

Abstract

Surfactant molecules are composed by hydrophilic and hydrophobic moieties whose opposite interactions with the solvent medium result in a particular self-aggregation behavior. However, despite the wide number of simulation, experimental and theoretical works, a microscopic understanding of the self-assembly process seems to be still incomplete. Looking for a deep knowledge of the micellization mechanisms and their impact on microscopic and macroscopic properties, this work is aimed to use the so-called single-chain mean-field (SCMF) theory for a diverse set of surfactant systems represented by a series of coarse-grained models.

In particular, the work coverages the following: (i) the study of static equilibrium properties of different surfactant systems, and, (ii) the development of a dynamic version of the SCMF to study the kinetic exchange phenomena in micellar systems. From the results, we obtained a detailed description of the surfactant architecture effects on equilibrium properties, as well as a microscopic analysis of the CMC deviations with increase of hydrophobic weight for nonionic gemini systems, and, a new coarse-grained model for Pluronic molecules. From the dynamic SCMF simulations the kinetic exchange of single monomers was studied through the calculation of autocorrelation functions, additionally, conformational changes of the copolymers when crossing the micellar region are calculated for the expulsion mechanism of Pluronic surfactants systems in equilibrium regime.

Table of Contents

Chapter 1

Introduction

The term *amphiphilic* refers to those compounds containing both, molecules that have affinity for water (water-like) and molecules that have affinity for oil (oil-like). Typically, amphiphilic molecules have molecular weights on the order of 500 g/mol. In particular, we can refer to the so-called *surfactants*, whose molecules are made up of one hydrophilic moiety (or *heads*) that are covalently bonded to one hydrophobic moiety (or *tails*) which can be branched or linear. The degree of the chain tail branchin, its length and the position of the head group as well as its length are parameters of importance for the physicochemical properties or the surfactants [1]. Depending on the nature of the hydrophilic group the surfactants can be classified as

- **Nonionic:** composed on noncharged head groups, e.g. those based on poly(ethylene oxide) segments

- **Anionic:** composed of negatively charged head groups, e.g. an alkyl sulfate

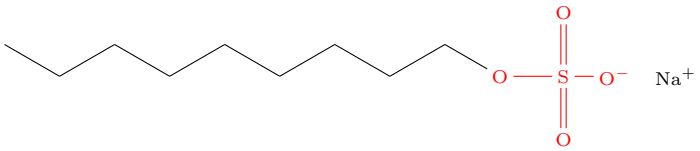

- **Cationic:** composed of positively charged head groups, e.g. an alkyl quaternary nitrogen system

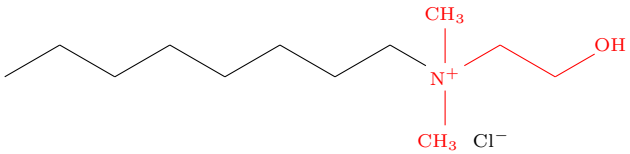

- **Zwitterionic:** composed of both positively and negatively charged head groups, e.g. an amine oxide

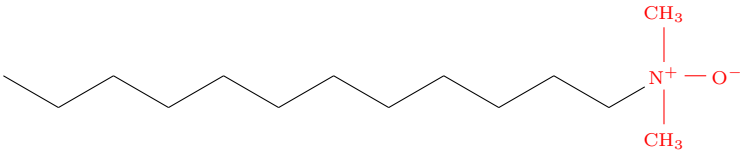

Additionally, there has been a recent interest in certain *oligomeric* surfactants, usually known as gemini, containing two hydrophobic tails and two head groups linked together with a short spacer. Also, it is of utmost interest amphiphile molecules whose molecular sizes are 10-100 times bigger than the common surfactants; these larger amphiphiles, known as block copolymers, are composed by blocks of one type of homopolymer and are joined in a sequential order to blocks of another type which are made up of hydrophilic and hydrophobic blocks. The hydrophilic block may be nonionic (e.g. poly(ethylene oxide)) or ionic (e.g. poly(acrylate)). In this thesis the term surfactant is used to refer to conventional surfactants as well as to oligomers or amphiphilic block

copolymers.

Because of the amphiphilic nature of a surfactant, the two parts of the same molecule interact very differently with the surrounding solvent (e.g. water); contacts of tail units with water molecules are energetically unfavorable in comparison to interactions of head units with the solvent. For hydrophobic blocks to avoid contacts with the solvent, some surfactants tend to accommodate at the air-water interface with the hydrophobic group placed in the air side of the interface while the heads are within the water volume, in consequence, an adsorbed layer of surfactant is formed and a reduction of the water surface tension is produced. As the surfactant concentration in solution is increased, the number of surfactants at the air-solution interface increases until the interface becomes saturated by the adsorbed surfactants, then, if more surfactants are added in the aqueous phase they will coexist in a molecularly dispersed form. Accordingly, as the concentration of surfactants in the bulk solution increases, the number of unfavorable contacts of tail units with water will also increases resulting in a rise of the free energy of the system, forcing, at a surfactant concentration known as the *critical micelle concentration* (CMC), the surfactants to self-associate into *micelles* to prevent further increases of the free energy. The physical mechanism responsible for this self-association in known as the hydrophobic effect, which arises from the tendency of surfactants to avoid contacts with water molecules, therefore, hydrophobic segments are in contact with one another forming an oily core surrounded by a shell composed by hydrophilic groups as can be observed in Figure 1.1 where the aggregation of surfactant molecules into spherical micelles is illustrated, in there, free monomers and aggregated surfactants are continuously exchanged in the equilibrium regime. Because of this

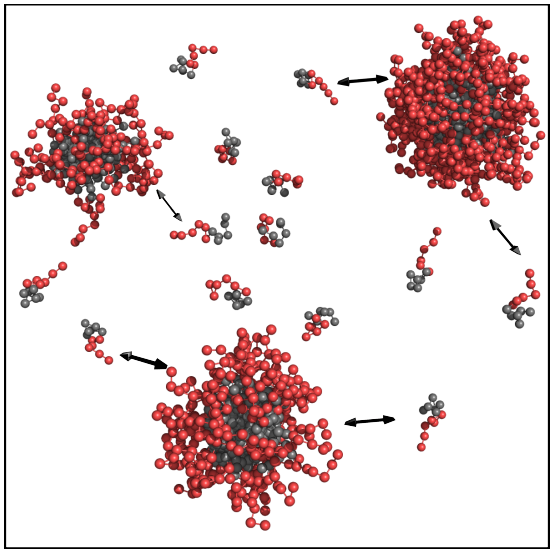

Figure 1.1: Schematic representation of the micellar structure and equilibrium exchange of singly dispersed and aggregated surfactants. Grey and red beads correspond to hydrophobic and hydrophilic units, respectively.

special aggregation behavior, surfactants have gained great importance in diverse industrial, technological and research processes including improving of solubility, stability and targeting of certain nanoparticles by coating surfactants on its surface [2], also, in the cleaning industry where the CMC is related to the concentration at which solubilization in the soil removal process occurs [3], as templates for the synthesis of mesoporous materials [4], in the purification of waste waters by solubilization and separation of toxic ingredients [5], and, in medical

research where surfactants have proven to increase drug potency in cancer therapy [6]. In particular, surfactants performance with specific attributes for the drug transport have been investigated, for instance, those with low CMC to decrease the concentration of surfactants precipitated in the blood [7], or, with non-linear architecture which improves the antitumor activity and therapeutic efficacy [8].

Depending on the structural and chemical properties of surfactants, micellar systems have been extensively studied by different experimental methods as surface tension [1], spectrophotometry, pyrene fluorescence [9], nuclear magnetic resonance, fluorimetry [10], light scattering [11], capillary electrophoresis [12], temperature jump [13], small-angle neutron scattering [14], fluorescence correlation spectroscopy [15] and time-resolved small-angle neutron scattering [16]. Nevertheless, time, cost, and accuracy constraints have encouraged researchers to seek alternative theoretical and simulation methods to study the micellization process.

In particular, computer simulations aim to provide a more complete understanding at a microscopic level than the current experimental techniques, to do so, thermodynamic observables (e.g. CMC, aggregates distribution, interfacial tension, micellar shape among others) must be predicted and compared with experiments in order to validate the simulation procedure and the surfactant model.

1.1 Modelling Techniques

The main purpose behind modelling surfactant systems is to predict macroscopic observables from an idealized microscopic level. In this sense, theoretical and simulation techniques have been widely developed and implemented to model a diverse set of surfactant systems through the years. Most relevant methods include Monte Carlo (MC) simulations [17, 18] where equilibrium of the system is reached by a series of random moves that are accepted depending on their energetic favorability, these moves generate an alteration of the phase space giving, in the long term, an appropriate sampling of the phase space, and in consequence, equilibrium can be accessed. Under this scheme, the ensemble averages for a system of N particles in a volume V at a temperature T are found to be

$$\langle A\rangle_{ensemble} = \frac{1}{Q}\int e^{-U(\vec{r}_1,\dots\vec{r}_N)/kT} A(\vec{r}_1,\dots\vec{r}_N)d\vec{r}_1\dots d\vec{r}_N, \tag{1.1}$$

where Q and k are the partition function of the system and the Boltzmann's constant, respectively, $\vec{r}_i$ and $U(\vec{r}_1,\dots\vec{r}_N)$ are the position of particle i and the potential energy of the system. Nonetheless, the time dimension is absent in MC simulations given the lack of a realistic dynamic trajectory, this is in contrast to molecular dynamics (MD) simulations [19, 20] which are based on the classical laws of motion from where it is possible to study equilibrium, structural and transport properties of diverse systems. Basically, MD is based on solving the Newton's second law for every particle i of the system

$$\vec{F}_i = m_i\frac{d^2\vec{r}_i(t)}{dt^2} = -\vec{\nabla}_i U(\vec{r}_1(t),\dots\vec{r}_N(t)), \tag{1.2}$$

where F_i is the force exerted on particle i by remaining particles and m_i is its corresponding mass. By computing the above equation it is possible to determine all the trajectories $\vec{r}_i(t)$ and velocities $\vec{v}_i(t)$ for all the particles of the system at any time t to reproduce the time evolution of the system in a dynamic form. The average for observable A obtained from MD simulations is calculated from

$$\langle A\rangle_{time} = \lim_{\tau\to\infty}\frac{1}{\tau}\int_0^\tau A(\vec{r}_1(t),\dots\vec{r}_N(t))dt. \tag{1.3}$$

However, only a short window of time can be reached by MD simulations because of the large amount of computation time needed to evolve the system according to the Newton's laws of motion, in general, this will cause difficulties in reaching equilibrium in certain systems as discussed further on.

In addition to MC and MD simulations, stochastic methods have been also considered. For instance, Brownian dynamics [21] includes frictional and random forces in the Newton's equations to correct the exclusion of the explicit solvent, that is, particles are considered to be in a continuum medium which in turn speed up the simulation time in comparison with standard MD simulations. In a similar manner, dissipative particle dynamics [22], simulations also obey the Newton's laws considering, extra dissipative and random force terms to include the viscous resistance of the monomers within the solvent and a correction in the energy due to the degrees of freedom suppressed in the coarse-grained process.

Alternative methods arising from mean field theories are also considered to predict macroscopic properties for a wide range of surfactant systems. In general, the free energy energy of the system, which is written in terms of sampling chains representing the surfactants, is minimized in order to address an equilibrium regime. In particular, the self-consistent field (SCF) [23, 24] and the single-chain mean-field (SCMF) [25, 17, 26] theories have been used in the study of short surfactants and block copolymer systems proving their effectiveness in the prediction of diverse equilibrium properties. In both cases the intermolecular interactions are considered through mean molecular fields while the intramolecular terms depend on the particular method, indeed, the SCF theory considers the sampling chains as ideals, that is, overlapping conformations are permitted affecting the intramolecular interactions and hence the free energy of the system. In contrast, the SCMF method can take into account self-avoiding conformations resulting in a more realistic model of surfactant systems and an accurate estimation of the free energy of the system. This thesis aims to study a series of static and dynamic equilibrium properties for a series of surfactant systems in an off-lattice space representation through a series of SCMF simulations.

1.2 Problem Statement

Although the wide number of simulation, experimental and theoretical works, a microscopic understanding of the self-assembly of surfactants into micellar aggregates seems to be still incomplete. For instance, theoretical free energy models [27] present a loss in the explicit microscopic information of the system given their semi-empirical foundations. Equilibration problems associated to slow dynamics events have been reported in MD simulations [20] for a series of nonionic short surfactants in a coarse-grained representation; despite reaching time scales close to milliseconds, static properties like aggregation numbers or the CMCs still deviate from their equilibrium values. Also, lattice space discretization used in MC or SCF simulations represents a difficulty when comparing with experiments either for static [28] or dynamic [29] equilibrium quantities. At a microscopic level, given that SCF simulations consider overlapping chain configurations to represent surfactants, excluded-volume interactions are missing in the intramolecular energetic terms of the system's free energy, thereby, it is unclear how this affects the prediction of several properties for surfactant systems, in particular, when the architecture of the surfactants is modified, or, explicit conformations of dispersed and aggregated monomers need to be taken into account. In light of the above arguments, it is expected that static and dynamic equilibrium proper-

ties to be difficult to predict given the sampling, spatial and temporal limitations in the current simulation and theoretical methods. This overall scenario is aggravated when copolymer surfactant systems are also considered.

In consequence, a detailed microscopic description of the micellization phenomena must be addressed by alternative methods able to guarantee equilibrium, and thereby, static and dynamic properties of the systems under study. Looking for a deep knowledge of the micellization process and its impact on microscopic and macroscopic properties, this work is aimed to use the SCMF theory for a diverse set of surfactants represented by a series of coarse-grained models. Therefore, the main purposes in this work are (i) to study static equilibrium properties of different surfactant systems by using SCMF simulations, and, (ii) to obtain dynamic equilibrium properties of block copolymer surfactant systems by development of a dynamic version of the SCMF scheme. In all cases, the results obtained are compared with experimental data when available.

1.3 Objectives

To attain the goals mentioned above the following objectives are proposed

1. To study the effect of the surfactant architecture on static equilibrium properties for a set of nonionic surfactants. In this work simulations are performed within the one dimensional spherical off-lattice SCMF scheme. Also, to understand how the monomers architecture impact on the aggregation process, calculation of the excess enthalpy and entropy quantities are carried out from simulations. The chain models and the energetic parameters are taken from a previous model for diblock poly(ethylene oxide) alkyl ethers C-PEO.

2. Based on the previous objective, we look for establishing a model for dimeric poly(ethylene oxide) surfactants to study, through SCMF simulations, the unexpected behavior of the CMC with the increase of the hydrophobic block length that has been reported in experiments. For this purpose, a combination of the results obtained by SCMF calculations with a kinetic model of micelle formation is proposed.

3. To develop a coarse-grained model for a series of poly(ethylene oxide)-poly(propylene oxide)-poly(ethylene oxide) molecules (PEO-PPO-PEO) at a constant temperature. Additionally, to determine structural and energetic parameters from the comparison between predicted and experimental CMCs for a set of PEO-PPO-PEO copolymers within the SCMF simulations in continuous space.

4. To develop a dynamic version of the SCMF theory to study the dynamic equilibrium phenomenology of surfactant systems when aggregate into micelles. In particular, to study the monomer exchange kinetics of PEO-PPO-PEO systems, and, to obtain detailed microscopic information of monomers when are exchanged between the micelles and the bulk solution.

1.4 Thesis Outline

The thesis is organized as follows. The physical considerations to formulate the SCMF together with their statistical mechanics and free energy formalisms are revised in Chapter 2, in addition, the mass action model

and the basic principles of micellization kinetics are also introduced together with the dynamic formulation of the SCMF simulations. In Chapter 3 we present the effects of the surfactant architecture on static equilibrium quantities like the CMC and the aggregation number, the results are obtained by a series of SCMF simulations in continuous space and subsequently compared with experimental data when available. A model representation for a set of nonionic gemini surfactants is implemented in Chapter 4, where, by combination of a micellization kinetic model and the free energy of the system predicted by the SCMF simulations, a deviation between experimental and theoretical CMC predictions with the increase of the hydrophobic weight is studied. The results suggest a combination of experimental limitations and a series of nonequilibrium effects as the main causes of the observed deviation. Chapter 5 is devoted to develop a coarse-grained model for a series of Pluronic surfactants, PEO-PPO-PEO. Fitting of the energetic parameters is evaluated from adjusting CMCs predicted by our simulations with the corresponding experimental values available in literature for a group of Pluronics. Besides, static equilibrium aggregation numbers and CMCs are studied based on the size of hydrophobic and hydrophilic blocks of the copolymers suggesting in the extreme cases the presence of nonequilibrium effects as the reported in Chapter 4. Based on the model for Pluronics developed in Chapter 5 and the dynamic versin of the SCMF developed in this work, we study in Chapter 6 the exchange kinetics mechanisms for copolymers when single copolymers are exchanged between the bulk solution and the micellar aggregates. In particular, expulsion rate constants are predicted and compared with available experimental data for the the Pluronics under study, also, conformational changes of the hydrophobic blocks when leaving the inner micelle core are analyzed in terms of explicit microscopic information obtained from the SCMF simulations. In Chapter 7 the relaxation kinetics of the expulsion process is studied from a series of dynamic SCMF simulations for a particular surfactant. Experimental deviations from theoretical calculations reported for analog systems are analysed in terms of the results obtained by our simulations together with solutions derived from analytical models. This enables us to identify the main physical mechanisms, that can not be accessed neither by experiments nor theory, responsible for these deviations. Finally, in Chapter 8 we present the concluding remarks and considerations for further research.

References

[1] L. Lee, J. Salimon, M. A. Yarmo, R. Syafri, and M. Hisam. *J. Dispersion Sci. Technol.*, 34(7):914–922, 2013.

[2] E. V. Batrakova and A. V. Kabanov. *J. Controlled Release*, 130(2):98 – 106, 2008.

[3] R. Zana and J. Xia. *Gemini Surfactants: Synthesis, Interfacial and Solution-Phase Behavior,and Applications*. Marcel Dekker, New York, 2003.

[4] A. May, A. Pasc, M. J. Stébé, J. M. Gutiérrez, M. Porras, and J. L. Blin. *Langmuir*, 28(25):9816–9824, 2012.

[5] A. V. Sineva, A. M. Parfenova, and A. A. Fedorova. *Colloids Surf., A*, 306(1-3):68 – 74, 2007.

[6] D. Y. Alakhova, Y. Zhao, S. Li, and A. V. Kabanov. *PLoS ONE*, 8(8):e72238, 2013.

[7] A. V. Kabanov and V. Y. Alakhov. Micelles of Amphiphilic Block Copolymers as Vehicles for Drug Delivery. In B. Lindman and P. Alexandridis, editors, *Amphiphilic Block Copolymers*, pages 347–376. Elsevier Science B.V., Amsterdam, 2000.

[8] H. Nakamura, E. Koziolová, T. Etrych, P. Chytil, J. Fang, K. Ulbrich, and H. Maeda. *Eur. J. Pharm. Biopharm.*, 90:90 – 96, 2015.

[9] M. Y. Kozlov, N. S. Melik-Nubarov, E. V. Batrakova, and A. V. Kabanov. *Macromolecules*, 33(9):3305–3313, 2000.

[10] A. A. Steinschulte, B. Schulte, S. Rutten, T. Eckert, J. Okuda, M. Moller, S. Schneider, O. V. Borisov, and F. A. Plamper. *Phys. Chem. Chem. Phys.*, 16:4917–4932, 2014.

[11] H. Altinok, G.-E. Yu, S. K. Nixon, P. A. Gorry, D. Attwood, and C. Booth. *Langmuir*, 13(22):5837–5848, 1997.

[12] W. Loh. *Block Copolymer Micelles*, volume 2 of *Encyclopedia of Surface and Colloid Science*. Taylor & Francis, Boca Raton, FL, 2006.

[13] I. Goldmints, J.F. Holzwarth, K.A. Smith, and T.A. Hatton. *Langmuir*, 13(23):6130–6133, 1997.

[14] L. Yang, P. Alexandridis, D. C. Steytler, M. J. Kositza, and J. F. Holzwarth. *Langmuir*, 16(23):8555–8561, 2000.

[15] D. Schaeffel, A. Kreyes, Y. Zhao, K. Landfester, H.-J. Butt, D. Crespy, and K. Koynov. *ACS Macro Lett.*, 3(5):428–432, 2014.

[16] S.-H. Choi, T. P. Lodge, and F. S. Bates. *Phys. Rev. Lett.*, 104:047802, 2010.

[17] A. D. Mackie, A. Z. Panagiotopoulos, and I. Szleifer. *Langmuir*, 13(19):5022–5031, 1997.

[18] A. Jusufi, A.-P. Hynninen, and A. Z. Panagiotopoulos. *J. Phys. Chem. B*, 112(44):13783–13792, 2008.

[19] S. A. Sanders and A. Z. Panagiotopoulos. *J. Chem. Phys.*, 132(11):114902, 2010.

[20] B. G. Levine, D. N. LeBard, R. DeVane, W. Shinoda, A. Kohlmeyer, and M. L. Klein. *J. Chem. Theory Comput.*, 7(12):4135–4145, 2011.

[21] M.-J. Hafezi and F. Sharif. *Langmuir*, 28(47):16243–16253, 2012.

[22] Z. Li and E. E. Dormidontova. *Soft Matter*, 7(9):4179–4188, 2011.

[23] P. N. Hurter, J. M. H. M. Scheutjens, and T. A. Hatton. *Macromolecules*, 26(21):5592–5601, 1993.

[24] V. G. de Bruijn, L. J. P. van den Broeke, F. A. M. Leermakers, and J. T. F. Keurentjes. *Langmuir*, 18(26): 10467–10474, 2002.

[25] A. Ben-Shaul, I. Szleifer, and W. M. Gelbart. *J. Chem. Phys.*, 83(7):3597–3611, 1985.

[26] A. Gezae Daful, J. Bonet Avalos, and A. D. Mackie. *Langmuir*, 28(8):3730–3743, 2012.

[27] T. A. Camesano and R. Nagarajan. *Colloids Surf. A*, 167(1-2):165–177, 2000.

[28] A. Z. Panagiotopoulos, M. A. Floriano, and S. K. Kumar. *Langmuir*, 18(7):2940–2948, 2002.

[29] T. Haliloğlu, I. Bahar, B. Erman, and W. L. Mattice. *Macromolecules*, 29(13):4764–4771, 1996.

Chapter 2

Theoretical Background

In this thesis the so-called single-chain mean-field (SCMF) theory [1] is considered to model and predict equilibrium, statical and dynamical behaviors for a series of surfactant systems described throughout this work. This theory was originally formulated to study dry core micellar aggregates [1], subsequently, solvent was included in the formalism for micellar systems [2] and grafted polymers [3]. The main idea behind the SCMF approach is to consider a central chain, representing the surfactant, in a mean molecular field as the reference state; those intermolecular fields (coming from the solvent and other surfactants) are determined by mean averages of the probability distribution function of the chain conformations together with the volume filling constraint, whereas the intramolecular interactions of the chain are known in an exact way. In this work the chains are self avoiding in nature, that is, they are non-Markovian because of the correlation between segments of the chain due to the excluded volume interactions, which implies the need of a complete knowledge of all chain conformations.
In this chapter we review the theoretical basis related to the SCMF scheme, in particular, statistical mechanics and free energy approaches are introduced and subsequently their equivalence is shown. Thereafter, we establish the thermodynamic and static kinetic relations used throughout this thesis together with their connection with the SCMF to later introduce the dynamic version of the SCMF along with some dynamic basic quantities.

Incompressibility Assumption Outlines

Consider a system of N chains, representing the surfactants, which are found to be surrounded by solvent molecules. We assume that the solution is incompressible, namely, the accessible volume is filled by either solvent or surfactant molecules. Considering the direction r in which the densities of the surfactants and solvent are inhomogeneous, we can adopt the term *layer* r which define the region of the space between r and $r + dr$ as shown in Fig. 2.1. As the available space in every layer is occupied by surfactants and solvent molecules, the volume fraction can be written as

$$\phi_s(\vec{r}) + \langle \phi(\vec{r}) \rangle_N = 1, \tag{2.1}$$

where $\phi_s(\vec{r})$ is the solvent volume fraction at point $\vec{r}$ while the brackets represent the ensemble average of the chain volume fraction $\phi(\vec{r})$ with the excluded-volume contributions taken into account. The ensemble averages can be related through the probability distribution, $P[\alpha_1, \ldots, \alpha_N]$, of the N chains where α_i represents the conformation of surfactant i, and the total volume fraction, $\phi(\alpha_1, \ldots, \alpha_N; \vec{r})$, of the chains at layer r

$$\phi_s(\vec{r}) + \sum_{\{\alpha_1,\ldots,\alpha_N\}} P[\alpha_1, \ldots, \alpha_N]\phi(\alpha_1, \ldots, \alpha_N; \vec{r}) = 1, \tag{2.2}$$

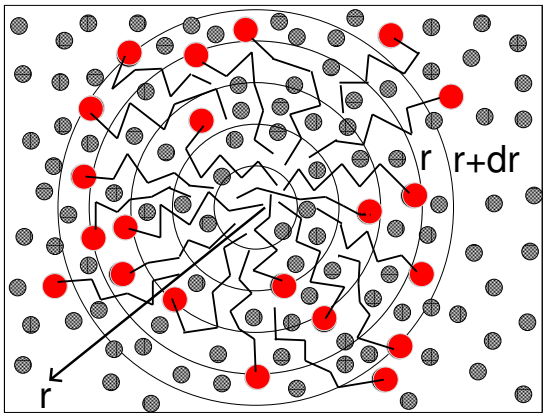

Figure 2.1: Diagram showing a set of surfactant molecules immersed in a solvent solution. Surfactant tail and head groups are represented by lines and filled red circles, respectively, while solvent is represented by dotted circles. In this example spherical symmetry has been considered where a layer r is the enclosed volume between shells r and r+dr.

where the sum is taken over all the possible configurations of the N chains. Also, the total volume fraction can be decomposed into contributions of the individual conformations α_i

$$\phi(\alpha_1, \ldots, \alpha_N; \vec{r}) = \sum_{i=1}^{N} \phi(\alpha_i, \vec{r}). \tag{2.3}$$

In order to construct a mean-field approach, it is necessary to consider that the N chains are equivalent, namely, the N configurational sum in Eq. 2.2 can be replaced by a single-chain average in the form

$$\phi_s(\vec{r}) + N \sum_{\alpha} P[\alpha]\phi(\alpha, \vec{r}) = 1, \tag{2.4}$$

with $P[\alpha]$ being the probability of finding a chain in conformation α while the sum goes over all the possible configurations of a single chain. The above equation can be written as

$$\phi_s(\vec{r}) + N\langle\phi(\vec{r})\rangle = 1, \tag{2.5}$$

where the term inside the angular brackets denote the average over all the possible conformations of a single chain molecule, thus, Eq. 2.5 represents the mean-field manner of how surfactant molecules and solvent are distributed to fill the available space. From here, it is necessary to determine the surfactant profiles that fulfill the incompressibility condition represented by the above equation, whereby, it will describe properly the thermodynamical properties of the system under study. This can be abridged in the properly prediction of the single chain probability distribution functions, (*pdf*), $P[\alpha]$. In particular, in this work we adopt the SCMF theory which is able to predict the *pdf* from the interactions of mean molecular fields with a single-chain.

2.1 Single-Chain Mean-Field Theory: Static Equilibrium Formulation

This theory assumes a central chain, whose interactions are taken to be: (i) intramolecular, which are determined in an exact way, and, (ii) intermolecular, with solvent and other surfactant chains considered through a

mean-field approach; this can be diagrammatically observed in Fig. 2.2. The associated probability of a chain

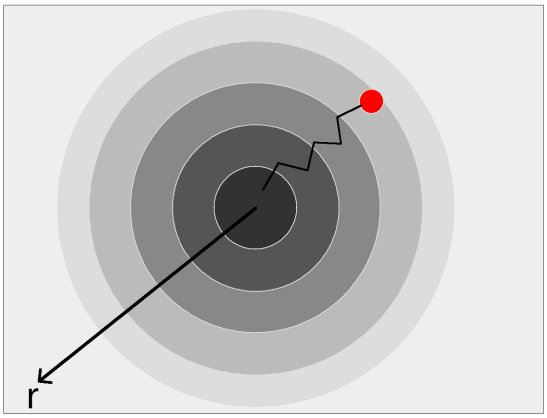

Figure 2.2: Representation of the central chain surrounded by the intermolecular mean field whose magnitude is depicted by the gray scale. Surfactant tail and head groups are represented by lines and filled red circles, respectively. The geometry and changes in the corresponding mean fields depend on the direction of the inhomogeneous density of surfactants and solvent.

configuration depends on its intramolecular and intermolecular interactions given by its distribution of segments coupled with the mean molecular fields. These molecular fields are given in terms of average properties of the chain, stating that, there is a relation between the average chain conformations and the probability for the chain to be in any conformation. Any thermodynamic property can be calculated from the chain averages, linking then the macroscopic behavior of the system with the explicit molecular properties of the chain molecules.
In view of this, the main purpose is to calculate the *pdf* for chain conformations to obtain the solvent and surfactant equilibrium densities together with average thermodynamic properties. In what follows two equivalent approaches to obtain the corresponding *pdf* are introduced.

2.1.1 Statistical Mechanics Formalism

Consider a canonical ensemble of N surfactant molecules and N_s solvent molecules in a volume V at a temperature T. The configurational partition function is

$$Z(N, N_s, V, T) = \int d^3r_1 \dots d^3r_{N_s} \sum_{\{\alpha_1,\dots\alpha_N\}} \exp\left[-\beta U(\vec{r}_1, \dots, \vec{r}_{N_s}; \alpha_1, \dots, \alpha_N)\right], \tag{2.6}$$

where $\beta = 1/kT$ and k is the Boltzmann's constant, while $U(\vec{r}_1, \dots, \vec{r}_{N_s}; \alpha_1, \dots, \alpha_N)$ is the total interaction energy of the N surfactants in configurations $\alpha_1, \dots, \alpha_N$ and the N_s solvent molecules in positions $\vec{r}_1, \dots, \vec{r}_{N_s}$. The sum in Eq. 2.6 represents a multiple integral including all the coordinates of the surfactants, indicating that the partition function consists of $N \times N_s \times n$ integrals, where n is the degree of polymerization of the chains. The probability of finding surfactant chains in configurations $\alpha_1, \dots, \alpha_N$ is

$$P[\alpha_1, \dots, \alpha_N] = \frac{\int d^3r_1 \dots d^3r_{N_s} \exp\left[-\beta U(\vec{r}_1, \dots, \vec{r}_{N_s}; \alpha_1, \dots, \alpha_N)\right]}{Z(N, N_s, V, T)}. \tag{2.7}$$

In particular, the singlet *pdf*, e.g. the probability for surfactant 1 to be in conformation α_1, can be obtained by integrating the all-chain probabilities in Eq. 2.7 over the $N-1$ remaining configurations

$$P[\alpha_1] = \frac{\int d^3r_1 \dots d^3r_{N_s} \sum_{\{\alpha_2,\dots\alpha_N\}} \exp\left[-\beta U(\vec{r}_1,\dots,\vec{r}_{N_s};\alpha_1,\dots,\alpha_N)\right]}{Z(N,N_s,V,T)}. \tag{2.8}$$

Taking now α instead of α_1 to refer to the central chain and decomposing the interaction total energy

$$U(\vec{r}_1,\dots,\vec{r}_{N_s};\alpha_1,\dots,\alpha_N) = u(\alpha,\vec{R}) + U(\vec{r}_1,\dots,\vec{r}_{N_s};\alpha_2,\dots,\alpha_N), \tag{2.9}$$

where, the first term in the right side of the above equation refers to the interactions of the central chain α with the remaining $N-1$ chains and the solvent molecules whose positions are represented by vector $\vec{R}$, and, the second term represents the interaction between the N-1 chains and the N_s solvent molecules. Hence, the *pdf* in Eq. 2.8 can be written in the following form

$$P[\alpha] = \frac{\int d^3r_1 \dots d^3r_{N_s} \sum_{\{\alpha_2,\dots\alpha_N\}} \exp\left[-\beta U(\vec{r}_1,\dots,\vec{r}_{N_s};\alpha_2,\dots,\alpha_N)\right] \exp\left[-\beta u(\alpha,\vec{R})\right]}{Z(N,N_s,V,T)}. \tag{2.10}$$

The central chain energy can be expressed as the sum of three terms; the first one depends on the intramolecular interactions of the central chain, $u_{intra}(\alpha)$, the second one takes into account the intermolecular mean-field interactions of the central chain with other surfactants and solvent molecules, $u_{inter}(\alpha)$. Both terms are position independent given that only depend on the central chain conformation and the mean density fields of solvent and remaining chains. Finally, the third term represents the repulsive interactions of the central chain with all other molecules, $u_{rep}(\alpha,\vec{R})$. With this, Eq. 2.10 can adopt the form

$$\begin{aligned} P[\alpha] =& \frac{\exp\left[-\beta\left(u_{intra}(\alpha)+u_{inter}(\alpha)\right)\right]}{Z(N,N_s,V,T)} \int d^3r_1 \dots d^3r_{N_s} \\ &\times \sum_{\{\alpha_2,\dots\alpha_N\}} \exp\left[-\beta U(\vec{r}_1,\dots,\vec{r}_{N_s};\alpha_2,\dots,\alpha_N)\right] \exp\left[-\beta u_{rep}(\alpha,\vec{R})\right]. \end{aligned} \tag{2.11}$$

Considering repulsive interactions of the hard-core type, means that, on the one hand, the term $u_{rep}(\alpha,\vec{R}) = 0$ if no overlapping is produced between the central chain and other molecules, and, on the other hand, $u_{rep}(\alpha,\vec{R}) \to \infty$ if it does. This choice leads to interpret the integral in Eq. 2.11 as the partition function of a system composed by $N-1$ chain surfactants and N_s solvent molecules at a temperature T in an available volume $\{V(\vec{r})\} - \int \phi(\alpha,\vec{r})d\vec{r}$, that is, the total volume of the system minus the volume occupied by the central chain α. With this, Eq. 2.11 can be written as

$$P[\alpha] = \exp\left[-\beta\left(u_{intra}(\alpha)+u_{inter}(\alpha)\right)\right] \frac{Z\left(N-1,N_s,\{V(\vec{r})\} - \int \phi(\alpha,\vec{r})d\vec{r},T\right)}{Z(N,N_s,\{V(\vec{r})\},T)}, \tag{2.12}$$

where the volume V is taken as the sum of the individual volumes $\{V(\vec{r})\}$. Expanding now $\log Z(N-1,N_s,\{V(\vec{r})\} - \int \phi(\alpha,\vec{r})d\vec{r},T)$ around $\log Z(N,N_s,\{V(\vec{r})\},T)$

$$\begin{aligned} \log Z\left(N-1,N_s,\{V(\vec{r})\} - \int \phi(\alpha,\vec{r})d\vec{r},T\right) =& \log Z(N,N_s,\{V(\vec{r})\},T) - \left(\frac{\partial \log Z}{\partial N}\right) \\ &- \int \left(\frac{\partial \log Z}{\partial V(\vec{r})}\right) \phi(\alpha,\vec{r})d\vec{r}, \end{aligned} \tag{2.13}$$

replacing Eq. 2.13 in Eq. 2.12 and reorganizing the terms we obtain the *pdf* for the central chain as

$$P[\alpha] = \frac{1}{Q} \exp\left[-\beta\left(u_{intra}(\alpha) + u_{inter}(\alpha) + \int \pi(\vec{r})\phi(\alpha,\vec{r})d\vec{r}\right)\right], \tag{2.14}$$

where $\log Q = \partial \log Z/\partial N = -\beta\mu$ is the work associated with the insertion of a chain to the system, while $\beta\pi(\vec{r}) = \partial \log Z/\partial V(\vec{r})$ represents the negative change in the free energy of the layer r as its volume increases and is interpreted as the lateral pressure acting on the chains. Normalization of the *pdf*, $\int d\alpha P[\alpha] = 1$, indicates that

$$Q = \int d\alpha \exp\left[-\beta\left(u_{intra}(\alpha) + u_{inter}(\alpha) + \int d\vec{r}\pi(\vec{r})\phi(\alpha,\vec{r})\right)\right], \tag{2.15}$$

which is the definition of the single-chain partition function.

2.1.2 Free Energy Formalism

A less detailed formalism based on the minimization of the free energy of the system subject to the incompressibility condition given in Eq. 2.5 may be used to determine the *pdf* of surfactant chain conformations $P[\alpha]$, accordingly, the density profiles of surfactants and solvent among other thermodynamic properties in equilibrium. The intermolecular repulsive interactions are included in the volume-filling constraint, as well as the intramolecular repulsions that are already implicitly taken in the set of single chains configurations, i.e. are self-avoiding in nature. The free energy terms are:

Internal energy: The intramolecular mean-field energy for a system composed by N surfactants, $\langle u_{intra}\rangle = N\int d\alpha P[\alpha]u_{intra}(\alpha)$, that is, the ensemble average over the *pdf* and the individual internal energies of the chains.

Intermolecular energy: Has the form $\langle u_{inter}\rangle = N\int d\alpha P[\alpha]u(\alpha)$, where the individual chain contributions are calculated through their interaction volumes together with the surrounding mean molecular fields. The fields for the central chain to interact depends on the pairwise interactions considered. In particular, considering the intermolecular energy in terms of chain-chain and chain-solvent interactions,

$$\langle u_{inter}\rangle = N\int d\alpha P[\alpha]\left[\frac{N-1}{2}\epsilon_{cc}\int d\vec{r}\Phi^{cc}_{int}(\alpha,\vec{r})\langle c(\vec{r})\rangle + \epsilon_{cs}\int d\vec{r}\Phi^{cs}_{int}(\alpha,\vec{r})c_s(\vec{r})\right], \tag{2.16}$$

where ϵ_{cc} and ϵ_{cs} are the interaction parameters for chain-chain and chain-solvent interactions, respectively. $d\vec{r}\Phi_{int}(\alpha,\vec{r})$ is the available volume at $\vec{r}$ for central chain to interact with chains and solvent through the average concentration fields $\langle c(\vec{r})\rangle$ and $c_s(\vec{r})$, respectively. The number of interaction parameters as well as the number of species represented by the concentration fields will depend on the coarse-grained level.

Entropy: Two entropic contributions are taken into account: $-kN\int d\alpha P[\alpha]\log P[\alpha]$, the conformational entropy of the chains, and, $-k\int d\vec{r}c_s(\vec{r})\log\phi_s(\vec{r})$, the translational entropy of the solvent molecules.

When summing all these contributions we obtain for the free energy $F = \langle E\rangle - T\langle S\rangle$ the equivalent mean-field expression

$$F = N\int d\alpha P[\alpha]\left(u_{intra}(\alpha) + u(\alpha)\right) + kT\left(N\int d\alpha P[\alpha]\log P[\alpha] + \int d\vec{r}c_s(\vec{r})\log\phi_s(\vec{r})\right). \tag{2.17}$$

The *pdf* and the solvent concentration $c_s(\vec{r})$ are found by minimization of the free energy F subject to the incompressibility condition in Eq. 2.5; namely, by insertion of a set of Lagrange multipliers $\pi(\vec{r})$ in the free

energy expression to then determine $\delta F/\delta P[\alpha] = 0$ and $\delta F/\delta c_s(\vec{r}) = 0$. Once this procedure is complete, it is possible to obtain the set of chain probabilities $P[\alpha]$ as can be reviewed in detail in Appendix A,

$$P[\alpha] = \frac{1}{Q} \exp\left[-\beta\left(u_{intra}(\alpha) + u_{inter}(\alpha) + \int d\vec{r}\pi(\vec{r})\phi(\alpha,\vec{r})\right)\right], \tag{2.18}$$

where Q is the term that ensures the correct normalization of the probabilities ($\int d\alpha P[\alpha] = 1$) and agrees with the expression given in Eq. 2.15. From the minimization procedure (see Appendix A for details) is obtained that $\phi_s(\vec{r}) \approx e^{-\beta v_s \pi(\vec{r})}$, with v_s as the volume of a solvent molecule, which reveals the physical meaning of the Lagrange multipliers: they are the osmotic pressure needed to hold constant the solvent chemical potential value as has been formally indicated from the partition function formalism. Nevertheless, as the Lagrange multipliers $\pi(\vec{r})$ emerge from the volume-filling constraint they can also be understood as the average repulsive intermolecular energy experienced by the chains due to the presence of surrounding solvent and surfactant molecules. In addition, the *pdf* in Eq. 2.18 obtained by the free energy formalism is the same as the one determined from the explicit expansion of the partition function as given in Eq. 2.14 and demonstrated in Section 2.1.1, thus validating the free energy procedure. From here, any equilibrium quantity, $\langle A \rangle$, can be estimated from the individual chain contributions, $A(\alpha)$, by means of

$$\langle A \rangle = \int d\alpha P[\alpha] A(\alpha). \tag{2.19}$$

Depending on the system under study different geometrical approaches can be taken into account; this work is devoted to study the self-aggregation phenomena in micellar systems, then, a reduction in the degrees of freedom can be made when only considering one dimensional spherical geometry which is found to be adequate to study this kind of systems, this can be admitted given simulation studies suggesting the earlier presence of spherical aggregates when micellization process is occurring [4]. Equilibrium properties for a system of N monomers through the SCMF formalism is achieved by determination of the single-chain probabilities $P[\alpha]$, the concentration average fields $\langle c(\vec{r}) \rangle$ and the Lagrange multipliers $\pi(\vec{r}) \approx -kT \log \phi_s(\vec{r})/v_s$ by evaluation of equations 2.5, 2.18 and 2.19. Solution of the system of nonlinear equation can be addressed by several numerical techniques. In this thesis we have discretized the space in spherical shells and in consequence all the concentration and interaction fields are given in terms of their individual contributions in the corresponding shell, in Appendix B a detailed description of the discretization procedure to solve the SCMF equations is shown.

Once the equations are solved, it is important to link the microscopic equilibrium quantities of the system with macroscopic observables; this can be reached when relating the mass action model with the quantities obtained within the SCMF theory as described in the following section.

2.1.3 Mass Action Model

A system of free and aggregated molecules in solvent medium is considered to be in thermodynamic equilibrium when the chemical potentials of surfactants in bulk solution (μ_1) or in aggregates ($\mu_2, \ldots, \mu_{N-1}, \mu_N$) have the same value [5],

$$\mu_1 = \mu_2 = \ldots = \mu_{N-1} = \mu_N. \tag{2.20}$$

The chemical potential is taken to be composed by ideal and excess contributions, $\mu = \mu^{id} + \mu^{exc}$, in particular, for surfactants in bulk solution

$$\mu_1 = \mu_1^* + kT \log X_1, \tag{2.21}$$

where X_1 is the concentration of free surfactants, and $\mu_1* = \mu_1^0 + \mu_1^{exc}$ with μ_1^0 as the standard chemical potential for free surfactants. Similarly, for surfactants in aggregates of size N the chemical potential is

$$\mu_N = \mu_N^* + \frac{kT}{N} \log \frac{X_N}{N}, \tag{2.22}$$

where X_N is the concentration of surfactants in aggregates of size N, and, $\mu_N^* = \mu_N^0 + \mu_N^{exc}$ where μ_N^0 corresponds to the standard chemical potential of aggregated surfactants. The second term in the right side of Eq. 2.21 is known as the translational entropy and implies that singly chains are free to move independently in space, in contrast, the analog term in Eq. 2.22 denotes that all surfactants in aggregates are forced to move together. Relating Eqs. 2.21 and 2.22 through Eq. 2.20 and assuming the surfactant system to behave ideally, that is, there are no interactions between the free surfactants ($\mu_1* = \mu_1^0$) and likewise between the aggregates ($\mu_N^* = \mu_N^0$), can be found the following relation

$$X_N = N \left(X_1 e^{-(\mu_N^0 - \mu_1^0)/kT} \right)^N. \tag{2.23}$$

The above equation is the expression of the mass action model (MAM) and states that formation of aggregates occurs when a difference between the free energies of singly and aggregated surfactants is produced ($\mu_N^0 < \mu_1^0$). Based on the former equation, the free surfactant concentration X_1 increases with total surfactant concentration $X_T = \sum_N X_N$, subsequently, from a specific X_T value X_1 takes a constant value referred as the CMC stating that any surfactant added to the system will prefer to aggregate rather than stay free in the bulk solution, this overall behavior is depicted in Fig. 2.3. To obtain the equilibrium distribution of micelles, X_N/N, from the

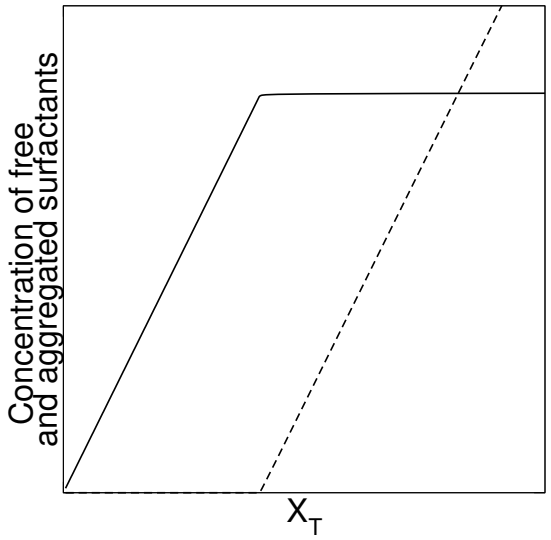

Figure 2.3: Schematic representation of the concentration of free (X_1, solid line) and aggregated ($\sum_{N=2} X_N$, dashed line) surfactants with total concentration of surfactants.

SCMF formalism it is necessary to relate the standard chemical potentials in Eq. 2.23 with the thermodynamic quantities obtained from the theory, to do so, a connection between the chemical potential of particles and the

SCMF is made by means of the following equation based on the mean-field approximation [6]

$$Q = N\, e^{-\mu/kT}, \tag{2.24}$$

where Q is the partition function in the SCMF scheme, as stated in the preceding section this can be calculated from the normalization of the single chain probabilities $P[\alpha] = e^{-H[\alpha]/kT}/Q$ where $H[\alpha]$ is known as the SCMF Hamiltonian for configuration α and can be obtained from Eq. 2.18

$$H[\alpha] = u_{intra}(\alpha) + u_{inter}(\alpha) + \int d\vec{r}\pi(\vec{r})\phi(\alpha, \vec{r}), \tag{2.25}$$

therefore, the following expression for Q can be obtained

$$Q = \int d\alpha e^{-H[\alpha]/kT}. \tag{2.26}$$

As can be observed, a direct way to relate the chemical potential of surfactants in a solvent medium with the SCMF theory is to equating the expressions of the partition function Q in Eqs. 2.24 and 2.26 to obtain

$$e^{-\mu/kT} = \frac{1}{N} \int d\alpha e^{-H[\alpha]/kT}. \tag{2.27}$$

Nevertheless, free and aggregated surfactants must be discussed separately; on the one hand, the SCMF scheme holds that the micelle is fixed in space which means that the chemical potential for aggregated surfactants in Eq. 2.22 does not contain the translational contribution, namely, $\mu_N = \mu_N^0$ in Eq. 2.27, then

$$e^{-\mu_N^0/kT} = \frac{1}{N} \int d\alpha e^{-H_N[\alpha]/kT}, \tag{2.28}$$

where the subscript N in the SCMF Hamiltonian is attached in order to distinguish from the case of free surfactants $H_1[\alpha]$. On the second hand, singly surfactants are free to be located in any region of space, as a consequence, when comparing with the expression for surfactants in micelles in Eq. 2.28 it is necessary to remove the translational contribution in the chemical potential when replacing in Eq. 2.27 in order to keep the same degrees of freedom in both cases, this is manifested by the emergence of the volume V of the system, thus

$$e^{-\mu_1^0/kT} = \frac{1}{V} \int d\alpha e^{-H_1[\alpha]/kT}. \tag{2.29}$$

Combining Eqs. 2.28 and 2.29, the following relation can be obtained

$$e^{-(\mu_N^0 - \mu_1^0)/kT} = \frac{V}{N} \frac{\int d\alpha e^{-H_N[\alpha]/kT}}{\int d\alpha e^{-H_1[\alpha]/kT}}. \tag{2.30}$$

Integrals in the previous equation include all possible chain configurations, nevertheless, a finite representative sample of these non-Markovian configurations can be considered as well, as a consequence, an approximation in these integrals must be taken in order to include this assumption [6]

$$e^{-(\mu_N^0 - \mu_1^0)/kT} \approx \frac{V}{N} \frac{\sum_\alpha e^{-H_N[\alpha]/kT}/W(\alpha)}{\sum_\alpha e^{-H_1[\alpha]/kT}/W(\alpha)}, \tag{2.31}$$

where the term $W(\alpha)$ is known as the Rosenbluth and Rosenbluth weight [7] and has been introduced to consider the inclusion of self-avoiding chain configurations α representing the surfactant. Importance of Eq. 2.31 lies in the fact that represents the connection between the macroscopic quantities X_1 and X_N through the MAM in Eq. 2.23 and the microscopic chain model in the SCMF approach. The procedure to generate nonoverlapping conformations and hence the Rosenbluth and Rosenbluth weight is introduced in the next section.

2.1.4 Self-Avoiding Random Walk

Chain configurations are obtained based on the Rosenbluth and Rosenbluth algorithm [7] which has been widely used in lattice [6] and off-lattice [8] SCMF simulations. The generation in continuous space of a chain surfactant, α, composed by m monomers proceeds as follows

- The first monomer is inserted at a random position into a cubic box of volume V, a partial weight $w_1(\alpha) = k$ is assigned to this monomer, where k is the number of initial trial positions as shown in Fig. 2.4.

- The next monomer, i, is located at one of the k new possible trial directions with probability

$$p_i(j) = \frac{e^{-\beta u^i_{intra}(j)}}{w_i(\alpha)},$$

  where j refers to one of the k trial directions with intramolecular energy $u^i_{intra}(j)$. The partial weight for the monomer is defined as

$$w_i(\alpha) = \sum_{j=1}^{k} e^{-\beta u^i_{intra}(j)}.$$

- The above steps are repeated until the chain is completely grown.

- The total weight of the chain is calculated as

$$1/W(\alpha) = \prod_{i=1}^{m} \frac{w_i(\alpha)}{k}. \tag{2.32}$$

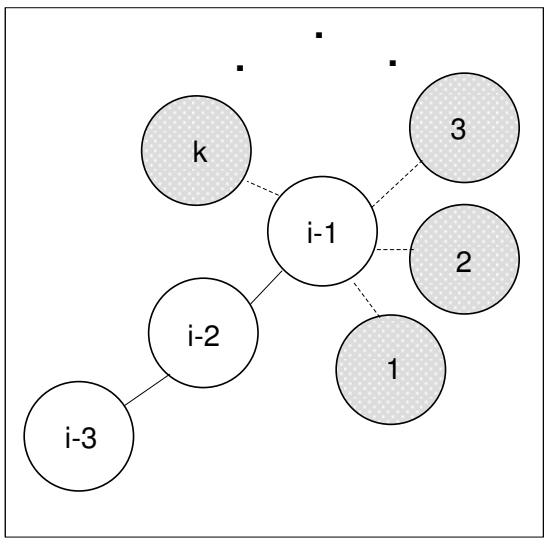

Figure 2.4: Chain generation based on the Rosenbluth and Rosenbluth self-avoiding procedure, where k trial directions connected to monomer $i-1$ are generated in order to place the next monomer i.

The values of the intramolecular energy $u^i_{intra}(j)$ depend on the molecular model to study the surfactant system. Up to this point we have introduced the main theoretical aspects of the SCMF scheme to predict equilibrium properties, like the CMC and size distribution X_N, for systems of two compounds that exhibit a self-aggregation

nature. In this sense, SCMF simulations predict a linear decreasing in the logarithmic scale [8] of the CMC with increasing the size of the chain hydrophobic block, nevertheless, experimental results for copolymer systems [9, 10, 11, 12] exhibit a deflection in this trend which is not observed in MC [13] or SCMF molecular simulations. This motivates us to relate kinetic association process with the SCMF in order to understand the physical nature of the CMC abnormality aforementioned. To do so, below are presented the basic concepts related to micellization as an activation process and its corresponding connection with the SCMF equations.

2.1.5 Micellization Kinetics

According to Nyrkova and Semenov [14], micellization and relaxation of surfactants can be expressed in terms of activation processes relating collective energy barriers, which, depending on their values, may suppress or diminish some relaxation paths. Essentially, fast and slow relaxation mechanisms are predicted, corresponding to unimer exchange and variation of the number of micelles respectively. The equilibrium distribution of aggregates,N, in a dilute solution of surfactants and aggregates is

$$\frac{X_N}{N} = X_1 e^{-\mathcal{F}(N,X_1)}, \tag{2.33}$$

where $\mathcal{F}(N, X_1)$ is the grand thermodynamic potential, that is, the difference between the total free energy of a micelle, $F(N)$, compared with that of unimers, $F(1)$,

$$\mathcal{F}(N, X_1) = F(N) - N\,F(1) - (N-1)\log X_1, \tag{2.34}$$

by considering the thermodynamic potential to be only described by the aggregation number and the concentration of free monomers, can be stated that single surfactants to associate into equilibrium micelles must be under a regime of minimal energy. Local minima along this path represents metastable micelles, which can suppress the growth to the equilibrium micellar state, and occasionally, completely reduce and stop growth. This means that micellization can be interpreted from the existence of collective energy barriers, arising from $\mathcal{F}(N, X_1)$, to overcome to form micelles from unimers. From the definition of the thermodynamic potential it is possible to define the CMC and the aggregation number, N_{agg}, in equilibrium by means of

$$\begin{aligned} \mathcal{F}(N_{agg}, \mathrm{CMC}^{\mathrm{eq}}) &= 0, \\ \left.\frac{\partial \mathcal{F}(N, \mathrm{CMC}^{\mathrm{eq}})}{\partial N}\right|_{N=N_{agg}} &= 0, \end{aligned} \tag{2.35}$$

where $\mathrm{CMC}^{\mathrm{eq}}$ is taken as the CMC in the equilibrium regime. Depending on the values of X_1 and taking as a reference $\mathrm{CMC}^{\mathrm{eq}}$, it is possible to visualize the behavior and aggregation significance of $\mathcal{F}(N, X_1)$ as shown in Fig. 2.5. As can be observed, can be identified an activation, F_a, and dissociation, F_d, barriers which are responsible of the formation and disintegration of micelles depending on the enthalpic/entropic balance influenced by the free monomer concentration, promoting: (i) association of monomers to form aggregates when the free monomer concentrations are higher than $\mathrm{CMC}^{\mathrm{eq}}$, (ii) release of surfactants from aggregates in the opposite case, and, (iii) an equal rate of association and dissociation of micelles meaning a constant number of aggregates over time when the concentration of free surfactants is the same as $\mathrm{CMC}^{\mathrm{eq}}$. The characteristic time for micellization is

$$T_a = T_0 e^{F_a}, \tag{2.36}$$

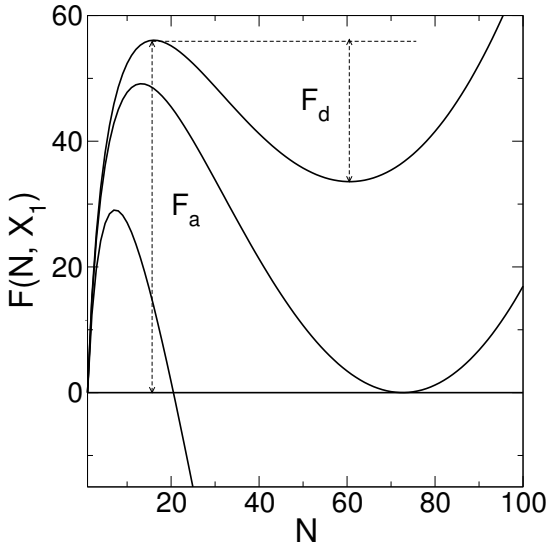

Figure 2.5: Grand thermodynamic potential $\mathcal{F}$ in kT units in function of X_1. The free energy of aggregated surfactants is calculated from $F(N) = \beta N^{3/2} + \gamma N^{2/3}$ with $\beta = 1$ and $\gamma = 60$. The curves from top to bottom are calculated for free monomers concentration close to 0.6CMC$^{\text{eq}}$, CMC$^{\text{eq}}$ and 10CMC$^{\text{eq}}$. Association, F_a, and dissociation, F_d, potentials are defined through the maximum and minimum of the thermodynamic potential respectively.

where the term T_0 is the elementary time association time. The association energy barrier is considered to include an additional entropic term arising from the noncontinuous nature of the aggregation process. Two mechanisms are considered in the elementary entrance of a surfactant into a micelle; on the one hand, a slow approaching of unimers to the micellar core, and on the second hand, diffusion of the hydrophobic block of the unimer into the micellar core. As the second process is usually favorable, the main contribution comes from the first substep, thus, the thermodynamic potential varies as

$$\mathcal{F}\left(N + \frac{1}{2}, X_1\right) = \mathcal{F}(N, X_1) - \log \Phi_1, \tag{2.37}$$

where $\Phi_1 = X_1 v_p$ being v_p the single surfactant molecular volume. Thus, the association energy in Eq. 2.36 can be defined as

$$F_a = \max\left\{\mathcal{F}\left(N + \frac{1}{2}, X_1\right)\right\}. \tag{2.38}$$

For copolymer systems has been shown that T_a can assume astronomical values, even in an equilibrium regime ($X_1 = \text{CMC}^{\text{eq}}$), for a series of concentrations of free monomers as shown in Fig. 2.6; this suggest that the CMC measured in experiments can be larger by several orders of magnitude when compared with the equilibrium CMC. This experimental CMC can be related to the apparent value CMC$^{\text{app}}$ which arises when aggregation is induced by increasing the concentration of free surfactants in the system up to CMC$^{\text{app}}$, leading then, to decrease F_a to F^{app} and in consequence to reach an available experimental time T^{app} through

$$T^{app} = T_0 e^{F^{app}}. \tag{2.39}$$

The importance of the above equation lies in the possibility of determining the value of CMC$^{\text{app}}$ by taking as an initial guess the experimental time of the micelle formation, T^{exp}, that is $T^{app} = T^{exp}$ in Eq. 2.39. Subsequently, an equivalent value of the association barrier F^{app} and finally an estimation of the apparent CMC can

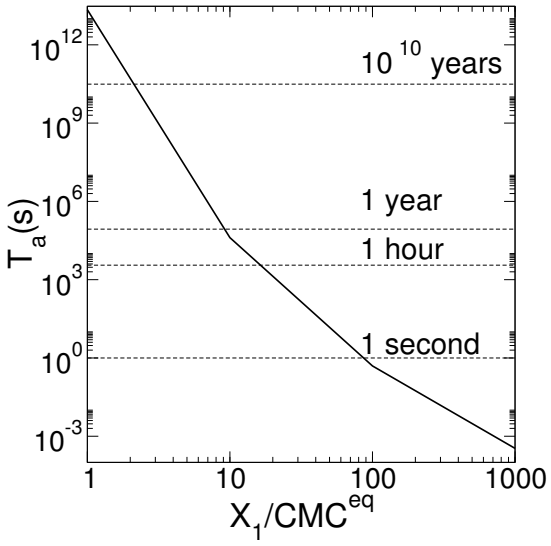

Figure 2.6: Characteristic micellization times as a function of the free monomer concentration. Horizontal axis represents the normalization of X_1 with the equilibrium CMC, while, dashed lines relate specifics times with their corresponding apparent CMCs.

be obtained by means of Eqs. 2.34, 2.37 and 2.38.

Connection of micellization kinetics formalism with the SCMF approach can be made through the aggregate size distributions predicted by the kinetic model and the MAM given by Eqs. 2.33 and 2.23, respectively

$$\mathcal{F}(N, X_1) = N\frac{\left(\mu_N^0 - \mu_1^0\right)}{kT} - (N-1)\log X_1,$$

according to Eqs. 2.31 and 2.40, the grand thermodynamic potential can be expressed in terms of the SCMF formalism through

$$\mathcal{F}(N, X_1) = N\log\left(\frac{N}{V}\frac{\sum_\alpha e^{-H_1[\alpha]/kT}/W(\alpha)}{\sum_\alpha e^{-H_N[\alpha]/kT}/W(\alpha)}\right) - (N-1)\log X_1,$$

as can be observed, the first term on the right side involves only enthalpic contributions for aggregated and free monomers which is consistent with the corresponding term provided by the SCMF scheme which resulted from the procedure to extract the entropic contributions to the chemical potential of free surfactants as stated in the analysis preceding Eq. 2.29; this means, that entropic contributions to the micellization process come only from the second term in the right side of Eq. 2.40 corresponding to the translational contributions of the free monomers.

The importance of Eq. 2.40 comes from the possibility to study experimental deviations from equilibrium values in surfactant systems based on SCMF predictions.

2.2 Single-Chain Mean-Field Theory: A Dynamical Approach

Once the relevant equations in the SCMF scheme have been identified, we proceed to establish a dynamic methodology which will allow to study equilibrium and nonequilibrium properties of surfactant systems. To

do so, we consider the set of sampling chains $\{\alpha\} = \alpha_1, \ldots, \alpha_0$ to be under the influence of a concentration field of solvent and surfactant molecules, then, generating a series of explicit moves which are accepted with a certain probability which depends on the relative change in the conformation energy caused by the the trial configuration it adopts. This can be seen as a system with a fixed number of chains which are uncorrelated one from each other i.e. they are independent by definition, from which a dynamics can be followed by the individual evolution of each of its members through a MC simulation where a trial move is generated simultaneously for each chain every MC cycle, then, is expected, in an equilibrium regime, a correct evaluation of dynamic events by following the collective behaviors of the sampling chains. The procedure to generate the move of the chains is taken as follows:

1. The starting point is to consider a representative number of configurations of the central chain α_o through a set of independent sampling chains $\{\alpha_o\}$, with all the interaction volumes $d\vec{r}\Phi^{cc}_{int}(\alpha_o, \vec{r})$ and $d\vec{r}\Phi^{cs}_{int}(\alpha_o, \vec{r})$, concentration $c(\alpha_o, \vec{r})$ and volume fraction $\phi(\alpha_o, \vec{r})$ fields and the corresponding mean fields $\langle c(\vec{r})\rangle$ and $\langle \phi(\vec{r})\rangle$ together with the solvent fields $c_s(\vec{r})$ and $\phi_s(\vec{r})$ by solution of Eqs. 2.5, 2.18 and 2.19 for the chain average fields mentioned above.

2. Subsequently, while keeping fixed the average fields $\langle c(\vec{r})\rangle$, $c_s(\vec{r})$ and $\phi_s(\vec{r})$, a trial move is generated simultaneously for each chain, α_o, with an individual probability of acceptance defined by the Metropolis formulation as described in the next section

$$p(\alpha_{o\to n}) = \min\left(1, \exp(-\Delta H\left[\alpha_{o\to n}\right]/kT)\right), \tag{2.40}$$

   where α_n refers to the new conformation of chain α_o given the trial move, $\Delta H[\alpha_{o\to n}] = H[\alpha_n] - H[\alpha_o]$ is the change in the SCMF Hamiltonian, given in the exponential term in Eq. 2.18, for the new and old conformations. With help of Eq. 2.16 the changes in the SCMF Hamiltonian are

$$\begin{aligned}\Delta H[\alpha_{o\to n}] \approx & \Delta u_{intra}(\alpha_{o\to n}) + (N-1)\int d\vec{r}\,\epsilon_{cc}\Delta\Phi^{cc}_{int}(\alpha_{o\to n}, \vec{r})\langle c(\vec{r})\rangle \\ & + \int d\vec{r}\,\epsilon_{cs}\Delta\Phi^{cs}_{int}(\alpha_{o\to n}, \vec{r})c_s(\vec{r}) - \frac{kT}{v_s}\int d\vec{r}\,\Delta\phi(\alpha_{o\to n}, \vec{r})\log\phi_s(\vec{r}),\end{aligned}$$

   where we have used the term $\pi(\vec{r}) \approx -kT/v_s \log\phi_s(\vec{r})$ in the last term of the SCMF energy. As can be observed, keeping unaltered the mean fields states that the changes in energy are caused by the changes in the internal energy, $\Delta u_{intra}(\alpha_{o\to n})$, the chain interaction volumes $d\vec{r}\Delta\Phi^{cc}_{int}(\alpha_{o\to n}, \vec{r})$ and $d\vec{r}\Delta\Phi^{cs}_{int}(\alpha_{o\to n}, \vec{r})$ and the individual volume fractions $\Delta\phi(\alpha_{o\to n}, \vec{r})$.

3. Once the moves for all the chains belonging to $\{\alpha_o\}$ have been individually accepted or rejected, a new set of sampling chains, $\{\alpha_n\}$, can be stated.

4. After the cycle has been completed, the concentration fields $\langle c(\vec{r})\rangle$, $\langle \phi(\vec{r})\rangle$, $c_s(\vec{r})$ and $\phi_s(\vec{r})$ are updated by solving Eqs. 2.5, 2.18 and 2.19.

5. All the procedure is repeated from step 1 for the new set of configurations after every cycle until equilibrium is reached.

Surfactant chains are generated based on the Rosenbluth and Rosenbluth procedure [7] to generate nonoverlapping chains with a biased probability distribution which is calculated through the chain statistical weight, $W(\alpha)$, and consequently removed when including in the corresponding SCMF probabilities in Eq. 2.18 as has been presented in sections 2.1.4 and 2.1.3, respectively.

As has been observed, in this section we have presented a method to study the dynamics of a systems of molecules in a solvent medium based on an extension of the SCMF scheme by evaluating trial moves over a set of independent sampling chains under the influence of intermolecular fields which are dependent on the evolution of individual chains. This method is suitable to study a wide number of phenomena that can not be deeply investigated by other traditional methods; as stated, dynamic SCMF simulations evaluate moves of noninteracting chains in a concentration field, that is, no pairwise interactions are calculated which results in a decrease in the simulation time, in particular this enables the study of polymeric systems which present interesting physical properties in timescales, e.g. diffusion of block copolymers through micellar aggregates [15], which are beyond the scope of common simulation schemes.

2.2.1 The Metropolis Method

The main objective is to determine the transition probability $\pi(o \to n)$ of going from an old state o to a new state n. Considering that in equilibrium the average number of accepted moves when going from o to n is the same as the opposite case leads to the *detailed balance condition*

$$N(o)\pi(o \to n) = N(n)\pi(n \to o), \tag{2.41}$$

where $N(o)$ and $N(n)$ are the probability densities of finding the system in the states o and n respectively. Formally, the transition probability can be written as

$$\pi(o \to n) = \alpha(o \to n) \times p(o \to n), \tag{2.42}$$

with $\alpha(o \to n)$ and $p(o \to n)$ as a symmetric matrix and the probability of accepting the trial move. Considering that $\alpha(o \to n) = \alpha(n \to o)$ in Eqs. 2.42 and 2.41

$$N(o) \times p(o \to n) = N(n) \times p(n \to o),$$

from the above equation can be found that

$$\frac{p(o \to n)}{p(n \to o)} = \frac{N(n)}{N(o)} = \exp(-\left(E(n) - E(o)\right)/kT), \tag{2.43}$$

where $E(n)$ and $E(o)$ are the energies of the system for the new and old states, respectively. In the Metropolis scheme the probability of accepting a move from state o to n is

$$p(o \to n) = \min\left(1, \exp(-\left(E(n) - E(o)\right)/kT)\right). \tag{2.44}$$

In this spirit, the procedure to accept or reject a trial move through the Metropolis scheme is as follows: firstly, a random trial move from an old configuration o to a new one n is generated; secondly, the calculation of the acceptance probability is calculated from the Eq. 2.44; thirdly, a random number $r \in [0, 1]$ is generated from a uniform distribution, and, fourthly, the trial move is accepted if $r < p(o \to n)$ or rejected in the opposite

case. In our case, the preceding procedure is adapted for calculating the probabilities of acceptance or rejection in Eq. 2.40 of new conformations of the sampling chains in the dynamic version of the SCMF presented in the previous section. From here, the dynamical behavior of a quantity across the time with respect to other variables or itself can be studied by means of time correlation functions which are introduced in the next section.

2.2.2 Time Correlation Functions

For time dependent quantities $A(t)$ and $B(t)$, let the correlation function $C_{AB}(t)$ to describe how the variables depend each other at a time t, it is defined as

$$C_{AB}(t) = \lim_{T\to\infty} \frac{1}{T} \int_0^T dt_0\, A(t_0)B(t_0 + t), \tag{2.45}$$

where T is the temporal length to perform the average, and, t_0 is the time origin which is arbitrary due to the equilibrium definition of the correlation function, i.e. $C_{AB}(t)$ is invariant under temporal translations. In terms of equilibrium averages, Eq. 2.45 can be written as

$$C_{AB}(t) = \langle A(t_0)B(t + t_0)\rangle, \tag{2.46}$$

with the term inside the brackets is taken as the average of quantities A and B in equilibrium. Analysing the two limiting cases; when $t = 0$ the temporal separation in Eq. 2.45 is no longer present in the values of the variables of interest, thereby, the correlation function becomes static

$$C_{AB}(0) = \langle A(t_0)B(t_0)\rangle = \langle AB\rangle. \tag{2.47}$$

In the second case, when $t \to \infty$ the two quantities will be decorrelated, that is

$$\lim_{t\to\infty} C_{AB}(t) = \langle A\rangle\langle B\rangle. \tag{2.48}$$

If $C_{AB}(t)$ does not decay to zero when A and B are no longer correlated, a shift for each variable around its mean value forces the convergence through

$$C'_{AB}(t) = \langle [A(t) - \langle A\rangle]\,[B(t) - \langle B\rangle]\rangle = C_{AB}(t) - \langle A\rangle\langle B\rangle, \tag{2.49}$$

the above expression can be normalized as $\hat{C}_{AB}(t) = C'_{AB}(t)/C'_{AB}(0)$, then, with help of Eq. 2.47

$$\hat{C}_{AB}(t) = \frac{C_{AB}(t) - \langle A\rangle\langle B\rangle}{\langle AB\rangle - \langle A\rangle\langle B\rangle}.$$

In case variables A and B are the same, $C_{AA}(t)$ is known as the autocorrelation function, and, in consequence, former equation turns into

$$\hat{C}_{AA}(t) = \frac{C_{AA}(t) - \langle A\rangle^2}{\langle A^2\rangle - \langle A\rangle^2}. \tag{2.50}$$

References

[1] A. BenShaul, I. Szleifer, and W. M. Gelbart. *J. Chem. Phys.*, 83(7):3597–3611, 1985.

[2] A. D. Mackie, A. Z. Panagiotopoulos, and I. Szleifer. *Langmuir*, 13(19):5022–5031, 1997.

[3] M. A. Carignano and I. Szleifer. *J. Chem. Phys.*, 98(6):5006–5018, 1993.

[4] A. Gezae Daful, J. Bonet Avalos, and A. D. Mackie. *Langmuir*, 28(8):3730–3743, 2012.

[5] J. N. Israelachvili. *Intermolecular and Surface Forces*. Elsevier, San Diego, CA, 2011.

[6] Z. A. Al-Anber, J. Bonet Avalos, and A. D. Mackie. *J. Chem. Phys.*, 122(10):104910, 2005.

[7] M. N. Rosenbluth and A. W. Rosenbluth. *J. Chem. Phys.*, 23(2):356–359, 1955.

[8] A. Gezae Daful, V. A. Baulin, J. Bonet Avalos, and A. D. Mackie. *J. Phys. Chem. B*, 115(13):3434–3443, 2011.

[9] F. M. Menger and C. A. Littau. *J. Am. Chem. Soc.*, 115(22):10083–10090, 1993.

[10] M. J. Rosen, J. H. Mathias, and L. Davenport. *Langmuir*, 15(21):7340–7346, 1999.

[11] B. Burczyk, K. A. Wilk, A. Sokołowski, and L. Syper. *J. Colloid Interface Sci.*, 240(2):552 – 558, 2001.

[12] P. A. FitzGerald, M. W. Carr, T. W. Davey, A. K. Serelis, C. H. Such, and G. G. Warr. *J. Colloid Interface Sci.*, 275(2):649 – 658, 2004.

[13] A. Nikoubashman and A. Z. Panagiotopoulos. *J. Chem. Phys.*, 141(4):041101, 2014.

[14] I. A. Nyrkova and A. N. Semenov. *Macromol. Theory Simul.*, 14(9):569–585, 2005.

[15] R. Zana, C. Marques, and A. Johner. *Adv. Colloid Interface Sci.*, 123-126:345–351, 2006.

Chapter 3

Chain Architecture and Micellization: A Mean-Field Coarse-Grained Model for Poly(ethylene oxide) Alkyl Ether Surfactants

J. Chem. Phys. **2015**, 142, 114902.

Fabián A. García Daza, Alexander J. Colville, and Allan D. Mackie

THE JOURNAL OF CHEMICAL PHYSICS **142**, 114902 (2015)

Chain architecture and micellization: A mean-field coarse-grained model for poly(ethylene oxide) alkyl ether surfactants

Fabián A. García Daza,[1] Alexander J. Colville,[2] and Allan D. Mackie[1,a)]
[1]*Department d'Enginyeria Química, ETSEQ, Universitat Rovira i Virgili, Avinguda dels Països Catalans 26, 43007 Tarragona, Spain*
[2]*Department of Chemical Engineering, Northeastern University, 360 Huntington Avenue, Boston, Massachusetts 02115-5000, USA*

(Received 24 December 2014; accepted 12 February 2015; published online 16 March 2015)

Microscopic modeling of surfactant systems is expected to be an important tool to describe, understand, and take full advantage of the micellization process for different molecular architectures. Here, we implement a single chain mean field theory to study the relevant equilibrium properties such as the critical micelle concentration (CMC) and aggregation number for three sets of surfactants with different geometries maintaining constant the number of hydrophobic and hydrophilic monomers. The results demonstrate the direct effect of the block organization for the surfactants under study by means of an analysis of the excess energy and entropy which can be accurately determined from the mean-field scheme. Our analysis reveals that the CMC values are sensitive to branching in the hydrophilic head part of the surfactant and can be observed in the entropy-enthalpy balance, while aggregation numbers are also affected by splitting the hydrophobic tail of the surfactant and are manifested by slight changes in the packing entropy. © *2015 AIP Publishing LLC*. [http://dx.doi.org/10.1063/1.4913960]

I. INTRODUCTION

Copolymer surfactants are widely used in industry for a variety of applications where their ability to self-assemble into micelles is key to their performance. For example, these micellar systems are of great utility for the drug delivery of pharmaceuticals, gene therapy, nanomaterial synthesis, food processing, and oil spill recovery.[1] As a result of the many applications of copolymer surfactants, much research has been conducted on the properties and molecular characteristics of them. Since the surfactants amphiphilic properties drive the self-assembly into micelles, the molecular structure of the surfactants is an essential part of the process. It is thus of great significance to fully understand and predict the effects of surfactant architecture on micelle thermodynamic properties as a step towards the design of tailor made surfactants for specific applications.

Many previous experimental works and reviews have looked at the utility of polymer architecture in drug delivery[2–6] and other applications. For example, Nakamura *et al.*[7] found star polymers to enhance therapeutic efficacy and antitumor activity in comparison to linear polymers when conjugated to drugs. These works highlight the promising potential for tailoring surfactant structure for unique and desirable characteristics. Numerous previous experimental works have sought to understand the thermodynamic properties behind the self-assembly of these complex surfactant shapes using techniques such as surface tension,[8] static and dynamic light scattering,[9] elution gel-permeation chromatography, dye solubilization,[10] electrical conductivity measurement, steady-state fluorescence measurement,[11,12] and microcalorimetry[13] to study critical micelle concentrations (CMCs) and aggregations numbers. Such experimental works have covered a variety of architectures including diblock, triblock, ring, gemini, bolaform, and branched among others.[14] However, time, cost, and accuracy constraints have spurred researchers in this field to pursue simulations in their study of copolymer characterization.[15] The experimental results have shown that there is a very wide parameter space to explore the effect of architecture on micelle formation.[16] The large variable space can be covered more cost effectively with simulations that are capable of providing detail on a more microscopic level than current experimental techniques. However, little simulation work has been done so far to investigate the effect of surfactant structure on micellar properties systematically.[17]

A few works have previously simulated the properties of copolymer micelles based on the effects of surfactant architecture using Molecular Dynamics (MD) simulations.[18,19] La Rosa *et al.*[18] investigated monolayers of surfactants with MD successfully. However, MD has limitations in the intensive computational power that the technique requires and the time scales necessary to reach equilibrium. While atomistic molecular simulations allow for greater accuracy and detail of the particles, mesoscale simulations allow for the study of larger surfactants over longer periods of time using coarse-graining. As a direct result, several groups have used Dissipative Particle Dynamics (DPD) to investigate the effects of block architecture.[20] For similar reasons, a lot of work utilizes Monte Carlo (MC) simulations in this area of research. Between DPD and MC, the available published work has looked at the effect of surfactant architecture in monolayers,[21] bilayer membranes,[22] and micelles.[23,24] These simulations have shown

a)Electronic mail: allan.mackie@urv.cat

success in investigating thermodynamic and micellar properties such as CMC and aggregation number for a great variety of surfactant architectures, in particular, Panagiotopoulos *et al.*[25] studied the micellization, CMC, and phase separation conditions for a series of diblocks, TH, and triblocks, THT and HTH, surfactants in a lattice grand-canonical MC. The abbreviation H is used for the head or hydrophilic group and T for the tail or hydrophobic group. In a similar fashion, Kim and Jo[26] studied the aggregation numbers and CMC for THT and HTH block copolymers, predicting higher values of both quantities for the HTH system at a fixed temperature, and a quantitative description of the aggregation process was analyzed in terms of the enthalpic and entropic contributions derived from the simulations.[26,27] Rekvig *et al.*[28] combined DPD and MC to test the impact of chain geometry for linear and branched surfactants on their efficiency at the oil-water interface yielding an advantage for branched molecules in terms of adsorbance and free monomer concentration in the bulk. Jackson *et al.*,[29] by means of a two-dimensional MC, studied the effect of asymmetry for a fixed number of hydrophobic/hydrophilic units for linear surfactants exhibiting a strong dependence on the CMC with respect to the number of spacers in the gemini-like case in comparison to the asymmetry. Also, mean-field techniques like the Self-Consistent Field (SCF) theory have been employed to describe the micellization process for series of surfactants. In this theory, polymers in solution are assumed to be ideal chains surrounded by interacting fields and it is possible to study equilibrium and geometrical properties of copolymers systems. Zhou and Shi[30] studied the most stable shape from one-dimensional simulations for linear diblock surfactants with different lengths. Hurter *et al.*[31] compared the partition coefficients in the case of triblock and Tetronic Pluronics when solubilized with different compounds. Symmetric surfactants have also been widely studied predicting phase behavior,[32,33] CMC, critical micelle temperature, and cloud point temperature.[34,35] In addition, symmetric and asymmetric THT and HTH triblocks have been studied by Monzen *et al.*[36] resulting in a more favorable formation of spherical micelles for the symmetric HTH case with respect to the THT system while the opposite case is true when the end blocks are highly asymmetric.

To our knowledge, there are only a very limited amount of simulation works, e.g., employing DPD and MC, that have quantitatively compared results with experimental findings. More research remains to be completed in order to fully understand the connection between DPD atomistic length-scale simulations and macroscopic experimental results. In addition, the discrete lattice model used in the MC and SCF simulations also causes difficulties in comparing directly to experimental results. Because of these limitations of previous works, this work utilizes the Single Chain Mean Field (SCMF) theory[37] that has been successfully used in previous studies of surfactant systems to predict and compare quantitatively with available experimental data.[38] The SCMF is a mean-field technique that is similar in spirit to SCF, nevertheless, the main difference comes from the connectivity related to the chains representing the surfactants; in the SCF scheme, the chains are ideal which means that they are Markovian in nature implying the possibility of the presence of overlapping configurations. In contrast, the SCMF considers non-Markovian chains leading to non-overlapping conformations, which allows for the explicit consideration of the excluded-volume interactions that are not considered in SCF.[39] This is essential in the present work where different chain architectures are compared and can be expected to have a direct impact on the free energy of the system. In particular, this paper seeks to further the study of the effects of surfactant architecture with a comparison between simulation values for CMCs and aggregation numbers across a more comprehensive set of surfactant structures: diblock (linear), branched, gemini, and triblock. The study also compares directly to experimental data when available.

II. SIMULATION AND MODEL DETAILS

A. Single chain mean field theory

The SCMF theory[37] is a free energy model that is based on the individual contributions of a single chain that belongs to the set of permitted conformations $\{\alpha\}$ representing the surfactant by means of its interaction with surrounding fields of solvent and surfactants. This is provided in the assignation of an individual probability $P[\alpha]$ for every conformation which leads to the calculation of average properties in equilibrium over these probabilities, particularly, the entropic and energetic effects due to the surfactant molecular structure. The starting point in the theory is the consideration of the explicit Helmholtz free energy F_N for an aggregate of size N,

$$F_N = \langle U_N \rangle - T\langle S_N \rangle, \tag{1}$$

where the first and the second terms refer to the energetic and the entropic contributions, respectively, and are defined by

$$\langle U_N \rangle = N \int d\alpha P[\alpha] U(\alpha, c_s(\vec{r})), \tag{2}$$

with $U(\alpha, c_s(\vec{r})) = U_{intra}(\alpha) + U_{inter}(\alpha, c_s(\vec{r}))$ as the total intramolecular and intermolecular energies for the corresponding conformation α depending on the solvent concentration $c_s(\vec{r})$. The exact form depends on the coarse-grained model chosen to represent the surfactant molecules and solvent as will be shown below. On the other hand, the entropy of surfactants and solvent is expressed as

$$\langle S_N \rangle = -kN \int d\alpha P[\alpha] \ln P[\alpha] - k \int d\vec{r} c_s(\vec{r}) \ln \phi_s(\vec{r}),$$

with k as the Boltzmann constant and $\phi_s(\vec{r}) = v_s c_s(\vec{r})$ the solvent volume fraction where v_s is the solvent bead volume. To determine the equilibrium state, it is necessary to minimize the free energy in Eq. (1) together with the volume-filling constraint, $\phi_s(\vec{r}) + N\langle \varphi_{exc}(\vec{r}) \rangle = 1$ by means of a Lagrange multiplier $\pi(\vec{r})$, where the second term is the volume fraction of the aggregate occupying the point $\vec{r}$. The physical meaning of the constraint resides in the condition that all regions of space are occupied by either surfactant or solvent molecules deriving from the steric hard-core repulsions for surfactant molecules. As can be observed from the expressions for $\langle U_N \rangle$ and $\langle S_N \rangle$, variations in the free energy depend on changes of the single-chain probabilities $P[\alpha]$ and the solvent concentration $c_s(\vec{r})$ leading to complete the minimization procedure from

the evaluation of the functional derivatives $\delta F_N/\delta P[\alpha] = 0$ and $\delta F_N/\delta c_s(\vec{r}) = 0$. As expected, this provides an expression for $P[\alpha] = e^{-H_N(\alpha)/kT}/Q$ which depends on $c_s(\vec{r})$ through the effective SCMF Hamiltonian $H_N(\alpha)$ and therefore the partition function Q ensuring $1 = \int d\alpha P[\alpha]$. Generally, the explicit form of $U(\alpha, c_s(\vec{r}))$ depends on the surfactant model and the intra and intermolecular interactions taken into account, while the expression for $P[\alpha]$ is influenced by the approximations considered in the minimization process. In this work, we consider a series of surfactants with different arrangements of the hydrophilic and hydrophobic units, where in order to describe the moieties involved, we implement the model developed by Gezae Daful *et al.*[38] for nonionic poly(ethylene oxide) alkyl ethers, where hydrophobic CH_2, hydrophilic CH_2CH_2O, and solvent groups are represented by beads of diameter σ. The distance between the centers of two consecutive beads belonging to the same surfactant is taken to be 1.42σ. The intermolecular interactions considered in the model are included via square well potentials with the corresponding volume $4\pi(r_{int}^3 - \sigma^3)/3$ from the center of each bead with $r_{int} = 1.61\sigma$. This potential has a depth ε, given in kT units, that depends on the interactions taken into account which in this case are those between hydrophobic, C, and hydrophilic, EO, and the solvent medium, S ($\varepsilon_{C,EO}$, $\varepsilon_{C,S}$ and $\varepsilon_{EO,S}$). From these considerations, the interaction energy for configuration α in this coarse-grained is taken to be

$$U(\alpha, c_s(\vec{r})) \approx U_{intra}(\alpha) + \frac{N-1}{2}\varepsilon_{C,EO}\int d\vec{r}d\beta P[\beta]\left(\Phi_C(\alpha,\vec{r})c_{EO}(\beta,\vec{r}) + \Phi_{EO}(\alpha,\vec{r})c_C(\beta,\vec{r})\right) + \int d\vec{r}\left(\varepsilon_{C,S}\Phi_C(\alpha,\vec{r}) + \varepsilon_{EO,S}\Phi_{EO}(\alpha,\vec{r})\right)c_s(\vec{r}), \tag{3}$$

the first term is calculated as the interaction energy $\varepsilon_{C,EO}$ times the number of non-consecutive intramolecular EO–C contacts for conformation α whose distance between centers lie in the range $[\sigma, 1.61\sigma]$, the second term indicates the interaction of conformation α through the available interaction volume $d\vec{r}\Phi(\alpha,\vec{r})$ at $\vec{r}$ with concentration fields $c(\beta,\vec{r})$ of conformation β for species EO and C, while the third term is the corresponding interaction of conformation α with the solvent medium (water). Once the interaction terms are known and the free energy minimization procedure is completed, the SCMF probabilities that minimize the free energy are found be

$$P[\alpha] = \frac{1}{Q}\exp\left[-\frac{1}{kT}\left(U_{intra}(\alpha) + (N-1)\varepsilon_{C,EO} \times \int d\vec{r}\left(\Phi_C(\alpha,\vec{r})\langle c_{EO}(\vec{r})\rangle + \Phi_{EO}(\alpha,\vec{r})\langle c_C(\vec{r})\rangle\right) + \int d\vec{r}\left(\varepsilon_{C,S}\Phi_C(\alpha,\vec{r}) + \varepsilon_{EO,S}\Phi_{EO}(\alpha,\vec{r})\right)c_s(\vec{r}) - \frac{kT}{v_s}\int d\vec{r}\phi_{ex}(\alpha,\vec{r})\ln\phi_s(\vec{r})\right)\right], \tag{4}$$

where the term in the exponential is referred to as the SCMF Hamiltonian $H_N(\alpha)$ for conformation α. We have used the averaged value for the concentration fields of the surfactant $\langle c(\vec{r})\rangle = \int d\alpha P[\alpha]c(\alpha,\vec{r})$ that along with Eq. (4) and the incompressibility condition forms a set of non-linear equations which can be solved iteratively giving as a result the values of $P[\alpha]$, $c_s(\vec{r})$ and hence $\langle c_{EO}(\vec{r})\rangle$ and $\langle c_C(\vec{r})\rangle$ for an aggregate of size N which ensures the minimum value of the free energy of the system given in Eq. (1).

B. Equilibrium properties

The connection between the microscopic nature and the macroscopic observables, particularly, the CMCs and concentration of aggregates in equilibrium is provided by the multiple equilibrium model[40]

$$\frac{X_N}{N} = X_1^N e^{-N(\mu_N^0 - \mu_1^0)/kT}, \tag{5}$$

where X_N and X_1 are the concentrations of surfactants in aggregates of size N and in the bulk, respectively, with their corresponding standard chemical potentials μ_N^0 and μ_1^0, which, in turn, can be obtained from the SCMF simulations[41]

$$\frac{\mu_N^0 - \mu_1^0}{kT} = -\log\left(\frac{V}{N}\frac{\sum_\alpha e^{-H_N(\alpha)/kT}/W(\alpha)}{\sum_\alpha e^{-H_1(\alpha)/kT}/W(\alpha)}\right), \tag{6}$$

with V as the volume of the simulation box, $W(\alpha)$, the corresponding correction to the bias generated in the generation of non-overlapping conformations according to the Rosenbluth and Rosenbluth method,[42] and $H_N(\alpha)$ and $H_1(\alpha)$, the SCMF Hamiltonians for surfactants in aggregates of size N and in the bulk solution respectively, which can be determined from Eq. (4)

$$H_N(\alpha) \approx U_{intra}(\alpha) + (N-1)\varepsilon_{C,EO} \times \int d\vec{r}\left(\Phi_C(\alpha,\vec{r})\langle c_{EO}(\vec{r})\rangle + \Phi_{EO}(\alpha,\vec{r})\langle c_C(\vec{r})\rangle\right) + \int d\vec{r}\left(\varepsilon_{C,S}\Phi_C(\alpha,\vec{r}) + \varepsilon_{EO,S}\Phi_{EO}(\alpha,\vec{r})\right)c_s(\vec{r}) - \frac{kT}{v_s}\int d\vec{r}\phi_{ex}(\alpha,\vec{r})\ln\phi_s(\vec{r}). \tag{7}$$

In order to compare the effect of chain architecture on the energetic and entropic quantities in equilibrium, we can use the relation between the standard chemical potentials and the excess enthalpy and entropy per molecule[26]

$$\frac{\mu_N^0 - \mu_1^0}{kT} = \frac{\Delta U^0}{kT} - \frac{\Delta S^0}{k}, \tag{8}$$

TABLE I. Surfactant chain architectures considered in this work.

Type	Chemical structure	Abbreviation
Diblock (linear)	$H(CH_2)_n(OCH_2CH_2)_mOH$	C_nE_m
Branched	$[H(CH_2)_{n/2-1}]_2CHCH_2(OCH_2CH_2)_mOH$	IC_nE_m
Gemini	$[H(CH_2)_{n/2-2}CHCH_2(OCH_2CH_2)_{m/2}OH]_2$	Gem_nE_m
Triblock	$HO(CH_2CH_2O)_{m/2}(CH_2)_n(OCH_2CH_2)_{m/2}OH$	$E_{m/2}C_nE_{m/2}$
Triblock	$H(CH_2)_{n/2}(OCH_2CH_2)_m(CH_2)_{n/2}H$	$C_{n/2}E_mC_{n/2}$

where the term on the left is given by SCMF calculations from Eq. (6), while the excess enthalpy representing the energetic favorability in the aggregation process, $\Delta U^0 = \langle U_N\rangle/N - \langle U_1\rangle$, for surfactants in aggregates and in the bulk solution can be obtained directly from the evaluation of Eq. (2). Once the standard chemical potential and the excess enthalpic contributions are known, using Eq. (8) it is possible to calculate the entropy of packing surfactants with a very-well defined architecture in equilibrium aggregates, $\Delta S^0 = \langle S_N\rangle/N - \langle S_1\rangle$. This quantity is related to the equilibrium size of the micelles depending on the surfactant geometry[26,43] as has previously been demonstrated for linear diblock and triblock copolymers. The use of Eq. (8) to calculate ΔS^0 is required to avoid translational entropic contributions contained in the SCMF formalism and is based on the standard chemical potential[41] and the energetic terms which are independent of the translational degrees of freedom. The determination of the enthalpic and entropic excess contributions enables us to directly analyze the effect of chain architecture on the relevant equilibrium properties such as the equilibrium aggregation number N_{agg} and CMC. In this work, the CMC is defined as the exponential of the minimum value of the standard chemical difference, namely, $CMC \approx \exp((\mu^0_{N_{agg}} - \mu^0_1)/kT)$. We have chosen four types of surfactants with different hydrophobic and hydrophilic block architectures as given in Table I. Examples of the different types of surfactants with various chain lengths can be observed in Figure 1 where typical configurations of surfactants in aggregates are shown. Note that the conformations are non-overlapping and flexible and were generated based on the Rosenbluth and Rosenbluth algorithm.[42]

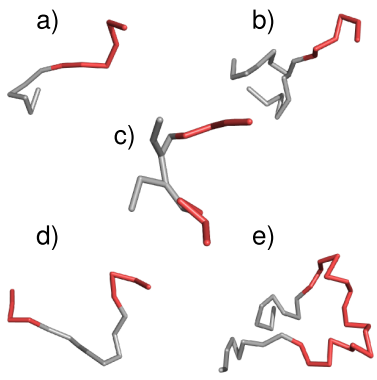

FIG. 1. Chain architectures studied using the SCMF scheme: (a) linear, (b) branched, (c) gemini and triblock with (d) hydrophobic and (e) hydrophilic central chains. In all cases, red and gray sticks refer to hydrophilic and hydrophobic units, respectively. The beads representing the moieties are omitted to represent the surfactants in a clear manner.

A series of simulations using a parallel OpenMP environment were performed for a set of 10 million conformations $\{\alpha\}$ for each surfactant system in simulation boxes with volumes between $(25\sigma)^3$ and $(60\sigma)^3$ depending on the total length of the surfactant under study. A one-dimensional spherical geometry has been assumed to discretize all the fields, this choice is due to our interest in the properties related to the initial appearance of micelles close to the CMC,[44,45] neglecting then the possibility of shape transitions which is beyond of the scope of this work. Both, 24-core and 32-core AMD workstations with RAM memories of 32 Gb and 128 Gb respectively, were used. After solving the SCMF equations, we obtained the standard chemical potential difference, $(\mu^0_{N_{agg}} - \mu^0_1)/kT$, the concentration profiles for each aggregate and solvent, $\langle c_C(\vec{r})\rangle$, $\langle c_{EO}(\vec{r})\rangle$, and $c_s(\vec{r})$, together with the probabilities distribution, $\{P[\alpha]\}$, the excess enthalpy contributions, ΔU^0, and from here the excess or packing entropy per surfactant, ΔS^0.

III. RESULTS AND DISCUSSION

Our results reveal the formation of spherical aggregates with a defined size distribution for a free monomer concentration close to the CMC. In Figure 2 are presented the schematic diagrams of the micelles for a series of surfactants with 16 hydrophobic and 18 hydrophilic units for the different surfactant architectures given in Table I. The micelles shown in these diagrams are not real conformations as obtained in standard MC, MD, or DPD simulations but instead are constructed from the most-probable configurations of the single-chain representing the surfactant in the equilibrium state. In this context, the configuration with the greatest probability is highlighted for every aggregate, which is a useful tool to help visualize the distribution of the different species composing the surfactant inside the micelles. As can be observed, the micelle cores are occupied by hydrophobic blocks and are surrounded by a non-uniform shell of hydrophilic units. The aggregation numbers N_{agg} and the CMCs predicted in this work at 25 °C under the SCMF theory are presented in Table II together with experimental available data. As expected, an increase in the aggregation number and a decrease of the CMC are found with an increase in the number of hydrophobic units for a given chain architecture. The validity of the results can be supported when comparing the CMC values predicted in this work with available experimental data for diblock (linear) and branched surfactants, where in both cases, a good quantitative agreement is obtained. The same trend has been reported in theoretical,[48] simulation,[27,38,49,50] and experimental[14,46,51,52] works. Of particular interest in this article is the behavior of the CMC with respect to the surfactant architecture keeping constant the total number of hydrophobic and hydrophilic blocks. To do so, we have chosen three series of surfactants with a constant number of units, see Figure 3, where a significant difference for the CMC depending on the surfactant geometry can be observed for all systems. For the sake of simplicity, we abbreviate the notation given in Table I for diblock (linear), branched, gemini, and triblock with central hydrophobic and hydrophilic blocks chain architectures to CE, ICE, GemE, ECE, and CEC respectively. Starting from the CE linear diblock surfactants, a

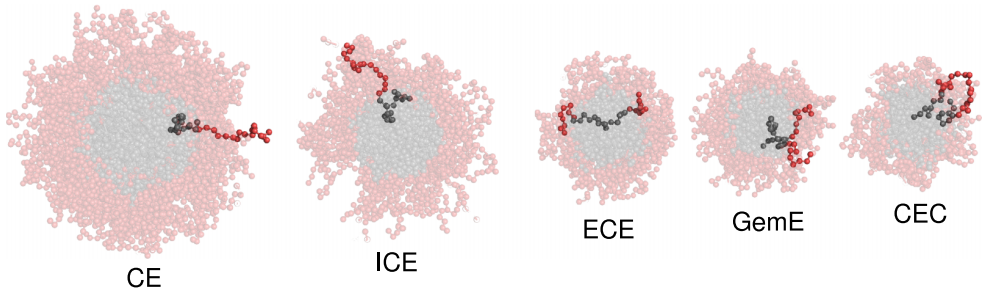

FIG. 2. Schematic cross-sections of aggregates corresponding to the minimum of the standard chemical potential for surfactants with $n = 16$ and $m = 18$ hydrophobic and hydrophilic units, respectively, for the geometries specified in Table II. The highlighted conformations refer to the surfactants with the highest probability while the others are half of the total aggregation number of the following most probable configurations.

slight increase of the CMC is observed for the branched ICE geometry which can be attributed to an increase in the steric interactions in the interior of the aggregates for the branched tail in comparison to the linear case, producing a higher free energy that causes the process to be less favorable thereby increasing the CMC. This result has also been reported in DPD simulations[49] and experimental measurements for nonionic surfactants[14] and can be explained also in terms of the enthalpic and entropic excess quantities for both cases as can be observed in Figure 4. Here, the enthalpy for the CE geometry is more negative than for the ICE case, indicating a more favorable energetic state, however, the entropy is slightly less negative for the ICE surfactant giving the opposite effect; that is, the packing of branched molecules is less adverse in comparison to the CE architecture. Despite this, the enthalpic-entropic balance favors the CE aggregation manifested in the lower CMC as stated. When considering triblock ECE and gemini GemE configurations, a general increase in the CMC of at least two times can be observed when comparing with the reference CE geometry. This is mainly due to a higher excess enthalpy produced by an increase of the interfacial core-water contact per surfactant coming from the two hydrophobic-hydrophilic contacts. On the other hand, a smaller loss of packing entropy is observed because of the hindrance of packing head groups outside the core. This can be observed when comparing analogous linear tail systems ECE and CE or branched tail GemE and ICE, but changing in both cases the number of hydrophilic blocks, as can be observed in Figure 4, this change will be consequently reflected in the changes of entropy and enthalpy excess values. Nevertheless, the enthalpic contribution is dominant in both cases with respect to the packing entropy, resulting in a less negative standard chemical potential indicating that the surfactants become more soluble thus giving a higher CMC as was reported in experiments[53] and in lattice MC simulations[25] for similar linear triblock and diblock systems.

TABLE II. Experimental and predicted CMCs from the SCMF theory together with aggregation numbers for the chain architectures under study. CMC values are given in mmol/L.

Surfactant	CMC_{SCMF}	CMC_{exp}	N_{agg}
	Diblock (linear)		
C_6E_6	117	68.5[a]	112
C_8E_6	10.4	9.80[b]	190
C_8E_8	13.6	10[b]	170
$C_{10}E_9$	1.46	1.30[a]	227
$C_{12}E_{20}$	0.518	0.1[c]	273
$C_{16}E_{18}$	0.0051	0.0003,[b] 0.002[d]	405
	Branched		
IC_6E_6	124	96.4[a]	94
IC_8E_6	12.4	21.4[a]	138
IC_8E_8	15.4	...	120
$IC_{10}E_9$	1.89	2.98[a]	143
$IC_{12}E_{20}$	0.551	...	156
$IC_{16}E_{18}$	0.0080	...	193
	Gemini		
Gem_8E_8	42	...	56
$Gem_{12}E_{20}$	2.37	...	54
$Gem_{16}E_{18}$	0.0207	...	96
	Triblock		
$E_4C_8E_4$	39	...	64
$E_{10}C_{12}E_{10}$	2.13	...	65
$EC_{16}E_9$	0.0210	...	120
$C_8E_{18}C_8$	0.151	...	89

[a]From Ref. 46 at 25 °C.
[b]From Ref. 47 at 25 °C.
[c]Value from Ref. 47 for surfactant $C_{12}E_{25}$.
[d]Value from Ref. 46 for surfactant $C_{16}E_{12}$.

A similar situation can be observed in the case of the triblock copolymers with two hydrophobic ends, CEC, where a high CMC is predicted in comparison with the other geometries. In this case, a less negative entropic penalty is found together with a less negative enthalpic compensation. In the case of the enthalpy, the two hydrophobic extremes of a surfactant must enter into the core of the micelle thus increasing the steric interactions and consequently the excess enthalpy similar to the GemE situation. For aggregates to form, the surfactants must form a loop, which is not the case of any of the other systems. Effectively, this situation will produce a packing entropy contribution. According to our calculations, for the ECE case, a surfactant in an equilibrium aggregate possesses a packing entropy $\langle S_N \rangle / N = -19.19\ k$ and enthalpy $\langle U_N \rangle / N = 29.69\ kT$ in contrast to the values of $-17.04\ k$ and $34.26\ kT$ for the CEC surfactants, which means that packing surfactants in CEC aggregates have a gain in entropy but a high energetic

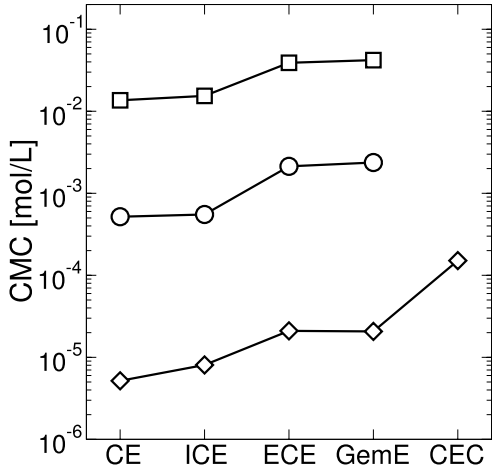

FIG. 3. Predicted CMC depending on the block architecture for three surfactants with defined numbers of hydrophobic, C_n, and hydrophilic, E_m, units. Empty squares refer to surfactants with $\{n,m\}=\{8,8\}$, empty circles represent the set $\{n,m\}=\{12,20\}$, and empty diamonds depict $\{n,m\}=\{16,18\}$. The solid line is included to help guide the eye.

cost when comparing to the ECE system. In both cases, similar excess contributions were found for the free surfactants in the bulk solution ($\langle S_1\rangle \approx 1.1\ k$ and $\langle U_1\rangle \approx 65\ kT$). Our results for the excess quantities are qualitatively similar to those found in previous lattice MC simulations[26] for triblock HTH and THT copolymers, as well as experimental CMCs[10,53] together with simulation predictions.[25,27,49]

Given that for the same number of monomers, similar CMCs are obtained in the case of CE and ICE or ECE and GemE, we turn our attention to another equilibrium property, namely, the equilibrium aggregation numbers N_{agg} which are presented in Figure 5. As can be observed, a systematic variation of the aggregation numbers depending on the block architecture is found. This situation is in contrast to the CMC where different architectures can exhibit a similar value. Keeping constant the hydrophilic block and varying the hydrophobic configurations, as in the case of CE and ICE, produces a decrease of the aggregation number for the branched case. This can be explained in terms of a compacting of the core for the ICE species in comparison with the linear one, resulting in a reduction of the free energy for a lower aggregation number, which is similar to some reported simulation results.[15,49] In the case of surfactants with two hydrophilic segments such as ECE and GemE, an increase of the interfacial area per surfactant between the core and the solvent is produced, leading to a decrease in the steric repulsion between hydrophilic units in the shell of the aggregate, thus requiring a lower number of surfactants to minimize the free energy in contrast to the diblock (linear) case. In addition to this, we have found a higher aggregation number for ECE surfactants compared to GemE. Despite a similar arrangement of the surfactants in the aggregated state, a slightly higher packing entropy penalty is imposed for the geminis due to the restriction in the accommodation of tails in the core because of the branching in the hydrophobic segments; contrarily, the triblock case can accommodate the tails more readily. This small entropic difference affects quantitatively the aggregation number in a similar manner for diblock (linear) surfactants with different head groups.[43] On the other hand, we have found a smaller value of the aggregation number for CEC when comparing with ECE case which is contrary to previous results given by grand-canonical MC techniques.[25–27] In particular, Kim and Jo[26] determined the excess entropy and enthalpy for symmetric triblock systems HTH and THT with fixed length. The excess quantities of the THT surfactants are found to be less negative in comparison to the HTH case,[26,27] which is qualitatively similar to the results presented in Figure 4. The behavior of the packing entropy is related to the value of the equilibrium aggregation number, N_{agg}, as has been stated before for linear triblock[26,27] and diblock[43] systems. For this reason, we believe that the qualitative discrepancy between our predictions for the aggregation numbers and the ones reported by Kim and Jo[26,27] and Panagiotopoulos *et al.*[25] is possibly due to the absence of dangling and bridge conformations in our SCMF calculations for the CEC surfactant which has been demonstrated to be relevant for the packing entropy and therefore the aggregation numbers. Despite the fact that we are limited by the one-dimensional geometry effectively at infinite dilution imposed in our simulations leading to neglect the possibility of dangling and bridge conformations that enables the

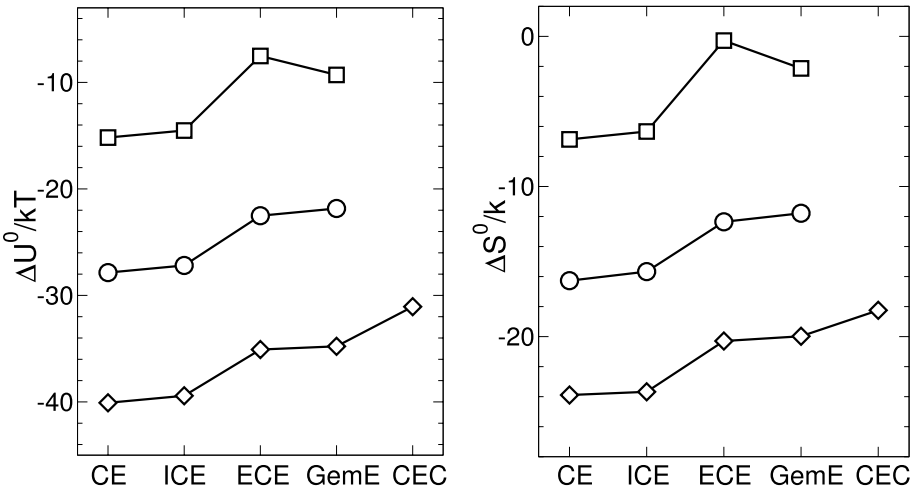

FIG. 4. Excess enthalpy and entropy per surfactant as a function of the surfactant architecture. Symbols and lines are as in Figure 3.

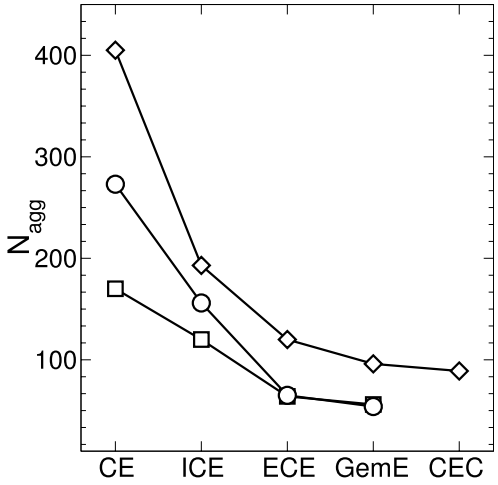

FIG. 5. Aggregation numbers for surfactants with different architectures. Symbols and lines are as in Figure 3.

possibility of connected aggregates, we expect that this will not substantially affect the calculation of the excess enthalpy but may result in an incomplete estimation of the packing entropy affecting directly the aggregation number. Although a two or even three-dimensional geometry can be implemented in the SCMF scheme to evaluate the impact of these kind of conformations, it is beyond the scope of the present work. On the other hand, these excess quantities depend on a fine balance between several contributions and so this difference with previous studies may be due instead merely to the model used or to inaccuracies from the mean-field approximation.

IV. SUMMARY

In this work, we have studied the equilibrium CMC and aggregation number for a series of poly(ethylene oxide) alkyl ethers surfactants with different block architectures but constant number of hydrophobic and hydrophilic groups. Our results reveal that, in general, triblock or branched conformations increase the solubility of the surfactants while the aggregation numbers exhibit a decreasing behavior. The behavior of the corresponding CMCs is evaluated from the excess enthalpic-entropic balance where an increase in both quantities is observed for different copolymer architectures taking as reference the diblock (linear) architectures. The results reported in this work highlight the ability of the SCMF theory to quantify the impact of the surfactant geometry on the relevant macroscopic quantities. This was carried out by means of an analysis of the thermodynamic excess variables involved in the aggregation process.

ACKNOWLEDGMENTS

F.A.G.D. acknowledges the financial support from URV through his Ph.D. scholarship.

[1]K. Kataoka, A. Harada, and Y. Nagasaki, Adv. Drug Delivery Rev. **64**, 37 (2012).
[2]C. Thompson, L. Tetley, and W. Cheng, Int. J. Pharm. **383**, 216 (2010).
[3]L. Qiu and Y. Bae, Pharm. Res. **23**, 1 (2006).
[4]Z. Wang, C. Chen, Q. Zhang, M. Gao, J. Zhang, D. Kong, and Y. Zhao, "Tuning the architecture of polymeric conjugate to mediate intracellular delivery of pleiotropic curcumin," Eur. J. Pharm. Biopharm. (published online).
[5]Y. Wang and S. M. Grayson, Adv. Drug Delivery Rev. **64**, 852 (2012).
[6]J. Liu, H. Duong, M. R. Whittaker, T. P. Davis, and C. Boyer, Macromol. Rapid Commun. **33**, 760 (2012).
[7]H. Nakamura, E. Koziolová, T. Etrych, P. Chytil, J. Fang, K. Ulbrich, and H. Maeda, "Comparison between linear and star-like HPMA conjugated pirarubicin (THP) in pharmacokinetics and antitumor activity in tumor bearing mice," Eur. J. Pharm. Biopharm. (published online).
[8]L. Lee, J. Salimon, M. A. Yarmo, R. Syafri, and M. Hisam, J. Dispersion Sci. Technol. **34**, 914 (2013).
[9]H. Altinok, G. Yu, S. K. Nixon, P. A. Gorry, D. Attwood, and C. Booth, Langmuir **13**, 5837 (1997).
[10]C. Booth, D. Attwood, and C. Price, Phys. Chem. Chem. Phys. **8**, 3612 (2006).
[11]X. Wang, J. Wang, Y. Wang, J. Ye, H. Yan, and R. K. Thomas, J. Phys. Chem. B **107**, 11428 (2003).
[12]A. A. Steinschulte, B. Schulte, S. Rutten, T. Eckert, J. Okuda, M. Moller, S. Schneider, O. V. Borisov, and F. A. Plamper, Phys. Chem. Chem. Phys. **16**, 4917 (2014).
[13]G. Bai, J. Wang, Y. Wang, H. Yan, and R. K. Thomas, J. Phys. Chem. B **106**, 6614 (2002).
[14]K. Kratzat and H. Finkelmann, Langmuir **12**, 1765 (1996).
[15]C. Lin, Y. Chen, Y. Sheng, and H. Tsao, React. Funct. Polym. **69**, 539 (2009).
[16]M. Zamurovic, S. Christodoulou, A. Vazaios, E. Iatrou, M. Pitsikalis, and N. Hadjichristidis, Macromolecules **40**, 5835 (2007).
[17]D. Liu and C. Zhong, Polymer **49**, 1407 (2008).
[18]M. La Rosa, A. Uhlherr, C. H. Schiesser, K. Moody, R. Bohun, and C. J. Drummond, Langmuir **20**, 1375 (2004).
[19]T. Taddese, P. Carbone, and D. L. Cheung, Soft Matter **11**, 81 (2015).
[20]A. G. Goicochea, M. Romero-Bastida, and R. López-Rendón, Mol. Phys. **105**, 2375 (2007).
[21]Z. Wang, Y. Li, Y. Guo, and H. Zhang, J. Dispersion Sci. Technol. **34**, 1020 (2013).
[22]G. Illya, R. Lipowsky, and J. C. Shillcock, J. Chem. Phys. **122**, 244901 (2005).
[23]V. Firetto, M. A. Floriano, and A. Z. Panagiotopoulos, Langmuir **22**, 6514 (2006).
[24]K. E. Hart, L. J. Abbott, M. Lísal, and C. M. Colina, J. Chem. Phys. **141**, 204902 (2014).
[25]A. Z. Panagiotopoulos, M. A. Floriano, and S. K. Kumar, Langmuir **18**, 2940 (2002).
[26]S. H. Kim and W. H. Jo, Macromolecules **34**, 7210 (2001).
[27]S. H. Kim and W. H. Jo, J. Chem. Phys. **117**, 8565 (2002).
[28]L. Rekvig, M. Kranenburg, J. Vreede, B. Hafskjold, and B. Smit, Langmuir **19**, 8195 (2003).
[29]D. R. Jackson, A. Mohareb, J. MacNeil, M. S. G. Razul, D. G. Marangoni, and P. H. Poole, J. Chem. Phys. **134**, 204503 (2011).
[30]J. Zhou and A. Shi, Macromol. Theory Simul. **20**, 690 (2011).
[31]P. N. Hurter, J. M. H. M. Scheutjens, and T. A. Hatton, Macromolecules **26**, 5592 (1993).
[32]P. Linse, J. Phys. Chem. **97**, 13896 (1993).
[33]A. De Nicola, T. Kawakatsu, and G. Milano, Macromol. Chem. Phys. **214**, 1940 (2013).
[34]V. G. de Bruijn, L. J. P. van den Broeke, F. A. M. Leermakers, and J. T. F. Keurentjes, Langmuir **18**, 10467 (2002).
[35]Y. Lauw, F. A. M. Leermakers, and M. A. Cohen Stuart, J. Phys. Chem. B **110**, 465 (2006).
[36]M. Monzen, T. Kawakatsu, M. Doi, and R. Hasegawa, Comput. Theor. Polym. Sci. **10**, 275 (2000).
[37]A. Ben-Shaul, I. Szleifer, and W. M. Gelbart, J. Chem. Phys. **83**, 3597 (1985).
[38]A. Gezae Daful, V. A. Baulin, J. Bonet Avalos, and A. D. Mackie, J. Phys. Chem. B **115**, 3434 (2011).
[39]J. Bonet Avalos, A. D. Mackie, and S. Díez-Orrite, Macromolecules **37**, 1143 (2004).
[40]J. N. Israelachvili, *Intermolecular and Surface Forces* (Elsevier, San Diego, CA, 2011).
[41]Z. A. Al-Anber, J. Bonet Avalos, and A. D. Mackie, J. Chem. Phys. **122**, 104910 (2005).
[42]M. N. Rosenbluth and A. W. Rosenbluth, J. Chem. Phys. **23**, 356 (1955).
[43]C. M. Care and T. Dalby, EPL **45**, 38 (1999).
[44]Z. A. Al-Anber, J. Bonet i Avalos, M. A. Floriano, and A. D. Mackie, J. Chem. Phys. **118**, 3816 (2003).

[45]A. G. Daful, J. B. Avalos, and A. D. Mackie, Langmuir **28**, 3730 (2012).
[46]M. Mattei, G. M. Kontogeorgis, and R. Gani, Ind. Eng. Chem. Res. **52**, 12236 (2013).
[47]A. Berthod, S. Tomer, and J. G. Dorsey, Talanta **55**, 69 (2001).
[48]R. Nagarajan, Chem. Eng. Commun. **55**, 251 (1987).
[49]Y. Lin, M. Wu, Y. Sheng, and H. Tsao, J. Chem. Phys. **136**, 104905 (2012).
[50]F. A. García Daza and A. D. Mackie, J. Phys. Chem. Lett. **5**, 2027 (2014).
[51]T. Kuwamura and H. Takahashi, Bull. Chem. Soc. Jpn. **45**, 617 (1972).
[52]W. L. Hinze and E. Pramauro, Crit. Rev. Anal. Chem. **24**, 133 (1993).
[53]C. Booth and D. Attwood, Macromol. Rapid Commun. **21**, 501 (2000).

Chapter 4

Low Critical Micelle Concentration Discrepancy between Theory and Experiment

J. Phys. Chem. Lett. **2014**, 5, 2027-2032.

Fabián A. García Daza and Allan D. Mackie

THE JOURNAL OF PHYSICAL CHEMISTRY Letters

Letter

pubs.acs.org/JPCL

Low Critical Micelle Concentration Discrepancy between Theory and Experiment

Fabián A. García Daza and Allan D. Mackie*

Department d'Enginyeria Química, ETSEQ, Universitat Rovira i Virgili, Avinguda dels Països Catalans 26, 43007 Tarragona, Spain

ABSTRACT: Experimental measurements for a variety of surfactants unexpectedly show that the critical micelle concentration (CMC) becomes constant with respect to increasing the size of the hydrophobic tail. This observation disagrees with theoretical models where it is expected to continue to decrease exponentially. Because of the lack of a satisfactory explanation for such a discrepancy from theory, we have studied these systems using a coarse-grained model within the single-chain mean field (SCMF) theory combined with relevant micellar kinetic effects. In particular, a microscopic model for poly(ethylene oxide) alkyl ether was applied to describe a series of nonionic gemini surfactants. When kinetic effects are used to correct the equilibrium CMC values from the SCMF scheme together with the loss of surfactants due to adsorption on the experimental recipient, it is possible to reproduce the correct order of magnitude of the experimental CMC results. Hence it appears that the experimental values disagree with the theoretical predictions because they are not true equilibrium values due to the fact that the time scales for these low CMC values become astronomically large.

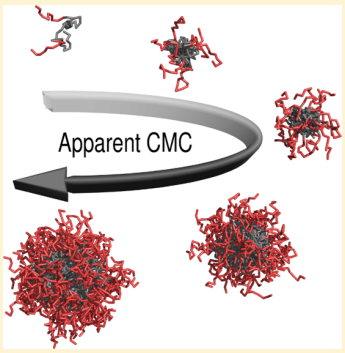

SECTION: Glasses, Colloids, Polymers, and Soft Matter

Surfactant molecules are of the utmost importance in a wide range of industries including environmental, pharmaceutical, material synthesis, and oil recovery, among others.[1−3] Key to their importance is their ability to associate into aggregates with well-defined geometrical shapes above a free surfactant concentration known as the critical micelle concentration (CMC). The ability to design surfactants to have specific properties can be expected to play a major role in various technological applications; for example, in the cleaning industry a lowering in surfactant CMC allows for a decrease in the concentration at which solubilization in the stain removal process occurs,[4] in emulsion polymerization the CMC and particle nucleation processes are related,[5] and in pharmacology surfactants with low CMC values are preferred to transport drugs to reduce the number of free monomers that can precipitate in the blood.[6]

Experimentally, surfactant systems exhibit an exponential decrease in the CMC value with respect to the size of the hydrophobic tail at constant temperature;[7,8] such a behavior has been predicted by theoretical models[9−11] and simulation studies.[12−14] However, for very low CMC values, a nonexponential decrease in the CMC can be observed starting from a certain length of the hydrophobic component, which depends on the surfactant chosen. This phenomenon has been reported in the case of ionic[15−17] and nonionic[18,19] surfactants. This Letter is aimed at understanding and explaining this discrepancy between the experimental CMC observation and expected theoretical behavior.

Theoretical models have been proposed for the formation of micelles in surfactant systems[9−11] to calculate the main factors that give rise to micelle shape, phase behavior, and the CMC. In particular, a description of cationic dimeric (gemini) surfactants has been realized.[20] These models are based on an arbitrary division of the free energy into several contributions, and a direct link to the underlying microscopic system is lost. The CMC is estimated mainly from the free energy contribution related to the transfer of the hydrophobic tail of the surfactant from the bulk to the inner core of an aggregate, together with additional contributions. Because this free energy can be related linearly to the size of the surfactant tail and the CMC depends on the exponential of the free energy of micelle formation, this results in an exponential decrease in the CMC on increasing the tail length.

Within the computational framework, molecular dynamics (MD) and Monte Carlo (MC) simulations have been widely used to explore micellization;[12,21−25] however, problems can be found when trying to determine the CMC. In particular, MC and MD calculations appear to be limited by spatial and temporal factors, resulting in sampling and equilibrium problems, a lack of long time kinetic effects, nonconvergence in the aggregate size distribution due to the slow dynamics of the aggregates, and in some cases no satisfactory CMC prediction. These effects have been reported in recent MD simulations using graphics processing units for a series of nonionic poly(ethylene glycol) surfactants for hydrophobic tails composed of 6 to 12 carbon atoms.[26]

In a similar fashion, mean-field methods have also been used such as the self-consistent field theory in lattice discretized space[27−29] and in continuous space;[30,31] however, the chains

Received: April 21, 2014
Accepted: May 20, 2014
Published: May 20, 2014

   dx.doi.org/10.1021/jz500790b | *J. Phys. Chem. Lett.* 2014, 5, 2027−2032

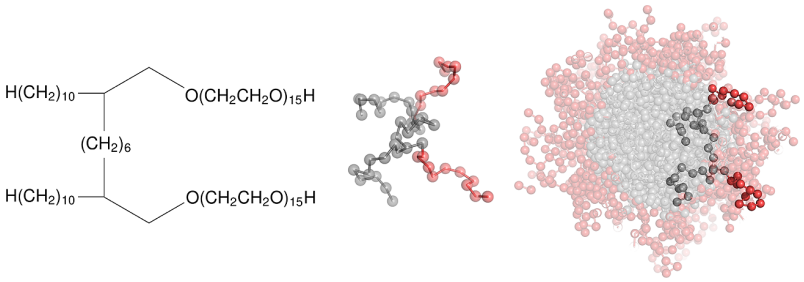

Figure 1. Coarse-grained model for $Gem_{12}EO_{10}$. Left: Chemical structure for the selected gemini surfactant. Center: The most probable conformation in the bulk. The groups with a central carbon atom and ethylene oxide unit are represented by gray and red beads, respectively. Right: Cross section for an aggregate of 100 gemini surfactants predicted with the SCMF, where the most probable configuration is highlighted.

representing the surfactants are described by Gaussian distributions, which implies the inclusion of overlapping conformations that ignore excluded volume intramolecular interactions terms in the free energy. Another mean-field simulation technique that has been successful in predicting the CMC is the so-called single-chain mean field (SCMF) theory,[32] which has been directly compared with MC[33,34] and MD[35] simulations. Recently, accurate predictions of the CMC for a wide number of polyoxyethylene alkyl ethers surfactants were performed by Gezae Daful et al.,[13] where a comparison with experimental values showed an excellent quantitative agreement.

In view of the concerns with standard simulations, which can be expected to be even more important for longer surfactants, the SCMF theory presents itself as an interesting alternative. This method uses the solution of a mean-field Hamiltonian and can be applied to relatively long surfactants. The main idea is to use nonoverlapping conformations of a single molecule that can be described at any desired coarse-grained level. The interactions with the other molecules and solvent medium are described in terms of mean molecular fields; these fields take into account the concentrations of the different species of the molecule and an incompressibility condition. The molecular fields are calculated from a self-consistent condition that specifies that the individual molecule conformations depend on the mean molecular fields, while these mean fields are calculated from the average values of these individual conformations. The microscopic level is close to the one employed in MC and MD simulations. The main advantage is that the free energy involved in the micellization process can be calculated directly, whereas it is difficult to obtain from MC or MD simulations. We employ the SCMF combined with a model for micellization kinetics to calculate the CMC to understand the deviations found between experimental data and the expected theoretical exponential decrease. In particular, we have chosen the nonionic gemini surfactant $(H(CH_2)_{n-2}CHCH_2O(CH_2CH_2O)_mH)_2(CH_2)_6$ synthesized by FitzGerald et al.[19] and denoted as Gem_nEO_m. This system has a strong deviation in the measured CMC with respect to the values predicted by theoretical free energy models as a function of the hydrophobic tail length n.

To describe nonionic gemini surfactants, we used the coarse-grained model developed in a previous work by Gezae Daful et al.[13] for poly(ethylene oxide) alkyl ether surfactants. Two classes of beads with the same diameter are employed: one type representing the group that contains a central carbon atom (C) and the other representing an ethylene oxide unit (EO). All length units are given in terms of the diameter of the beads: the distance between two consecutive beads is 1.42, and the interactions of a bead with the surrounding fields are given by means of square well potentials with internal and external radii of 1.0 and 1.6, respectively. Finally, the only interactions considered are those between unlike molecular type of the surfactant and the solvent, that is, C-EO, C-Solvent, and EO-Solvent, with values of 0.34, 3.984, and 0.5, respectively. (In the original work, ref 13, a factor of 1.66 was missing and is incorrectly stated. The value should be 3.984, as given in this work to correctly reproduce the CMC values.) It should be noted that no additional adjustment of these parameters was made for the gemini surfactants. The chemical formula and a typical configuration of the coarse-grained model adopted in this work is shown in Figure 1 for a $Gem_{12}EO_{10}$ surfactant.

In the SCMF, a set of nonoverlapping conformations, $\{\alpha\}$, of the surfactant molecule is generated, and each one of these conformations is represented by an associated probability $P[\alpha]$ enabling the calculation of any average property by means of $\langle A \rangle = \int d\alpha\, P[\alpha]A[\alpha]$, where $A[\alpha]$ is the quantity measured for each conformation. This probability follows a Boltzmann distribution, which means that $P[\alpha] = e^{-H^N_{MF}[\alpha]/kT}/Q$, where $H^N_{MF}[\alpha]$ is the SCMF Hamiltonian for a system containing N surfactants, k is the Boltzmann constant, T is the temperature, and Q is the partition function, which ensures the correct normalization of the probabilities. The mean-field Hamiltonian includes: (i) the exact internal energy of configuration α, (ii) the interaction of the configuration with the surrounding fields of solvent and surfactants molecules calculated in a self-consistent way, and (iii) a steric repulsion term representing the incompressibility condition of the system. The concentration of aggregates in equilibrium can be extracted from the equality of the chemical potential between aggregated and free surfactants according to the mass action model[36]

$$\frac{X_N}{N} = [X_1 e^{-(\mu_N^0 - \mu_1^0)/kT}]^N \tag{1}$$

where X_1 and X_N are the concentrations of surfactants in the bulk and those in aggregates of size N, while μ_1^0 and μ_N^0 are the corresponding standard chemical potentials for free chains and surfactants in aggregates of size N, respectively. The macroscopic connection with the SCMF is obtained from the relation of eq 1 with the Hamiltonian,[34] which is given as

$$e^{-(\mu_N^0 - \mu_1^0)/kT} \approx \frac{V}{N} \frac{\sum_\alpha e^{-H^N_{MF}[\alpha]/kT}/W(\alpha)}{\sum_\alpha e^{-H^1_{MF}[\alpha]/kT}/W(\alpha)} \tag{2}$$

where $H^1_{MF}[\alpha]$ refers to the SCMF Hamiltonian for free surfactants in the bulk solution and V and $W(\alpha)$ are the

simulation box volume and the statistical weight associated with the Rosenbluth and Rosenbluth method used to generate nonoverlapping conformations[37] of the surfactants.

It is possible to establish a direct relationship between the standard chemical potentials and the association/dissociation thermodynamic potential $F(N, X_1)$, which gives rise to the energetic barriers[38,39] involved in micelle formation. To do so, we relate the concentration of aggregates given by the mass action model in eq 1 with the dimensionless potential $F(N, X_1)$ by means of

$$\frac{X_N}{N} = X_1 e^{-F(N,X_1)} \tag{3}$$

From the relation between eqs 1 and 3, we can state that

$$F(N, X_1) = N\frac{(\mu_N^0 - \mu_1^0)}{kT} - (N-1)\log X_1 \tag{4}$$

The first term on the right-hand side of eq 4 is related to the interaction between surfactants in aggregates as compared with those in the bulk solution and can be determined by the SCMF method by means of eq 2. The second term is related to the translational entropy of free monomers. From here, the CMC in equilibrium (CMC^{eq}) can be defined as the free surfactant concentration at which $F(M^{agg}, CMC^{eq}) = 0$ and $[(\partial F(N,CMC^{eq}))/(\partial N)]|_{N=M}{}^{agg} = 0$, where M^{agg} is the aggregation number in the equilibrium state.

A series of simulations were performed for a set of 16 gemini surfactants Gem_nEO_m, with n = 6, 8, 10, 12, 14, 16, 18, and 20 and m = 10 and 15. Sets of 3 to 8 million conformations were generated to represent the corresponding surfactant configurations. From the solutions of the SCMF equations, we can derive all equilibrium properties such as the average volume fractions for aggregates of size N and estimate the standard chemical potentials favoring the micellization process in eq 2, leading to the determination of the association/dissociation potentials from eq 4. In Figure 2, the potential $F(N, X_1)$ for three values of the free surfactant concentration is presented,

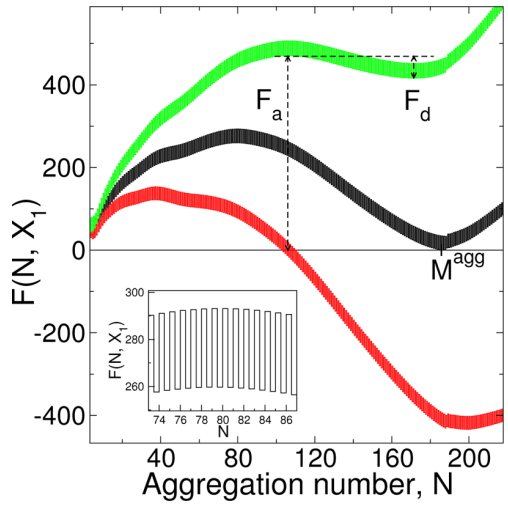

Figure 2. Aggregation potentials $F(N, X_1)$ as a function of aggregation number, N, for surfactant $Gem_{16}EO_{10}$ with F_a, F_d, and M^{agg} as the association/dissociation barriers and the equilibrium aggregation number, respectively. From top to bottom, $X_1 \approx CMC^{eq}/10$, $X_1 \approx CMC^{eq}$, and $X_1 \approx 10CMC^{eq}$. The inset shows the maximum for $X_1 \approx CMC^{eq}$ in the range N = 73−87.

where F_a and F_d, the activation and dissociation energy barriers, are given for the lowest surfactant concentration of $CMC^{eq}/10$. It should be noted, however, that they are defined for any free surfactant concentration. As can be seen, when $X_1 < CMC^{eq}$ (green line), the association barrier is higher than the dissociation one, meaning that the energetic cost for surfactants to associate into aggregates is higher, in comparison with the dissociation, indicating that most surfactants will be in a nonaggregated state. When $X_1 = CMC^{eq}$ (black line), the association/dissociation rates are the same, indicating that over an interval of time the number of aggregates per unit volume per unit time that associate is the same as the ones that dissociate ($F_a = F_d$). Finally, if $X_1 > CMC^{eq}$ (red line), the barrier F_a to form aggregates can be more easily overcome; however, the dissociation barrier is relatively higher, making it more difficult to pass in the opposite direction (i.e., releasing surfactants from the aggregates), leading to the possible formation of aggregates that are not in equilibrium. This last state is of particular importance to understand the experimental results for the gemini surfactants studied in this work.

To obtain a reasonable correspondence between the association/dissociation scheme with the step-by-step nature of the micellization process, we have to include an entropic contribution related to the probability for surfactants to be in contact with aggregates in the estimation of the potential $F(N, X_1)$ and hence the values of F_a and F_d. This negative contribution is taken to be $-\log\Phi_1$ and modifies the aggregation potential given in eq 4 as follows[38]

$$F\left(N + \frac{1}{2}, X_1\right) = F(N, X_1) - \log \Phi_1 \tag{5}$$

where Φ_1 refers to the free surfactant volume fraction of the system and is taken in this Letter to be approximately $X_1 V_{mol}$, with V_{mol} being the single surfactant molecular volume.[8] The effect of such corrections in the association/dissociation potentials can be observed in the inset in Figure 2, which exhibits a step behavior due to the intrinsically discrete mechanism of micelle formation, where one chain has to be added at a time. From the information provided by $F(N, CMC^{eq})$ and $F(N+1/2, CMC^{eq})$, an estimation of the characteristic time scale of micelle formation can be performed by means of $T_a = T_0 e^{F_a}$, where T_0 is the primary association time that is taken to be $T_0 = 6\pi\eta_{sol}R_1^3/M^{agg}kT$, where η_{sol} is the solvent viscosity and R_1 is the surfactant hydrodynamic radius. This time scale is obtained from the relationship of maximum free chain concentration in aggregates with the rate of micelle formation per unit volume and unit time and the dimer lifetime.[38] In our case, we have roughly estimated the hydrodynamic radius for each selected surfactant to be in the interval $R_1 \approx 0.42$ to 0.56 nm; in all cases, the aggregation number is $M^{agg} \approx 54-203$, the viscosity of water at 298.15 K is $\eta_{sol} \approx 8.91 \times 10^{-4}$ kg/m·s, and $kT \approx 4.11 \times 10^{-3}$ kg·nm^2/s^2. From here we find that T_0 is on the order 10^{-12} s. Given that we are considering micellization as a closed association process carried out by a step-by-step growth, the activation barrier F_a must be overcome to achieve a complete micellization process at the CMC^{eq}. By considering that according to the SCMF results $F_a \approx 35-293$, we can infer for $n \geq 12$ (where $F_a > 150$) that the time needed to obtain a complete micelle formation in equilibrium becomes astronomical, $T_a \approx 10^{50}$ to 10^{100} s, leading to the conclusion that it is not feasible to determine experimentally the correct CMC for the longer surfactants on the time scales available in the laboratory.

dx.doi.org/10.1021/jz500790b | J. Phys. Chem. Lett. 2014, 5, 2027−2032

In Figure 3, the equilibrium CMCs calculated in this work using the SCMF theory for the nonionic gemini surfactants

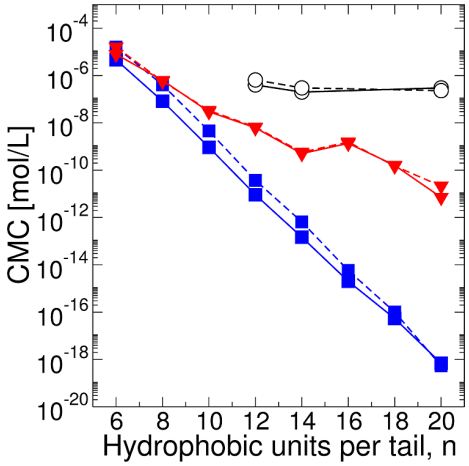

Figure 3. Experimental CMC data (○) as a function of the number of hydrophobic tail units, n, taken from ref 19 for nonionic gemini surfactants, predicted equilibrium values from the SCMF (CMC^{eq}, ■), and corrected for kinetic factors (CMC^{app}, ▼). The lines are guides for the eye, where the dashed line represents Gem_nEO_{15} and the solid line represents Gem_nEO_{10}.

(filled squares) studied in this Letter are shown as well as the available literature experimental values. As can be observed, CMC^{eq} is found to follow a linear behavior on the logarithmic scale with respect to the number of carbon atoms in the alkyl chain, as has already been found in experiments for shorter CxEOy surfactants and has been predicted in theoretical models.[8,13] When the experimental data (empty circles) are compared with the predictions obtained from SCMF for CMC^{eq}, a discrepancy of four orders of magnitude is observed for geminis with the shorter hydrophobic chain (n = 12). Such a deviation dramatically increases as the number of methylene CH_2 units rises, reaching a difference of 11 orders of magnitude in the case of $Gem_{20}E_m$. A similar scenario was presented in a previous work[20] for a free energy model for bis(quaternary ammonium bromide) surfactants. The authors justify the difference by suggesting that a recoil or collapse of the free surfactants, an effect not included in the empirical model used, may be responsible for changing the intramolecular interactions and thereby the transfer free energy and result in an increase in the CMC in the experimental systems. However, this is not observed in the SCMF calculations performed in this Letter, where the free chain conformations are explicitly included in a homogeneous concentration field. Indeed, we have not noted any collapse of the surfactants either in the bulk or in the aggregates, as can be observed in Figure 1. Thus, we need to look to other possible explanations to understand the discrepancy between experimental and theoretical CMC values and so we turn our attention to the kinetic effects.

As already mentioned, from the estimation of the time T_a needed to achieve the micellization process in equilibrium, we can infer that the aggregation process is extremely slow for these systems. However, the formation of aggregates can be modified by means of an arbitrary increase in the free surfactant concentration X_1 above CMC^{eq} following eqs 4 and 5, leading to a nonequilibrium formation of micelles in the experimental time scales T^{app} that are typically used. This action of arbitrarily increasing the surfactant concentration above the unattainable CMC^{eq} reduces the activation energy barrier $F_a = \max\{F(N + 1/2, X_1)\}$ until a value F^{app}, which can be overcome during the experimental time scale $T^{app} = T_0 e^{F^{app}}$. The observed result will be an equivalent or apparent CMC (referred to here as CMC^{app}), as previously suggested.[38] In this work, we arbitrarily consider that the necessary experimental time to observe a complete micellization for the geminis in the laboratory is T^{app} = 1 m; this is equivalent to a reduction of F_a until $F^{app} \approx 30$, resulting in a correction in the CMC predicted values seen in Figure 3 (filled triangles). The CMC^{app} and CMC^{eq} from the SCMF scheme show a relative difference that increases progressively to 10^7 with respect to the number of hydrophobic units in the gemini surfactants. Comparing the CMC^{app} with the experimental values, we observe an improved agreement, where the predicted values are now within a factor of 10^2 of the experimental values when n = 12 or 14. However, the difference between these values increases for n = 20 to a relative difference of $\sim 10^4$. Although no experimental CMC values are available in the case of n = 16, 18, we can expect an intermediate difference between these two values when comparing with the predicted CMC^{app}, in contrast with n = 6, 8, 10, where minor discrepancies can be expected. Experimental data are unfortunately also unavailable for these shorter surfactants. The cause of the deviation between CMC^{app} and the experimental CMC is still unclear; however, we have not considered the possible effects of the loss of surfactants due to adsorption and how this might affect the equilibrium CMC and equivalent CMC^{app} predicted values. In this respect, FitzGerald et al.[19] suggested that for measured CMCs close to 10^{-7} to 10^{-6} mol/L it is plausible to estimate that the concentration of free surfactants in the bulk should be around 10^{-10} to 10^{-8} mol/L. Such an assertion is based on the assumption that an important amount of surfactant can be adsorbed onto the walls of the recipient that contains the solution, leading to an increase in the measured experimental CMC. This means that an experimental CMC of $\sim 10^{-7}$ mol/L would possibly correspond to 10^{-10} mol/L in the bulk, which is on the same order of magnitude with the predicted CMC^{app} in this Letter for n = 12, 14 and relatively close in the case of n = 20.

According to our calculations for geminis with n = 6, 8, and 10, we have observed that the aggregation numbers N corresponding to the association barriers $F^{app} = \max\{F(N + 1/2, CMC^{app})\}$ lie in the range $10 \leq N \leq 20$. In every case this barrier is easily overcome, producing a small relative difference between the apparent and equilibrium CMC, as can be observed in Figure 3. This is contrary to the case when geminis with $n \geq 12$ are considered where the barriers F^{app} are usually found in the range $N \leq 10$. At these very low aggregate numbers the limit of validity of our spherical mean-field approximation can be reached, and it would be interesting to check these calculations with other techniques. However, precisely in the case of these longer gemini such as $Gem_{20}EO_{15}$, there are 76 beads representing each surfactant, and we expect that the mean-field approximation may be reasonable even at very low aggregation numbers. Furthermore, the inclusion of the standard chemical potential difference $(\mu_N^0 - \mu_1^0)kT$ in the corresponding association/dissociation potentials $F(N, X_1)$ for very small aggregation numbers, such as dimers and trimers, which are currently missing from our mean field approach and kinetic calculations, is expected to lead to an increase in CMC^{app}. This change is not expected to be large and would

dx.doi.org/10.1021/jz500790b | J. Phys. Chem. Lett. 2014, 5, 2027−2032

give rise to an improved agreement with experimental data. We thus believe that despite these limitations to our calculations our overall conclusions will not be significantly affected, namely, that the difference between the simulation SCMF value and the experimental one can be attributed to both kinetic and adsorption effects in the experimental measurements.

To identify the effect on CMC^{app} determined with SCMF and kinetic theory with respect to the time scale used to study micellization in the laboratory, T^{app}, we performed a series of calculations with T^{app} = 1 s, 1 h, and 6 h. The CMC^{app} obtained in every case shows a tendency to decrease with respect to increasing T^{app}, as expected. In the extreme cases, a decrease of two orders of magnitude and an increase of one order of magnitude were obtained for T^{app} = 6 h and T^{app} = 1 s, respectively, with respect to our reference time of 1 m. These results reveal that although the kinetic effects are susceptible to changes in the laboratory time scales the changes are not so large so as to affect our overall conclusions. To finish, we propose that the experimental values disagree with the theoretical predictions for the gemini surfactants studied in this work because they are not true equilibrium values. This is a consequence of the extremely large time scales found for the equilibration of micelles for these low concentrations values, leading to apparent CMCs that are orders of magnitude above the equilibrium values. When these kinetic factors are used to estimate an apparent CMC, and are combined with the possible adsorption effects on the experimental equipment as reported in the literature, we are able to find the same order of magnitude between the experimental CMCs and our predicted values. We also observe a change in the exponential decrease in the CMC with tail length, where the CMC decreases less rapidly in our calculations. Although we have only calculated the case for nonionic gemini surfactants, we expect the same conclusions to be valid for all surfactants with sufficiently low CMCs.

AUTHOR INFORMATION

Corresponding Author

*E-mail: allan.mackie@urv.cat.

Notes

The authors declare no competing financial interest.

ACKNOWLEDGMENTS

F.A.G.D. acknowledges financial support from URV through his Ph.D. scholarship.

REFERENCES

(1) Shah, D. *Micelles: Microemulsions, and Monolayers: Science and Technology*; Marcel Dekker: New York, 1998.
(2) Schramm, L. L.; Stasiuk, E. N.; Marangoni, D. G. Surfactants and Their Applications. *Annu. RepProg. Chem., Sect. C: Phys. Chem.* **2003**, *99*, 3−48.
(3) May, A.; Pasc, A.; Stébé, M. J.; Gutiérrez, J. M.; Porras, M.; Blin, J. L. Tailored Jeffamine Molecular Tools for Ordering Mesoporous Silica. *Langmuir* **2012**, *28*, 9816−9824.
(4) Zana, R.; Xia, J. In *Gemini Surfactants: Synthesis, Interfacial and Solution-Phase Behavior, and Applications*; Zana, R., Xia, J., Eds.; Marcel Dekker: New York, 2003; pp 296−315.
(5) Chern, C. S. *Principles and Applications of Emulsion Polymerization*; Wiley: Hoboken, NJ, 2008.
(6) Kabanov, A. V.; Alakhov, V. Y. In *Amphiphilic Block Copolymers*; Alexandridis, P., Lindman, B., Eds.; Elsevier: Amsterdam, 2000; pp 347−376.
(7) Rosen, M.; Kunjappu, J. *Surfactants and Interfacial Phenomena*; Wiley: Hoboken, NJ, 2012.
(8) Berthod, A.; Tomer, S.; Dorsey, J. G. Polyoxyethylene Alkyl Ether Nonionic Surfactants: Physicochemical Properties and Use for Cholesterol Determination in Food. *Talanta* **2001**, *55*, 69−83.
(9) Tanford, C. Theory of Micelle Formation in Aqueous Solutions. *J. Phys. Chem.* **1974**, *78*, 2469−2479.
(10) Tanford, C. *The Hydrophobic Effect: Formation of Micelles and Biological Membranes*; Wiley: New York, 1973.
(11) Nagarajan, R.; Ruckenstein, E. Theory of Surfactant Self-Assembly: A Predictive Molecular Thermodynamic Approach. *Langmuir* **1991**, *7*, 2934−2969.
(12) Jusufi, A.; Sanders, S.; Klein, M. L.; Panagiotopoulos, A. Z. Implicit-Solvent Models for Micellization: Nonionic Surfactants and Temperature-Dependent Properties. *J. Phys. Chem. B* **2011**, *115*, 990−1001.
(13) Gezae Daful, A.; Baulin, V. A.; Bonet Avalos, J.; Mackie, A. D. Accurate Critical Micelle Concentrations from a Microscopic Surfactant Model. *J. Phys. Chem. B* **2011**, *115*, 3434−3443.
(14) Sanders, S. A.; Sammalkorpi, M.; Panagiotopoulos, A. Z. Atomistic Simulations of Micellization of Sodium Hexyl, Heptyl, Octyl, and Nonyl Sulfates. *J. Phys. Chem. B* **2012**, *116*, 2430−2437.
(15) Song, L. D.; Rosen, M. J. Surface Properties, Micellization, and Premicellar Aggregation of Gemini Surfactants with Rigid and Flexible Spacers. *Langmuir* **1996**, *12*, 1149−1153.
(16) Rosen, M. J.; Mathias, J. H.; Davenport, L. Aberrant Aggregation Behavior in Cationic Gemini Surfactants Investigated by Surface Tension, Interfacial Tension, and Fluorescence Methods. *Langmuir* **1999**, *15*, 7340−7346.
(17) Menger, F. M.; Littau, C. A. Gemini Surfactants: A New Class of Self-Assembling Molecules. *J. Am. Chem. Soc.* **1993**, *115*, 10083−10090.
(18) Burczyk, B.; Wilk, K. A.; Sokołowski, A.; Syper, L. Synthesis and Surface Properties of N-Alkyl-N-methylgluconamides and N-Alkyl-N-methyllactobionamides. *J. Colloid Interface Sci.* **2001**, *240*, 552−558.
(19) FitzGerald, P. A.; Carr, M. W.; Davey, T. W.; Serelis, A. K.; Such, C. H.; Warr, G. G. Preparation and Dilute Solution Properties of Model Gemini Nonionic Surfactants. *J. Colloid Interface Sci.* **2004**, *275*, 649−658.
(20) Camesano, T. A.; Nagarajan, R. Micelle Formation and CMC of Gemini Surfactants: A Thermodynamic Model. *Colloids Surf., A* **2000**, *167*, 165−177.
(21) Smit, B.; Esselink, K.; Hilbers, P. A. J.; Van Os, N. M.; Rupert, L. A. M.; Szleifer, I. Computer Simulations of Surfactant Self-Assembly. *Langmuir* **1993**, *9*, 9−11.
(22) Pool, R.; Bolhuis, P. G. Accurate Free Energies of Micelle Formation. *J. Phys. Chem. B* **2005**, *109*, 6650−6657.
(23) Shinoda, W.; DeVane, R.; Klein, M. L. Multi-Property Fitting and Parameterization of a Coarse Grained Model for Aqueous Surfactants. *Mol. Simul.* **2007**, *33*, 27−36.
(24) Shinoda, W.; DeVane, R.; Klein, M. L. Coarse-Grained Molecular Modeling of Non-Ionic Surfactant Self-Assembly. *Soft Matter* **2008**, *4*, 2454−2462.
(25) Sanders, S. A.; Panagiotopoulos, A. Z. Micellization Behavior of Coarse Grained Surfactant Models. *J. Chem. Phys.* **2010**, *132*, 114902.
(26) Levine, B. G.; LeBard, D. N.; DeVane, R.; Shinoda, W.; Kohlmeyer, A.; Klein, M. L. Micellization Studied by GPU-Accelerated Coarse-Grained Molecular Dynamics. *J. Chem. Theory Comput.* **2011**, *7*, 4135−4145.
(27) Hurter, P. N.; Scheutjens, J. M. H. M.; Hatton, T. A. Molecular Modeling of Micelle Formation and Solubilization in Block Copolymer Micelles. 1. A Self-Consistent Mean-Field Lattice Theory. *Macromolecules* **1993**, *26*, 5592−5601.
(28) Hurter, P. N.; Scheutjens, J. M. H. M.; Hatton, T. A. Molecular Modeling of Micelle Formation and Solubilization in Block Copolymer Micelles. 2. Lattice Theory for Monomers with Internal Degrees of Freedom. *Macromolecules* **1993**, *26*, 5030−5040.

(29) Linse, P. Micellization of Poly(ethylene oxide)-Poly(propylene oxide) Block Copolymers in Aqueous Solution. *Macromolecules* **1993**, *26*, 4437−4449.
(30) Ginzburg, V. V.; Chang, K.; Jog, P. K.; Argenton, A. B.; Rakesh, L. Modeling the Interfacial Tension in Oil-Water-Nonionic Surfactant Mixtures Using Dissipative Particle Dynamics and Self-Consistent Field Theory. *J. Phys. Chem. B* **2011**, *115*, 4654−4661.
(31) Thompson, R. B.; Jebb, T.; Wen, Y. Benchmarking a Self-Consistent Field Theory for Small Amphiphilic Molecules. *Soft Matter* **2012**, *8*, 9877−9885.
(32) Ben-Shaul, A.; Szleifer, I.; Gelbart, W. M. Chain Organization and Thermodynamics in Micelles and Bilayers. I. Theory. *J. Chem. Phys.* **1985**, *83*, 3597−3611.
(33) Mackie, A. D.; Panagiotopoulos, A. Z.; Szleifer, I. Aggregation Behavior of a Lattice Model for Amphiphiles. *Langmuir* **1997**, *13*, 5022−5031.
(34) Al-Anber, Z. A.; Bonet Avalos, J.; Mackie, A. D. Prediction of the Critical Micelle Concentration in a Lattice Model for Amphiphiles Using a Single-Chain Mean-Field Theory. *J. Chem. Phys.* **2005**, *122*, 104910.
(35) Guerin, C. B. E.; Szleifer, I. Self-Assembly of Model Nonionic Amphiphilic Molecules. *Langmuir* **1999**, *15*, 7901−7911.
(36) Israelachvili, J. N. *Intermolecular and Surface Forces*; Elsevier: San Diego, CA, 2011.
(37) Rosenbluth, M. N.; Rosenbluth, A. W. Monte Carlo Calculation of the Average Extension of Molecular Chains. *J. Chem. Phys.* **1955**, *23*, 356−359.
(38) Nyrkova, I. A.; Semenov, A. N. On the Theory of Micellization Kinetics. *Macromol. Theory Simul.* **2005**, *14*, 569−585.
(39) Thiagarajan, R.; Morse, D. C. Micellization Kinetics of Diblock Copolymers in a Homopolymer Matrix: A Self-Consistent Field Study. *J. Phys.: Condens. Matter* **2011**, *23*, 284109.

Chapter 5

Mean-Field Coarse-Grained Model for Poly(ethylene oxide)-Poly(propylene oxide)-Poly(ethylene oxide) Triblock Copolymer Systems

Langmuir **2015**, 31, 3596-3604.

Fabián A. García Daza, Alexander J. Colville, and Allan D. Mackie

Langmuir

Article

pubs.acs.org/Langmuir

Mean-Field Coarse-Grained Model for Poly(ethylene oxide)-Poly(propylene oxide)-Poly(ethylene oxide) Triblock Copolymer Systems

Fabián A. García Daza,[†] Alexander J. Colville,[‡] and Allan D. Mackie*,[†]

[†]Departament d'Enginyeria Química, ETSEQ, Universitat Rovira i Virgili, Avinguda dels Països Catalans 26, 43007 Tarragona, Spain

[‡]Department of Chemical Engineering, Northeastern University, 360 Huntington Avenue, Boston, Massachusetts 02115-5000, United States

ABSTRACT: The microscopic modeling of surfactant systems is of the utmost importance in understanding the mechanisms related to the micellization process because it allows for prediction and comparison with experimental data of diverse equilibrium system properties. In this work, we present a coarse-grained model for Pluronics, a trademarked type of triblock copolymer, from simulations based on a single-chain mean-field theory (SCMF). This microscopic model is used to quantify the micellization process of these nonionic surfactants at 37 °C and has been shown to be able to quantitatively reproduce experimental data of the critical micelle concentration (CMC) along with other equilibrium properties. In particular, these results correctly capture the experimental behavior with respect to the lengths of the hydrophobic and hydrophilic moieties of the surfactants for low and medium hydrophobicities. However, for the more highly hydrophobic systems with low CMCs, a deviation is found which has been previously attributed to nonequilibrium effects in the experimental data (García Daza, F. A.; Mackie, A. D. Low Critical Micelle Concentration Discrepancy between Theory and Experiment. *J. Phys. Chem. Lett.* **2014**, 5, 2027−2032).

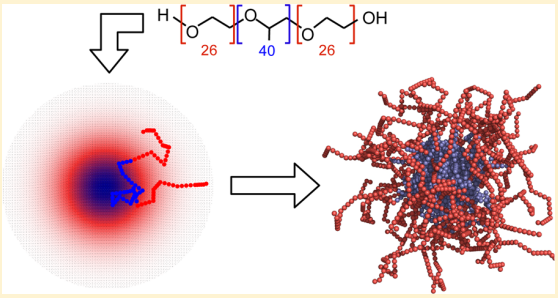

INTRODUCTION

Poly(ethylene oxide)-poly(propylene oxide)-poly(ethylene oxide) molecules, a type of linear triblock nonionic copolymer surfactant commercially available as Pluronics, Synperonics, and Poloxamers, have gained popularity for a wide variety of applications including biomedical uses. Pluronics contain a central hydrophobic poly(propylene oxide) (PPO) chain connected to two hydrophilic poly(ethylene oxide) (PEO) chains. At sufficiently high concentrations of surfactant, the molecules spontaneously self-assemble into micelles[1] and later into worm-like aggregates.[2] The broad use of Pluronics stems from their unique properties in solution as well as their customizable length and size. As a result, it is very valuable to be able to accurately predict the structure, dynamics, and properties of Pluronics under a variety of conditions such as in vivo, and this study works toward that goal.

These nonionic surfactants have been used in a wide variety of important industrial sectors including pharmaceuticals, cosmetics, oil recovery, and drug and gene nanocarriers for targeted drug delivery.[3] Some of the surfactants have been coated on the surface of nanoparticles to improve desirable qualities of the particles such as solubility, stability, and targeting.[4] Recently, medical research has shown some of the copolymers to elicit biological responses in vitro and in vivo.[5] Certain classifications of Pluronics have enhanced gene transcription,[6] improved drug potency of chemotherapeutics such as doxorubicin against cancer cells,[7] and modified other biological responses. The copolymers can be blended into polymeric matrices to form hydrogels and other drug carriers with highly specific release rates.

The self-assembly of micelles is caused by the forces of chemical equilibrium,[1] where the interactions between the hydrophilic and hydrophobic groups with the solvent and each other must all balance with any effects of entropy changes due to organization; therefore, the self-assembly of surfactants into micelles is controlled by changes in free energy. Such assembly into aggregates comes about over a small range of surfactant concentrations. This narrow range can be quantified as a useful parameter known as the critical micelle concentration (CMC),[8,9] which represents the point of spontaneous micelle aggregation from free surfactants. This transformation in conformation and aggregation exhibits changes in the physical and chemical properties of a solution such as surface tension, osmotic pressure, solubilization, detergent activity, turbidity, and conductivity.[10] The transition at the CMC is very important for applications of the product micelles as well as for models of the micellization process.

The CMC of many surfactants has been determined experimentally through a number of techniques including surface tension, light scattering, spectrophotometry, nuclear

Received: December 16, 2014
Revised: March 2, 2015
Published: March 6, 2015

DOI: 10.1021/la504884m
Langmuir 2015, 31, 3596−3604

magnetic resonance, fluorimetry, and capillary electrophoresis.[11] The micellization and subsequent experimental CMC values for Pluronic surfactants have been studied extensively; however, experimental concentrations for PEO-PPO-PEO block copolymer micelles have faced issues in reproducibility and speed.[12] Such inconsistencies and costs have pushed researchers to seek alternative methods of studying micellization.

Computer simulations have been used to predict the thermodynamic properties of only a select group of simple surfactants. Thermodynamic parameters of the micellization process for surfactants include the CMC, phase behavior, and associated free-energy change. Previous works have included the analysis of free-energy contributions,[13] molecular dynamics (MD),[14] Monte Carlo simulations (MC),[9] and mean-field models.[15]

MD and MC simulation methods have proven to be effective for the simulation of atom-based models of surfactants in the micellization process when the micelles are preassembled; however, these methods are computationally expensive for the determination of the CMC and other equilibrium properties when the systems are required to self-assemble[16] due to the slow kinetics of micelle formation. This is particularly the case for Pluronic micelles because of the large size of the surfactants.[17,18] As a result, MD and MC methods have been found to take prohibitive amounts of time to reach equilibrium even for short nonionic diblock surfactants.[14] These computational problems associated with MD and MC simulation efforts suggest that alternative techniques need to be explored in order to be able to adequately study the formation of micelles in surfactant solutions. One such technique is the single-chain mean-field theory[19] (SCMF) used in this work where a coarse-grained model similar to that in conventional molecular simulations is used; but the estimation of the equilibrium properties is simplified by solving for single chains in a mean field of the other species in the system. In this sense, the SCMF is similar to the standard self-consistent field theory[2,18,20] (SCF), where surfactants are modeled as Gaussian chains interacting with surrounding concentration fields. Nonetheless, the possibility of overlapping chains in the SCF comes from its Markovian nature, implying the absence of excluded-volume repulsions and, as a consequence, an incomplete estimation of the free energy of the system. In contrast, the SCMF considers non-Markovian connections between segments of the same chain, and thus only nonoverlapping configurations are used to estimate the free-energy contributions. The SCMF has already been successfully employed in the study of diblock surfactants[9,15] as well as gemini surfactants[21] and has been recommended specifically for the study of Pluronic micelles.[22] To our knowledge, a comprehensive list of theoretical CMCs for Pluronic micelles has not been published, and the extension of the SCMF to Pluronics in this study attempts to reach this goal.

In the current study, we have conducted a series of simulations within the SCMF to construct a coarse-grained model for the PEO-PPO-PEO surfactants in water for a temperature of 37 °C focused mainly on the reproduction of experimental CMCs. First, the details of the microscopic model and the simulation protocols are given. Afterward, the related model parameters are optimized and a series of SCMF simulations are implemented for a set of Pluronics to obtain predictions of the CMCs together with the corresponding aggregation numbers and micellar profiles. In the Results and Discussion section, the SCMF predictions are compared to the available experimental data including CMCs, aggregation numbers, and the volume fraction profiles. The results are discussed in the context of observed experimental discrepancies manifested by several authors and the deviation found in this work of the CMC between experimental and predicted data for the most hydrophobic surfactants.

MODEL AND SIMULATION METHOD

Single-Chain Mean-Field Theory. In the SCMF scheme, the intermolecular energetic contributions of surfactants belonging to an aggregate of size N are taken into account through the interactions of a single coarse-grained chain, representing the surfactant, with a set of concentration fields of solvent and surfactants while the intramolecular interactions are obtained in an exact manner. The expression for the energy in this system is given in terms of averaged energetic values of configurations of the surfactant, $\{\gamma\}$, weighted by its individual probabilities, $P[\gamma]$, and is given by

$$\langle E\rangle = N\int \mathrm{d}\gamma\, P[\gamma](U_{\mathrm{intra}}[\gamma] + U_{\mathrm{inter}}[\gamma]) \tag{1}$$

where $U_{\mathrm{intra}}[\gamma]$ is the exact internal energy of conformation γ and $U_{\mathrm{inter}}[\gamma]$ refers to the intermolecular energy related to the interactions of the configuration with the other surfactants and solvent medium and is given as

$$U_{\mathrm{inter}}[\gamma] = \frac{N-1}{2}\int \mathrm{d}\vec{r}\ \mathrm{d}\beta\ P[\beta]U_{\mathrm{inter}}[\gamma,\beta,\vec{r}] + \int \mathrm{d}\vec{r}\ c_{\mathrm{s}}(\vec{r})\ U_{\mathrm{inter}}[\gamma,\vec{r}] \tag{2}$$

The first term on the right side represents the intermolecular surfactant interactions of conformation γ with the remaining $N-1$ surfactants in the system by means of the interaction with configuration β together with its associated probability $P[\beta]$ and the corresponding energetic contribution $U_{\mathrm{inter}}[\gamma,\beta,\vec{r}] = \sum_{i,j}\epsilon_{i,j}\Phi_i(\gamma,\vec{r})c_j(\beta,\vec{r})$. The terms in this summation are the interaction parameters, $\epsilon_{i,j}$, together with the interaction volume $\mathrm{d}\vec{r}\ \Phi_i(\gamma,\vec{r})$ available for configuration γ to interact at $\vec{r}$ with the remaining conformations $\{\beta\}$ through their corresponding concentration, $c_j(\beta,\vec{r})$, for the appropriate species i, j that make up the surfactant in the coarse-grained model. The second term represents the interaction of configuration γ with the solvent medium through its concentration field $c_{\mathrm{s}}(\vec{r})$ at $\vec{r}$ by means of $U_{\mathrm{inter}}[\gamma,\vec{r}] = \Sigma_i\ \epsilon_{i,\mathrm{s}}\Phi_i(\gamma,\vec{r})$ with respect to the coarse-grained solvent and surfactant−solvent interaction parameters $\epsilon_{i,\mathrm{s}}$. The terms given in eq 2 account only for attractive intermolecular interactions, for which the repulsive terms are included by means of steric hard-core repulsions given by the following volume-filling constraint

$$\phi_{\mathrm{s}}(\vec{r}) + N\sum_i \langle\phi_i^{\mathrm{exc}}(\vec{r})\rangle = 1 \tag{3}$$

which means that all regions of physical space are occupied either by solvent or surfactant molecules by means of the corresponding volume fractions $\phi_{\mathrm{s}}(\vec{r})$ and $\langle\phi_i^{\mathrm{exc}}(\vec{r})\rangle$ respectively, with this last term representing the correct excluded-volume contributions. The term inside the angular brackets in eq 3 comes from the single-chain values of $\phi_i^{\mathrm{exc}}(\gamma,\vec{r})$, interpreted as the total physical volume fraction of species i of conformation γ at $\vec{r}$ that cannot be accessed by solvent or other surfactant molecules, weighted by the individual

DOI: 10.1021/la504884m
Langmuir 2015, 31, 3596−3604

probabilities giving the average excluded-volume fraction of the surfactant

$$\langle \phi_i^{\mathrm{exc}}(\vec{r})\rangle = \int \mathrm{d}\gamma\ P[\gamma]\ \phi_i^{\mathrm{exc}}(\gamma, \vec{r}) \tag{4}$$

Similarly, the concentration fields of the surfactant monomers can be predicted in general from

$$\langle c_i(\vec{r})\rangle = \int \mathrm{d}\gamma\ P[\gamma]\ c_i(\gamma, \vec{r}) \tag{5}$$

From here, the determination of the associated probabilities $P[\gamma]$ is given by a minimization of the system free energy $\langle F\rangle = \langle E\rangle - T\langle S\rangle$, where the entropy contains the configurational surfactant contributions and the solvent translational entropy

$$\langle S\rangle = -Nk \int \mathrm{d}\gamma\ P[\gamma] \log P[\gamma] - k \int \mathrm{d}\vec{r}\ c_s(\vec{r}) \log \phi_s(\vec{r}) \tag{6}$$

with k and T as Boltzmann's constant and the temperature of the system, respectively. Minimizing $\langle F\rangle$ from $\delta\langle F\rangle/\delta\ P[\gamma] = 0$ subject to the volume-filling constraint in eq 3 with the inclusion of Lagrange multipliers $\lambda(\vec{r})$, which in turn can be found from the evaluation of $\delta\langle F\rangle/\delta c_s(\vec{r}) = 0$, provides the individual probabilities in equilibrium

$$P[\gamma] = \frac{\mathrm{e}^{-H_N[\gamma]/kT}}{Q} \tag{7}$$

where Q is the partition function of the system ensuring the normalization of the associated probabilities. Finally, from eq 7 we can establish the SCMF Hamiltonian $H_N[\gamma]$ associated with conformation γ that contains the intramolecular and intermolecular interactions for the corresponding surfactant with the surrounding fields. In addition, intermolecular steric repulsions are also derived from the Lagrange multipliers definition with constraints in eq 3. The analytical expression of the Hamiltonian is found to be

$$\begin{aligned} H_N[\gamma] \approx\ & U_{\mathrm{intra}}[\gamma] + (N-1) \int \mathrm{d}\vec{r} \sum_{i,j} \epsilon_{i,j} \Phi_i(\gamma, \vec{r}) \langle c_j(\vec{r})\rangle \\ & + \int \mathrm{d}\vec{r} \sum_i \epsilon_{i,s} \Phi_i(\gamma, \vec{r})\ c_s(\vec{r}) \\ & - kT \int \mathrm{d}\vec{r} \frac{\log \phi_s(\vec{r})}{v_s} \sum_i \phi_i^{\mathrm{exc}}(\gamma, \vec{r}) \end{aligned} \tag{8}$$

where v_s is the volume of the solvent molecules. From the set of nonlinear equations given in eqs 3−5, 7, and 8, it is possible to determine the individual probabilities $P[\gamma]$ in eq 7 and hence the equilibrium properties for aggregates of size N and densities and concentrations through eq 5. In the SCMF approach the necessary inputs are the set of conformations $\{\gamma\}$ of a single surfactant in the simulation box with the estimation of the concentrations $c_i(\gamma, \vec{r})$, excluded-volume fractions $\phi_i^{\mathrm{exc}}(\gamma, \vec{r})$, and interaction volume fractions $\Phi_i(\gamma, \vec{r})$ for each conformation.

To relate the SCMF to the full micellization process, it is necessary to link the properties of the single micelles to the macroscopic system. This is achieved by calculating the standard chemical potentials of free chains, μ_1^0, and those from micelles of size N, μ_N^0, and substituting them into the well-known equilibrium condition between free surfactants in solution and micelles of an arbitrary size, namely,[1]

$$\frac{X_N}{N} = \left(X_1 e^{-(\mu_N^0 - \mu_1^0)/kT}\right)^N \tag{9}$$

where X_N and X_1 are the concentrations of aggregated and free surfactants, respectively. The calculation of the standard chemical potential in the SCMF can be achieved in terms of the following expression[23] that has been used in earlier studies related to the prediction of equilibrium properties for surfactant systems in solvent media such as poly(ethylene oxide) alkyl ethers[15] and more recently a series of nonionic gemini surfactants,[21]

$$\frac{\mu_N^0 - \mu_1^0}{kT} \approx -\log\left(\frac{V}{N} \frac{\sum_\gamma \mathrm{e}^{-H_N[\gamma]/kT} W[\gamma]}{\sum_\gamma \mathrm{e}^{-H_1[\gamma]/kT} W[\gamma]}\right) \tag{10}$$

where $H_1[\gamma]$ is the Hamiltonian for surfactants in the bulk solution, V is the volume of the simulation box, and $W[\gamma]$ is the statistical weight associated with the Rosenbluth and Rosenbluth algorithm to generate nonoverlapping chain conformations.[24]

Simulation Protocols. In this work, the Pluronic block copolymers are modeled as linear chains composed of two kinds of beads with the same diameter σ; the first one represents the hydrophilic CH_2CH_2O groups, and the second one represents the hydrophobic $CH(CH_3)CH_2O$ groups. The choice of the same-sized EO and PO units is similar to that employed by other research groups for coarse-grained models of Pluronic surfactants.[25,26] The distance between the centers of two consecutive beads is taken to be σ. The chain stiffness, as indicated by the number of Kuhn segments, has been included by using rigid sections of four consecutive monomers in the case of PO and five monomers in the case of EO species[27,28] whereas the joints between the segments are free to rotate (e.g., Figure 1). The intermolecular interactions in eq 8 are modeled

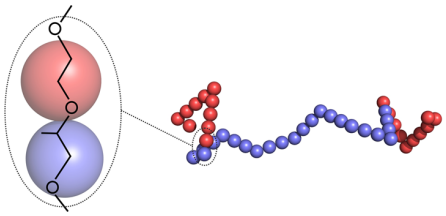

Figure 1. Coarse-grained model for Pluronic L44 $EO_{10}PO_{23}EO_{10}$. Right: Typical self-avoiding conformation generated by the Rosenbluth and Rosenbluth method. Left: Detailed coarse-grained extrapolation in the SCMF technique employed in this work, where red and blue beads represents EO and PO groups, respectively.

by means of square well potentials with a hard core repulsive interaction up to σ and then an attractive well up to r_{int}. The interaction radius r_{int} has been adjusted to a value of 1.62σ for all species composing the surfactant in order to have a coordination number of 26 as was used in previous models.[15,21] This gives a volume for attractive interactions of $v_{\mathrm{int}} = {}^4/_3\pi(r_{\mathrm{int}}^3 - \sigma^3)$ for each monomer. Three independent intermolecular interactions have been used, namely, EO−solvent, PO−solvent, and EO−PO with their corresponding numerical values $\epsilon_{\mathrm{EO,S}}$, $\epsilon_{\mathrm{PO,S}}$, and $\epsilon_{\mathrm{EO,PO}}$. With these assumptions for the interactions and species, we can state the specific complete nonlinear set of equations in order to describe the equilibrium properties. In the first place, the indexes in the whole equation system are reduced to i, j = EO, PO, and in the Hamiltonian in eq 8, we

DOI: 10.1021/la504884m
Langmuir 2015, 31, 3596−3604

have to relate interaction parameter $\epsilon_{i,j}$ to the analogous Flory–Huggins parameter in the symmetric case $\chi_{i,j} = \chi_{j,i}$ by means of $\epsilon_{i,j} = kT\chi_{i,j}/z$, where $z = 26$ is the coordination number. This choice will affect the excluded-volume term in the SCMF Hamiltonian. For more details, see ref 15. The Hamiltonian can be written now as

$$H_N[\gamma] \approx U_{\text{intra}}[\gamma] + (N-1)\frac{kT}{z}\int d\vec{r}\sum_{i\neq j}\chi_{i,j}\Phi_i(\gamma,\vec{r})\langle c_j(\vec{r})\rangle + \frac{kT}{z}\int d\vec{r}\sum_i \chi_{i,s}\Phi_i(\gamma,\vec{r})\, c_s(\vec{r}) - kT\int d\vec{r}\frac{\log \phi_s(\vec{r})}{v_s}\sum_i \phi_i^{\text{exc}}(\gamma,\vec{r}) \tag{11}$$

Once the relevant intermolecular interactions and the species describing the surfactant and solvent in the coarse-grained model are defined, the SCMF equations can be solved. To do so, we divide the procedure into two stages. In the first stage, a set of nonoverlapping conformations $\{\gamma\}$ are randomly generated according to the Rosenbluth and Rosenbluth algorithm[24] in a simulation box of volume V, and all of the intrinsic properties such as concentrations $c_i(\gamma,\vec{r})$, excluded-volume fractions $\phi_i^{\text{exc}}(\gamma,\vec{r})$, interaction volume fractions $\Phi_i(\gamma,\vec{r})$, and intramolecular energy $U_{\text{intra}}[\gamma]$ are calculated for every conformation γ. In the second stage, the SCMF system of equations is solved self-consistently, that is, from calculated fields $\langle c_i(\vec{r})\rangle$ and $\langle \phi_i^{\text{exc}}(\vec{r})\rangle$ in eqs 4 and 5; calculations of $\phi_s(\vec{r})$, $H_N[\gamma]$, and the corresponding probability $P[\gamma]$ can be realized by means of eqs 3, 7, and 11, respectively, again enabling the calculation of the mean fields over the calculated probabilities, making the whole process self-consistent. Once the structural characteristics are assigned, only the intermolecular interaction parameters $\chi_{\text{EO,S}}$, $\chi_{\text{PO,S}}$, and $\chi_{\text{EO,PO}}$ need to be determined. For this purpose, we have performed an error minimization of the difference between predicted and experimental CMCs by means of the gradient method. To capture the overall CMC dependence with respect to the numbers of EO and PO monomers, we have chosen to optimize the experimental CMCs for three Pluronics surfactants, two in which the number of EO units is smaller than the corresponding number of PO units L44 and L64, and F87, a surfactant which has significantly more EO than PO units.

Optimization Procedure. To find the optimal values of the Flory–Huggins parameter, we take as initial estimates, $\chi_{\text{EO,S}} = 0.4$ and $\chi_{\text{PO,S}} = 2.0$ from ref 29 and $\chi_{\text{EO,PO}} = 0.006$ from refs 30 and 31. These parameters are obtained directly or indirectly by fitting to experimental data. To continue, we start by considering the minimization of the function

$$F[\chi] = \frac{1}{n}\sum_{i=1}^{n}\frac{(\text{CMC}_i^{\text{sim}} - \text{CMC}_i^{\text{exp}})^2}{s_i^2} \tag{12}$$

where $n = 3$ is the total number of data points, which in our case consists of the experimental CMCs for Pluronics L44, L64, and F87 represented by $\text{CMC}_i^{\text{exp}}$ with its associated uncertainty s_i^2 and the SCMF predictions $\text{CMC}_i^{\text{sim}}$. The minimization procedure can be done via the gradient method[32] by determining in an iterative scheme the optimal values from

$$\chi_j^{\text{new}} = \chi_j^{\text{old}} - \alpha\nabla_j F[\chi^{\text{old}}] \tag{13}$$

where α is the step size and index j refers to the energy parameter to be adjusted. In particular, from eq 12 we can state

$$\nabla_j F[\chi] = \frac{2}{3}\sum_{i=1}^{3}\frac{(\text{CMC}_i^{\text{sim}} - \text{CMC}_i^{\text{exp}})}{s_i^2}\frac{\partial \text{CMC}_i^{\text{sim}}}{\partial\chi_j} \tag{14}$$

To find the derivatives in the last equation, we can start from the definition of CMC^{sim} adopted in this work, namely, that the CMC is taken based on the micelle of size M with a minimum standard chemical potential, $\log \text{CMC}_i^{\text{sim}} = \min((\mu_N^0 - \mu_1^0)/kT) = ((\mu_M^0 - \mu_1^0)/kT)$. The relevant derivatives for this specific case are then $\partial\text{CMC}_i^{\text{sim}}/\partial\chi_j = \text{CMC}_i^{\text{sim}}(\partial/\partial\chi_j)[(\mu_M^0 - \mu_1^0)/kT]$. To develop the partial derivative, we made use of the relation between the standard chemical potentials in the SCMF theory given in eq 10

$$\frac{\partial \text{CMC}_i^{\text{sim}}}{\partial\chi_j} \approx -\frac{\text{CMC}_i^{\text{sim}}}{kT}\left[\frac{\sum_\gamma e^{-H_1[\gamma]/kT}/W[\gamma]}{Q_1}\frac{\partial H_1[\gamma]}{\partial\chi_j} - \frac{\sum_\gamma e^{-H_M[\gamma]/kT}/W[\gamma]}{Q_M}\frac{\partial H_M[\gamma]}{\partial\chi_j}\right] \tag{15}$$

where $Q_1 = \sum_\gamma e^{-H_1[\gamma]/kT}/W[\gamma]$ and $Q_M = \sum_\gamma e^{-H_M[\gamma]/kT}/W[\gamma]$ are the unbiased partition functions for free and aggregated chains, respectively. From the SCMF Hamiltonian in eq 11 and assuming that the concentration fields and the probabilities remain invariant with respect to the interaction parameters close to the minimum in $F[\chi]$, we can find in general the following set of partial derivatives

$$\begin{aligned}
\frac{\partial H_N[\gamma]}{\partial\chi_{\text{EO,PO}}} &\approx \frac{\partial U_{\text{intra}}[\gamma]}{\partial\chi_{\text{EO,PO}}} + (N-1)\frac{kT}{z}\int d\vec{r}\,[\Phi_{\text{EO}}(\gamma,\vec{r})\langle c_{\text{PO}}(\vec{r})\rangle + \Phi_{\text{PO}}(\gamma,\vec{r})\langle c_{\text{EO}}(\vec{r})\rangle],\\
\frac{\partial H_N[\gamma]}{\partial\chi_{\text{EO,S}}} &\approx \frac{kT}{z}\int d\vec{r}\;\Phi_{\text{EO}}(\gamma,\vec{r})\, c_s(\vec{r}),\\
\frac{\partial H_N[\gamma]}{\partial\chi_{\text{PO,S}}} &\approx \frac{kT}{z}\int d\vec{r}\;\Phi_{\text{PO}}(\gamma,\vec{r})\, c_s(\vec{r})
\end{aligned} \tag{16}$$

This set of equations can be exactly determined in the SCMF simulations for every surfactant chosen to adjust the energy parameters. With this, the fitting procedure for the energy parameters can be done by means of eq 13. To this end, the partial derivatives in eq 14 must be solved through the values given in eq 15 which in turn can be evaluated from the SCMF results obtained in order to calculate the expressions in eqs 16.

The coarse-grained dimensions as well as the optimized energy interaction values are presented in Table 1 upon completion of the fitting process. As can be seen, the final values are close to the parameters derived from experiment, thus validating the physical model that we have used in our study. Although the differences from the initial guesses are small, they do have a significant effect on the CMC values, and

Table 1. Coarse-Grained Structural and Energy Specifications

diameter (σ)	1.0
bond length (σ)	1.0
interaction radius (σ)	1.62
EO–PO interaction parameter ($\chi_{\text{EO,PO}}$)	0.006
EO–S interaction parameter ($\chi_{\text{EO,S}}$)	0.5
PO–S interaction parameter ($\chi_{\text{PO,S}}$)	2.1

DOI: 10.1021/la504884m
Langmuir 2015, 31, 3596–3604

Table 2. Physical Properties and Predictions for Pluronics Block Copolymers under Study

				aggregation number		CMC [mol/L]	
polymer	MW	m	$2n$	pred.	exp.	pred.	exp.[a]
L44	2200	23	20	145(1)		$4.00(0.01) \times 10^{-3}$	3.6×10^{-3}
L64	2900	30	26	187(7)	37[b]	$3.55(0.04) \times 10^{-4}$	4.8×10^{-4}
P65	3400	29	36	145(12)	11−21[c]	$0.84(0.01) \times 10^{-3}$	2.94×10^{-3} [j]
F68	8400	29	152	33(1)	22[d]	$18.9(0.5) \times 10^{-3}$	0.48×10^{-3}, $>8.33 \times 10^{-3}$ [k]
P84	4200	43	34	279(10)	44−54[e]	$3.87(0.05) \times 10^{-6}$	71×10^{-6}
P85	4600	40	52	218(4)	57(16)[f]	$2.55(0.03) \times 10^{-5}$	6.5×10^{-5}
F87	7700	40	122	66(10)		$1.77(0.04) \times 10^{-4}$	0.91×10^{-4}
F88	11 400	39	208	46(11)	17[g]	$6(1) \times 10^{-4}$	2.5×10^{-4}
F98	13 000	45	236	40(9)		$1.51(0.05) \times 10^{-4}$	0.77×10^{-4}
P105	6500	56	74	318(17)		$1.54(0.05) \times 10^{-7}$	62×10^{-7} [l]
F127	12 600	65	200	120(16)	145[h]	$1.3(0.3) \times 10^{-7}$	28.0×10^{-7}
F108	14 600	50	266	34(10)	13(3)[i]	$2.0(0.3) \times 10^{-5}$	2.2×10^{-5}

[a]Taken from ref 35. Measured through a pyrene solubilization technique at 37 °C unless otherwise specified. [b]From ref 36 at 37.5 °C using SANS. [c]In the range of 36−40 °C from ref 37, obtained from SLS. [d]At 54 °C from ref 21 cited in ref 38. [e]Based on SANS in the range of 35−40 °C from ref 39. [f]From light scattering and centrifugation at 37 °C from ref 38. [g]At 40 °C from ref 40. [h]From ref 28 at 35 °C based on SANS. [i]At 37 °C from ref 38. [j]Using the dye solubilization technique at 36 °C from ref 41. [k]Taken from ref 41 at 40 °C. [l]Taken from ref 42 at 37 °C.

the optimization procedure gives an important improvement in the final fit. The success of the optimization can be observed by a decrease of the objective function in eq 12 from 47.2 to 2.7 when going from the initial guesses, $\chi_{PO,S} = 2.001$, $\chi_{EO,S} = 0.48$, and $\chi_{EO,PO} = 0.006$ (these values were used after a preliminary study rather than the aforementioned literature Flory−Huggins parameters), to the fitted values of $\{\chi_{i,j}\}$, respectively, indicating that the difference between the experimental and SCMF results is close to the reported experimental error, assumed to be 30% in all cases. For the optimization procedure and final results, a series of simulations were performed where space was discretized into concentric layers separated by a distance $\delta = 0.8\sigma$ for shorter surfactants with less than 100 monomers, whereas for longer surfactants we assume $\delta = 1.4\sigma$. In all simulations, the radius of the first layer is taken to be 2δ to improve the statistics. This choice provides 1D spherical symmetry where the only coordinate is the radial distance to the center of the simulation box and is supported by experimental evidence using small-angle neutron scattering (SANS),[33] static light scattering (SLS), and dynamic light scattering (DLS),[34] which suggest a spherical shape for micellar aggregates of Pluronic systems for concentrations close to and above the CMC. Depending on the Pluronic under study, we used simulation boxes with dimensions of between $40 \times 40 \times 40$ and $100 \times 100 \times 100$ in units of the beads diameter σ. Between 5 and 10 million conformations $\{\gamma\}$ were generated for each Pluronic, and the simulations were run on 12-core Intel machines and 24-core and 32-core AMD machines with RAM memory of 64, 32, and 128 GB, respectively.

RESULTS AND DISCUSSION

In Table 2, the physical properties of Pluronics $EO_nPO_mEO_n$ at a temperature of 37 °C are given, including the molecular weight MW, the number of PO and EO units (m and $2n$, respectively), the predicted CMCs, and aggregation number values of the SCMF from this work together with available experimental data. The CMCs reported in this work follow the expected behavior with respect to the length of the hydrophobic PO units. An increase in the PO length increases the repulsive interaction between the surfactant and solvent medium, causing a decrease in the free energy of micellization, thus yielding a lower CMC together with an increase in the aggregation number. The increase in aggregation number occurs as additional PO monomers increase the available volume to be occupied by the hydrophobic species that can be accommodated in the core of the micelle. Both of these results are exemplified for Pluronics F68, F88, and F127, where the hydrophilic contribution is almost constant (Table 2). In the reverse case, an increase in the number of EO units while the number of PO units remains constant was shown to increase the solubility of the Pluronics in the solvent medium, leading to a gradual increase in the CMC. The increase in the number of EO units leads to higher repulsive interactions between hydrophilic units in the corona of the micelle, forcing the formation of micelles with smaller aggregation numbers. These expected trends were evidenced within all three of the subdivisions of Table 2.

From an analysis of the aggregation numbers presented in Table 2, clear differences can be observed between the experimental and SCMF values. In some cases, the experimental data reported by different groups are similar, for instance, for P85 where Mortensen and Pedersen[33] using SANS reported aggregation numbers of 37−78 in the range of 20−40 °C, similar to the value 57(16) given by Kabanov et al.[38] at 37 °C and the values 37−55 based on SANS with a concentration of 1−5% at 40 °C as reported by Goldmints et al.[43] Nonetheless, in other cases the aggregation numbers derived from experimental measurements can be highly variable. For example, Yang et al.[36] reported a value of 37 for a temperature of 37.5 °C in the case of L64; however, Wu et al.[44] using SANS reported an aggregation number of 69(7) at 35 °C, in contrast to Almgren et al.[45] who reported a value of 19 for 40 °C. These values are contrary to the expected increase in aggregation number with an increase in temperature. A similar situation is presented in the case of copolymer F127, where Wanka et al.[37] and Mortensen[28] presented aggregation numbers of 82 and 145, respectively, for a temperature of 35 °C. In the case of F108, Alexandridis et al.[8] reported aggregation numbers of 43−61 between 35 and 40 °C, in contrast to the value of 13 for a temperature of 37 °C reported by Kabanov et al.,[38] giving a

DOI: 10.1021/la504884m
Langmuir 2015, 31, 3596−3604

difference of more than 3-fold. These contrasts between reported values may be due to the type of experiment and the model considered to describe the physical properties of the micelles, such as in the case of results given by DLS and SLS and discussed by Nolan et al.[34] and Yang et al.[36] Despite these differences between experimental values, the SCMF predictions are in general much larger. This difference may be due to the model being too simple to correctly capture the correct fine balance between entropic and enthalpic factors. It may also be due to the approximations used in the SCMF itself. For example, in this work spherical symmetry is assumed for the micelles without fluctuations, which may affect the micelle free energy of formation by small fractions of kT. Although small compared to the formation of the micelle, these approximations may affect the preferred aggregation number.[9,15] Despite this, the model is able to correctly reproduce qualitative trends such as a decrease in the aggregation number with an increase in the EO units while maintaining the PO units relatively constant as in the cases of P84, P85, F87, and F88, which has also been observed experimentally for P104 and F108 by Alexandridis et al.,[8] P85, F87, and F88 by Mortensen and Brown,[46] and P103, P104, and P105 by Nolan et al.[34] Moreover, an increase in the aggregation number with the number of PO units while EO monomers remain constant is also observed, as in the case of P65, L64, and P84, and has been experimentally reported by Booth and Attwood[47] for a series of Pluronic surfactants.

A comparison between experimental CMC values and those determined with SCMF from Table 2 can be found in Figure 2.

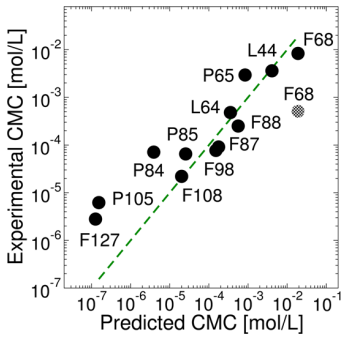

Figure 2. Experimental CMC versus theoretical values predicted in the SCMF scheme for Pluronics studied in this work. The dashed line represents the ideal scenario where experimental and theoretical values match exactly. Error bars in the theoretical data are smaller than the diameter of the filled circles.

In general, good quantitative agreement between experimental and predicted values can be observed. For CMCs above 10^{-6} mol/L, most data points are close to the dashed line, indicating excellent quantitative agreement between the SCMF predictions and the experimental values, giving a high level of confidence in the model results. Nevertheless, this is not the case for F68, where two values are given. This is mainly because of the discrepancy between the experimental data reported by Batrakova et al.[35] and Alexandridis et al.[41] In the latter, the reported CMC is 8.33×10^{-3} mol/L above 40 °C and 11.9×10^{-3} mol/L for 33 °C, which establishes an interval for our target of 37 °C and supports the idea that in the case of F68 the CMC for a temperature of 37 °C could be near 10^{-2} mol/L, which is the same order of magnitude as the value reported in this work, although contrary to the value reported by Batrakova et al.,[35] which is on the order of 10^{-4} mol/L. This is also supported when comparing the experimental CMCs for a selection of Pluronics in Table 2 with the same PO weight but a varying EO presence. For example, (i) in the case of P105 and F108, an increase close to 3 times the EO content results in an increase in the CMC within the same proportion and (ii) similar to P85 and F88, where the hydrophilic units increase 4 times as well as the corresponding CMCs, an extrapolation to the case of L64 and F68 where the PEO increases 5 times leads one to expect a similar tendency in the CMC value. Another exception in Figure 2 is that of the most hydrophobic Pluronics P105 and F127 together with P84, which reveal underpredicted values by more than 1 order of magnitude with respect to experimental data.

To understand the nature of such discrepancies, we have selected a series of Pluronics with hydrophilic units in a specific range which ensures that the changes in the CMC are not significantly affected by the increase or decrease in EO units in this interval. In this case, the effect of the hydrophobic PO length on the CMC can be better appreciated. Specifically, we have considered those Pluronics that contain EO units in the range of 20−74. The CMC dependence when hydrophobic PPO units increase in both experimental and predicted values with the SCMF can be observed in Figure 3. Below 40 PO

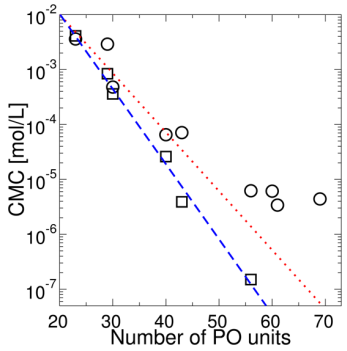

Figure 3. CMC dependence with respect to the hydrophobic length of Pluronics $EO_nPO_mEO_n$ for short head lengths ($20 \leq 2n \leq 74$). Empty circles refer to experimental data given in Table 2 with the exception of the three most hydrophobic copolymers (P103, P104, and P123, respectively), which are not included in the table but are given in ref 35. Empty squares are SCMF predictions together with the best fit represented by the dashed blue lines; the red dotted line is the best fit for the four highest CMC experimental points.

units, there is a good agreement between predictions and experimental values that corresponds to high CMCs; however, above a value of 43 PO units (Pluronic P84), a strong deviation from the linear behavior in the experimental data is observed and is not predicted in the results of the model implemented in this work.

Following this procedure, we can also analyze those surfactants with a total number of hydrophilic units EO in the range of 122−266, also including the experimental CMCs reported by Alexandridis et al.[41] in a range of temperature between 35 and 40 °C with the exception of F68 (n = 29), whose lowest temperature is 33 °C. The resulting graph is shown in Figure 4.

As can be observed, the experimental values reported in ref 41 for CMCs above 10^{-5} mol/L are close to the predictions of this work. However, on increasing the hydrophobic units above 50 PO units, a deviation between experiment and SCMF is

DOI: 10.1021/la504884m
Langmuir 2015, 31, 3596−3604

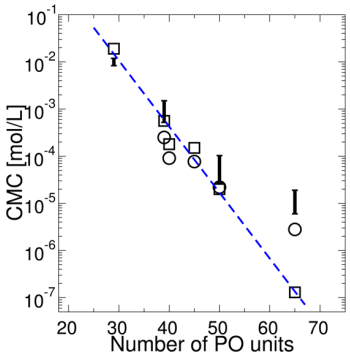

Figure 4. CMC dependence with respect to the hydrophobic length of Pluronics $EO_nPO_mEO_n$ for long head groups ($122 \leq 2n \leq 266$). Empty circles refers to experimental data reported in ref 35, which is given in Table 2; bars are the CMCs in a temperature range between 35 and 40 °C given in ref 41 and empty squares are the SCMF predictions together with the best fit represented by the dashed blue line.

found. This break in the logarithmic CMC behavior with respect to a large number of hydrophobic units is similar to the experimental reports for diblock copolymers[48] and gemini surfactants.[49] From a theoretical point of view, free-energy models do not predict such a deviation.[13] Also, recent simulations using grand canonical MC simulations for nonionic surfactants exhibit the usual exponential decrease, rejecting the collapse of the hydrophobic block as an explanation for such a deviation.[50] Indeed, our previous work on gemini surfactants suggests that this deviation occurs because the experimental results are not true equilibrium values due to the long time scales found for these systems.[21] These nonequilibrium effects would explain the discrepancy between experimental P105 and F127 CMCs in comparison to the values reported in this work. In the case of P84, the CMC values are higher and are not expected to be affected by equilibration issues. However, the experimental data for the CMC of P84 is clearly inconsistent with that of P85, where despite having a larger number of PO and lower EO units, which is expected to give a lower CMC, P84 has a larger CMC. This suggests that the discrepancy between experimental and SCMF values for P84 may come from experimental issues different from nonequilibrium effects.

Although aggregates conformed by real conformations as in the usual MD, MC, or DPD simulations cannot be obtained from the SCMF results, it is possible to construct schematic diagrams of the aggregates for surfactants under study from the set of the configurations with the highest probability $\{P[\gamma]\}$. In particular, a micelle for Pluronic F68 is shown in Figure 5, where the snapshot is generated for visualization purposes and should not be interpreted as a real aggregate. As can be observed, the micelles have a large concentration of hydrophobic PO units in its core, which decreases with respect to distance from the center of the micelle. This core is surrounded by a nonuniform shell of hydrophilic EO units that starts to increase from the center of the micelle, reaching a maximum value, and then decays smoothly with distance. A quantitative description of the density profiles of the micelle is presented in Figure 6.

In all cases under study, similar behavior in the equilibrium state volume fraction profile has been observed where the shape of the PO and EO volume fractions depends on the corresponding number of units. The number of PO and EO

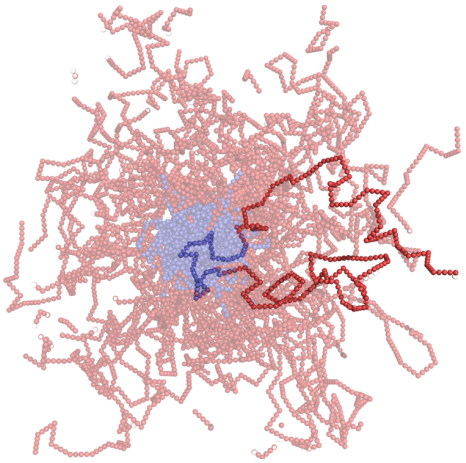

Figure 5. Cross-sectional scheme of an aggregate for Pluronic F108 ($EO_{133}PO_{50}EO_{133}$) for an aggregation number of 34. The conformation with the highest probability is highlighted, and the remaining configurations are half of the next 33 most probable conformations. Red beads represent the PEO units forming the corona, and the PPO units are represented in blue.

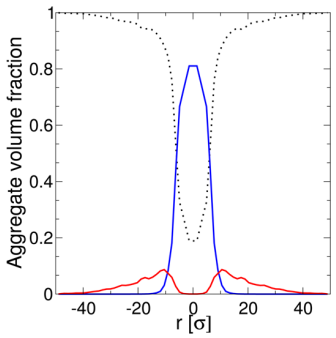

Figure 6. Volume fraction profile for the most stable micelle in the case of Pluronic F108 with an aggregation number of $N = 34$. Blue lines represents the PO percentage inside and outside the micelle, red lines refers to the volume fraction of EO units, and black dotted lines are related to the corresponding profile of the solvent.

units of a chosen Pluronic system was shown to modify the solvent profile which is found to be between 20 and 30% in the center of the micelle. This hydration in the center of the micelle has been reported in several simulation works[2,17,18,20,22] and is also derived from the analysis of SANS data for a variety of Pluronics: P85 with a concentration of 5% was found to contain a water content in the core between 60 and 10% for a range of temperature from 31.4 to 40 °C,[43] P84 and P104 at temperatures of 35 and 45 °C in concentrations of 2.6 and 4.2%, respectively,[39] contained water content fractions in the core of 20 and 6%, and L64 at a temperature of 37.5 °C and a concentration of 2.5% was reported to have fractions of solvent in the core of 40 and 80% in the corona.[36]

CONCLUSIONS

We have presented a coarse-grained model for Pluronic systems for 37 °C based on SCMF simulations. The estimates of our model for the CMC are found to be in excellent agreement with experimental data for a wide range of surfactants. On the other hand, the SCMF aggregation numbers are generally much larger than the ones reported from experiments. However, it is

DOI: 10.1021/la504884m
Langmuir 2015, 31, 3596−3604

difficult to extract the aggregation numbers from the experiments, and significant discrepancies between different groups can be found in the literature. Our findings reveal that an increase in the number of PO units with EO units held relatively constant yields a decrease in the CMC and an increase in the aggregation number. Increasing the hydrophilic EO units results in a slight increase in the CMC and a decrease in the aggregation number. This overall scenario agrees qualitatively with the available experimental and theoretical reports. From a comparison between our CMC predictions and available experimental data, we find evidence of a deviation from the expected exponential trend in the case of experimental CMCs for the most hydrophobic Pluronics. On the basis of our confidence of the CMCs predicted in this work when compared to experimental data down to 10^{-6} mol/L and previous SCMF and MC studies, we suggest that this deviation can be explained as a consequence of nonequilibrium effects in the experiments.

AUTHOR INFORMATION

Corresponding Author

*E-mail: allan.mackie@urv.cat.

Notes

The authors declare no competing financial interest.

ACKNOWLEDGMENTS

F.A.G.D. acknowledges financial support from URV through his Ph.D. scholarship.

REFERENCES

(1) Israelachvili, J. N. *Intermolecular and Surface Forces*; Elsevier: San Diego, CA, 2011.
(2) Linse, P. Micellization of Poly(ethylene oxide)-Poly(propylene oxide) Block Copolymers in Aqueous Solution. *Macromolecules* **1993**, *26*, 4437−4449.
(3) Park, T., Cohen, S., Langer, R. 1994 U.S. Patent. Controlled Drug Delivery Using Polymer/Pluronic Blends; US5330768 A1.
(4) Batrakova, E. V.; Kabanov, A. V. Pluronic block copolymers: Evolution of drug delivery concept from inert nanocarriers to biological response modifiers. *J. Controlled Release* **2008**, *130*, 98−106.
(5) Murhammer, D. W.; Goochee, C. F. Scaleup of Insect Cell Cultures: Protective Effects of Pluronic F-68. *Nat. Biotechnol.* **1988**, *12*, 1411−1418.
(6) Sriadibhatla, S.; Yang, Z.; Gebhart, C.; Alakhov, V. Y.; Kabanov, A. Transcriptional activation of gene expression by pluronic block copolymers in stably and transiently transfected cells. *Mol. Ther.* **2006**, *13*, 804−813.
(7) Alakhova, D. Y.; Zhao, Y.; Li, S.; Kabanov, A. V. Effect of Doxorubicin/Pluronic SP1049C on Tumorigenicity, Aggressiveness, DNA Methylation and Stem Cell Markers in Murine Leukemia. *PLoS One* **2013**, *8*, e72238.
(8) Alexandridis, P.; Nivaggioli, T.; Hatton, T. A. Temperature Effects on Structural Properties of Pluronic P104 and F108 PEO-PPO-PEO Block Copolymer Solutions. *Langmuir* **1995**, *11*, 1468−1476.
(9) Mackie, A. D.; Panagiotopoulos, A. Z.; Szleifer, I. Aggregation Behavior of a Lattice Model for Amphiphiles. *Langmuir* **1997**, *13*, 5022−5031.
(10) Rangel-Yagui, C. O.; Pessoa, A.; Tavares, L. C. Micellar solubilization of drugs. *J. Pharm. Pharm. Sci.* **2005**, *8*, 147−163.
(11) Loh, W. In *Encyclopedia of Surface and Colloid Science*, 2nd ed. Somasundaran, P., Ed.; Taylor & Francis: Boca Raton, FL, 2006; Vol. *2*, pp 1014−1025.
(12) Goldmints, I.; Holzwarth, J. F.; Smith, K. A.; Hatton, T. A. Micellar Dynamics in Aqueous Solutions of PEO-PPO-PEO Block Copolymers. *Langmuir* **1997**, *13*, 6130−6134.
(13) Camesano, T. A.; Nagarajan, R. Micelle Formation and CMC of Gemini Surfactants: A Thermodynamic Model. *Colloids Surf., A* **2000**, *167*, 165−177.
(14) Levine, B. G.; LeBard, D. N.; DeVane, R.; Shinoda, W.; Kohlmeyer, A.; Klein, M. L. Micellization Studied by GPU-Accelerated Coarse-Grained Molecular Dynamics. *J. Chem. Theory Comput.* **2011**, *7*, 4135−4145.
(15) Gezae Daful, A.; Baulin, V. A.; Bonet Avalos, J.; Mackie, A. D. Accurate Critical Micelle Concentrations from a Microscopic Surfactant Model. *J. Phys. Chem. B* **2011**, *115*, 3434−3443.
(16) Carbone, P.; Avendaño, C. Coarse-grained methods for polymeric materials: enthalpy- and entropy-driven models. *WIREs Comput. Mol. Sci.* **2014**, *4*, 62−70.
(17) Bedrov, D.; Smith, G. D.; Yoon, J. Structure and Interactions in Micellar Solutions: Molecular Simulations of Pluronic L64 Aqueous Solutions. *Langmuir* **2007**, *23*, 12032−12041.
(18) de Bruijn, V. G.; van den Broeke, L. J. P.; Leermakers, F. A. M.; Keurentjes, J. T. F. Self-Consistent-Field Analysis of Poly(ethylene oxide)-Poly(propylene oxide)-Poly(ethylene oxide) Surfactants: Micellar Structure, Critical Micellization Concentration, Critical Micellization Temperature, and Cloud Point. *Langmuir* **2002**, *18*, 10467−10474.
(19) Ben-Shaul, A.; Szleifer, I.; Gelbart, W. M. Chain organization and thermodynamics in micelles and bilayers. I. Theory. *J. Chem. Phys.* **1985**, *83*, 3597−3611.
(20) Hurter, P. N.; Scheutjens, J. M. H. M.; Hatton, T. A. Molecular Modeling of Micelle Formation and Solubilization in Block Copolymer Micelles. 1. A Self-Consistent Mean-Field Lattice Theory. *Macromolecules* **1993**, *26*, 5592−5601.
(21) García Daza, F. A.; Mackie, A. D. Low Critical Micelle Concentration Discrepancy between Theory and Experiment. *J. Phys. Chem. Lett.* **2014**, *5*, 2027−2032.
(22) Bedrov, D.; Ayyagari, C.; Smith, G. D. Multiscale Modeling of Poly(ethylene oxide)-Poly(propylene oxide)-Poly(ethylene oxide) Triblock Copolymer Micelles in Aqueous Solution. *J. Chem. Theory Comput.* **2006**, *2*, 598−606.
(23) Al-Anber, Z. A.; Bonet Avalos, J.; Mackie, A. D. Prediction of the Critical Micelle Concentration in a Lattice Model for Amphiphiles Using a Single-Chain Mean-Field Theory. *J. Chem. Phys.* **2005**, *122*, 104910.
(24) Rosenbluth, M. N.; Rosenbluth, A. W. Monte Carlo Calculation of the Average Extension of Molecular Chains. *J. Chem. Phys.* **1955**, *23*, 356−359.
(25) De Nicola, A.; Kawakatsu, T.; Milano, G. A Hybrid Particle-Field Coarse-Grained Molecular Model for Pluronics Water Mixtures. *Macromol. Chem. Phys.* **2013**, *214*, 1940−1950.
(26) Nawaz, S.; Carbone, P. Coarse-Graining Poly(ethylene oxide)-Poly(propylene oxide)-Poly(ethylene oxide) (PEO-PPO-PEO) Block Copolymers Using the MARTINI Force Field. *J. Phys. Chem. B* **2014**, *118*, 1648−1659.
(27) Aharoni, S. M. On entanglements of flexible and rodlike polymers. *Macromolecules* **1983**, *16*, 1722−1728.
(28) Mortensen, K. Structural studies of aqueous solutions of PEO - PPO - PEO triblock copolymers, their micellar aggregates and mesophases; a small-angle neutron scattering study. *J. Phys.: Condens. Matter* **1996**, *8*, A103−A124.
(29) Malcolm, G. N.; Rowlinson, J. S. The thermodynamic properties of aqueous solutions of polyethylene glycol, polypropylene glycol and dioxane. *Trans. Faraday Soc.* **1957**, *53*, 921−931.
(30) Bailey, A.; Salem, B.; Walsh, D.; Zeytountsian, A. The interfacial tension of poly(ethylene oxide) and poly(propylene oxide) oligomers. *Colloid Polym. Sci.* **1979**, *257*, 948−952.
(31) Helfand, E.; Tagami, Y. Theory of the interface between immiscible polymers. *J. Polym. Sci., Part B: Polym. Lett.* **1971**, *9*, 741−746.
(32) Press, W. H., Teukolsky, S. A., Vetterling, W. T., Flannery, B. P. Numerical Recipes. *The Art of Scientific Computing*, 3rd ed.; Cambridge University Press: New York, 2007; pp 515−520.

DOI: 10.1021/la504884m
Langmuir 2015, 31, 3596−3604

(33) Mortensen, K.; Pedersen, J. S. Structural study on the micelle formation of poly(ethylene oxide)-poly(propylene oxide)-poly-(ethylene oxide) triblock copolymer in aqueous solution. *Macromolecules* **1993**, *26*, 805−812.
(34) Nolan, S. L.; Phillips, R. J.; Cotts, P. M.; Dungan, S. R. Light Scattering Study on the Effect of Polymer Composition on the Structural Properties of PEO-PPO-PEO Micelles. *J. Colloid Interface Sci.* **1997**, *191*, 291−302.
(35) Batrakova, E.; Lee, S.; Li, S.; Venne, A.; Alakhov, V.; Kabanov, A. Fundamental Relationships Between the Composition of Pluronic Block Copolymers and Their Hypersensitization Effect in MDR Cancer Cells. *Pharm. Res.* **1999**, *16*, 1373−1379.
(36) Yang, L.; Alexandridis, P.; Steytler, D. C.; Kositza, M. J.; Holzwarth, J. F. Small-Angle Neutron Scattering Investigation of the Temperature-Dependent Aggregation Behavior of the Block Copolymer Pluronic L64 in Aqueous Solution. *Langmuir* **2000**, *16*, 8555−8561.
(37) Wanka, G.; Hoffmann, H.; Ulbricht, W. Phase Diagrams and Aggregation Behavior of Poly(oxyethylene)-Poly(oxypropylene)-Poly-(oxyethylene) Triblock Copolymers in Aqueous Solutions. *Macromolecules* **1994**, *27*, 4145−4159.
(38) Kabanov, A. V.; Nazarova, I. R.; Astafieva, I. V.; Batrakova, E. V.; Alakhov, V. Y.; Yaroslavov, A. A.; Kabanov, V. A. Micelle Formation and Solubilization of Fluorescent Probes in Poly(oxyethylene-b-oxypropylene-b-oxyethylene) Solutions. *Macromolecules* **1995**, *28*, 2303−2314.
(39) Liu, Y.; Chen, S.-H.; Huang, J. S. Small-Angle Neutron Scattering Analysis of the Structure and Interaction of Triblock Copolymer Micelles in Aqueous Solution. *Macromolecules* **1998**, *31*, 2236−2244.
(40) Alexandridis, P.; Hatton, T. A. Poly(ethylene oxide)-poly-(propylene oxide)-poly(ethylene oxide) block copolymer surfactants in aqueous solutions and at interfaces: thermodynamics, structure, dynamics, and modeling. *Colloids Surf., A* **1995**, *96*, 1−46.
(41) Alexandridis, P.; Holzwarth, J. F.; Hatton, T. A. Micellization of Poly(ethylene oxide)-Poly(propylene oxide)-Poly(ethylene oxide) Triblock Copolymers in Aqueous Solutions: Thermodynamics of Copolymer Association. *Macromolecules* **1994**, *27*, 2414−2425.
(42) Kozlov, M. Y.; Melik-Nubarov, N. S.; Batrakova, E. V.; Kabanov, A. V. Relationship between Pluronic Block Copolymer Structure, Critical Micellization Concentration and Partitioning Coefficients of Low Molecular Mass Solutes. *Macromolecules* **2000**, *33*, 3305−3313.
(43) Goldmints, I.; von Gottberg, F. K.; Smith, K. A.; Hatton, T. A. Small-Angle Neutron Scattering Study of PEO-PPO-PEO Micelle Structure in the Unimer-to-Micelle Transition Region. *Langmuir* **1997**, *13*, 3659−3664.
(44) Wu, G.; Chu, B.; Schneider, D. K. SANS Study of the Micellar Structure of PEO/PPO/PEO Aqueous Solution. *J. Phys. Chem.* **1995**, *99*, 5094−5101.
(45) Almgren, M.; Bahadur, P.; Jansson, M.; Li, P.; Brown, W.; Bahadur, A. Static and dynamic properties of a (PEO-PPO-PEO) block copolymer in aqueous solution. *J. Colloid Interface Sci.* **1992**, *151*, 157−165.
(46) Mortensen, K.; Brown, W. Poly(ethylene oxide)-poly(propylene oxide)-poly(ethylene oxide) triblock copolymers in aqueous solution. The influence of relative block size. *Macromolecules* **1993**, *26*, 4128−4135.
(47) Booth, C.; Attwood, D. Effects of block architecture and composition on the association properties of poly(oxyalkylene) copolymers in aqueous solution. *Macromol. Rapid Commun.* **2000**, *21*, 501−527.
(48) Burczyk, B.; Wilk, K. A. Sokołowski, A.; Syper, L. Synthesis and Surface Properties of N-Alkyl-N-methylgluconamides and N-Alkyl-N-methyllactobionamides. *J. Colloid Interface Sci.* **2001**, *240*, 552−558.
(49) Rosen, M. J.; Mathias, J. H.; Davenport, L. Aberrant Aggregation Behavior in Cationic Gemini Surfactants Investigated by Surface Tension, Interfacial Tension, and Fluorescence Methods. *Langmuir* **1999**, *15*, 7340−7346.
(50) Nikoubashman, A.; Panagiotopoulos, A. Z. Communication: Effect of solvophobic block length on critical micelle concentration in model surfactant systems. *J. Chem. Phys.* **2014**, *141*, 041101.

DOI: 10.1021/la504884m
Langmuir 2015, 31, 3596−3604

Chapter 6

Micellar Kinetic Exchange of Pluronic Surfactants by a Dynamic Single-Chain Mean-Field Method

To be submitted to *Macromolecules*.

6.1 Introduction

The ability of amphiphilic block copolymer systems to self-aggregate into well-defined geometric structures is of paramount importance in a wide range of technological applications including: foaming [1] and emulsion [2] processes, stabilization of nanoparticles [3], and, transport and controlled release of drugs [4, 5]. This behavior emerges when the concentration of copolymers in a selective solvent exceeds a value known as the critical micelle concentration, CMC, where diverse physicochemical system properties like surface tension experience a significant change. Although the equilibrium properties of copolymer systems have been extensively studied from experimental, theoretical and simulation frameworks, there is a lack of information related to the dynamic and kinetic behavior. Research on the kinetic mechanisms have been carried out by a broad number of experimental techniques including temperature jump [6], fluorescence correlation spectroscopy [7] and time-resolved small-angle neutron scattering [8, 9, 10, 11, 12, 13] (TR-SANS). Experiments carried out by these techniques are considered to be near the equilibrium regime where expulsion and insertion of single monomers in micellar aggregates is observed to be dominant when comparing with micellar fusion and fission as has been manifested theoretically for block copolymer surfactants [14] based on the analysis of the Aniansson and Wall mechanism [15, 16]. In particular, recent experiments for triblock poly(ethylene oxide)-poly(propylene oxide)-poly(ethylene oxide) copolymer (PEO-PPO-PEO) surfactants, also known as Pluronics, revealed that fusion and fission rates are six orders of magnitude less than insertion and expulsion events [17].

Even under equilibrium conditions detailed information of the microscopic behavior of chains involving exchange processes is still incomplete. For instance, TR-SANS experimental data of experimental correlation functions obtained from scattering intensities has been contradictory interpreted as indicating both a collapse [8, 9, 18] or a stretching [12] of the insoluble blocks conforming the surfactant copolymers when leaving the micellar aggregates. Although theoretical studies [14, 15, 16] can identify the main mechanisms responsible for the exchange processes, explicit microscopic information is still missing. This motivates the need for computer simulations given their ability to directly access detailed information at a microscopic level. In this scenario, Monte Carlo (MC) [19, 20] and Brownian dynamics [21] simulations for diblock copolymers have been implemented to study the exchange of surfactants in the presence of micelles through a series of correlation functions. Molecular dynamics (MD) [22] was used to determine the effect of aggregates size on the monomer exchange mechanism for a short nonionic diblock surfactant. Also, the exchange of monomers was studied by dissipative particle dynamics (DPD) [23] simulations for a set of diblock surfactants where the expulsion process of single monomers is identified as the dominant mechanism. Notwithstanding, lattice space discretization inhibits a quantitative comparison with real experimental systems for certain stochastic MC simulations [19], and, difficulties to reach equilibrium prohibits a satisfactory analysis even for the case of short coarse-grained surfactants [22]. This overall situation and the absence of a reliable model for block copolymer systems, that, together with an efficient simulation technique, are capable to provide dynamic information in an equilibrium regime, call for alternative methods. In particular, in this chapter we consider the single-chain mean-field (SCMF) theory [24] which defines a central chain whose intermolecular interactions are described by mean molecular fields, thereby, all macroscopic properties can be formulated in terms of the central chain contributions. The sampling chains used in the SCMF simulations can be constructed in a self-avoiding way at any molecular level of detail,

which differs from the standard self-consistent field [25] scheme where overlapping conformations are used thus affecting the estimation of the system's free energy. Static equilibrium properties calculated from the SCMF formalism are obtained by minimization of the free energy, and have been reported for nonionic short surfactants [26, 27, 28], block copolymer systems [29] and have successfully been quantitatively compared with experimental data [30, 29], standard MC [27, 28] and MD [26] simulations. Although a considerable number of studies on surfactant systems in equilibrium based on SCMF calculations have been reported, only a few of them are devoted to the dynamic properties of these systems, as reported in the case of protein adsorption on surfaces [31, 32] where the dynamics is determined by solution of combined SCMF and diffusion equations. However, the explicit evolution of the particles composing the system is lost due to the static nature of the sampling conformations used to solve the SCMF equations. This is in contrast to alternative SCMF simulations for polymer systems where explicit dynamics of independent sampling chains are followed by the evolution of the mean molecular fields [33]. As far as we know, there is a lack in comparisons of simulation studies for copolymer surfactants with experimental quantities related to kinetic exchange processes in equilibrium, in particular the expulsion of monomers from micellar aggregates, and this chapter aims to achieve this goal for a series of Pluronic surfactants.

In the present chapter we have carried out a series of simulations based on a dynamic SCMF scheme for a series of Pluronic systems within a coarse-grained model developed in a recent study [29]. Theoretical aspects related with the SCMF formalism in equilibrium and dynamic regime are introduced, and the coarse-grained details are presented under the dynamic version of the SCMF. The autocorrelation function associated to the kinetic expulsion process is defined to provide information on the expulsion rate constants for the systems under study. In the Results and Discussion section the predictions obtained in this chapter are compared to experimental data when available. In particular, the expulsion rate constants, hydrophobic radius of gyration and angle between blocks are examined. The results are discussed in terms of the conformational changes experienced by the hydrophobic blocks when diffusing across the micellar region, which differ from the commonly accepted in analog copolymer systems of collapsed [14, 8, 9] or stretched [12] configurations.

6.2 Computational Methodology

The starting point is to consider a central chain that interacts with the surrounding external mean molecular fields whilst its intramolecular interactions are explicitly known. All thermodynamic quantities are determined through the chain probability density functions, *pdf*, where the individual contributions of the single chain α, belonging to the set of configurations $\{\alpha\}$, are averaged with its corresponding probability $P[\alpha]$. The *pdf* is obtained through the SCMF formalism by considering the free energy of a system of N chains in a solvent medium at a temperature T,

$$F = \langle U \rangle - T\langle S \rangle \tag{6.1}$$

where the first term corresponds to the mean energy of the system given in terms of the single-chain individual contributions, $\langle U \rangle = N \int d\alpha P[\alpha] \left(U_{intra}(\alpha) + U_{inter}(\alpha) \right)$, with $U_{intra}(\alpha)$ and $U_{inter}(\alpha)$ as the intramolecular and intermolecular contributions respectively, the latter being dependent on the average concentrations of the mean-fields of the remaining $N-1$ chains and the solvent molecules. The second term includes the configu-

rational and translational entropy of chains and solvent, $\langle S\rangle = -kN\int d\alpha P[\alpha]\log P[\alpha] - k\int d\vec{r}c_s(\vec{r})\log\phi_s(\vec{r})$, respectively; k is Boltzmann's constant, $\vec{r}$ is a position vector, $c_s(\vec{r})$ is the concentration of solvent molecules at point $\vec{r}$, and, $\phi_s(\vec{r}) = v_s c_s(\vec{r})$ is the solvent volume fraction with v_s as the volume of a solvent molecule. Intermolecular energetic contributions are attractive by definition whereas the repulsive terms are included by an incompressibility condition

$$\phi_s(\vec{r}) + N\langle\phi(\vec{r})\rangle = 1 \tag{6.2}$$

where $\langle\phi(\vec{r})\rangle = \int d\alpha P[\alpha]\phi(\alpha,\vec{r})$ with $\phi(\alpha,\vec{r})$ as the total volume fraction of conformation α at position $\vec{r}$. The former equation includes the intermolecular excluded volume interactions, that is, a volume region in space that can only be filled by either solvent or surfactant molecules. Determination of the single-chain probabilities, and the solvent concentration profile, is made by minimizing the free energy functional in Eq. 6.1 subject to the volume-filling constraint given in Eq. 6.2 by the inclusion of a set of Lagrange multipliers and a direct evaluation of the functional derivatives $\delta F/\delta P[\alpha] = 0$, and, $\delta F/\delta c_s(\vec{r}) = 0$. Once the minimization procedure has been completed, the *pdf* is found to follow a Boltzmann distribution

$$P[\alpha] = \frac{e^{-H[\alpha]/kT}}{Q} \tag{6.3}$$

where Q is a constant which ensures the normalization of the central chain probabilities, $\int d\alpha P[\alpha] = 1$. The explicit form of the SCMF Hamiltonian depends on the level of detail in the surfactant and solvent models and therefore the number of interactions taken into account which will directly affect the number of concentration mean-fields existing in the Hamiltonian.

After the SCMF equations have been established, the dynamics of the system can be evaluated by local displacements of the set of sampling chains $\{\alpha\}$. The local displacement are accepted or rejected with a certain probability which depends on the change of energy between the trial and the original moves. This procedure is similar to other mean-field simulations [33] for polymer systems. For a finite set of independent chains representing the surfactant $\{\alpha\}_o$, the probability for a chain to change its configurational state α_o to a new one α_n is

$$p(\alpha_o \to \alpha_n) = \min\left(1, e^{-(H[\alpha_n]-H[\alpha_o])/kT}\right) \tag{6.4}$$

where $H[\alpha_n]$ is the SCMF Hamiltonian calculated for the trial state. Once the probability in Eq. 6.4 has been evaluated for every sampling chain, the new solvent and chain concentration mean-fields are determined by solution of Eqs. 6.2 and 6.3. The procedure is repeated until the mean-fields agree with the ones determined from the equilibrium formalism. In addition, to recovering the same equilibrium state of our previous methodology it is also possible to follow the temporal evolution of the system, and, in consequence, the dynamic properties of the system under study can be examined. In the following section we present the details of the coarse-grained copolymer surfactant model chosen in this chapter to study the kinetics of the exit of surfactants in micellar aggregates and the corresponding SCMF approximations.

6.2.1 Simulation Protocols

In this chapter, the Pluronic copolymers are modeled by a coarse-grained model from a recent work [29] where hydrophobic PO, $CH(CH_3)CH_2O$, and hydrophilic EO, CH_2CH_2O, groups are represented by beads of the same

diameter σ. The stiffness of the chain is introduced by a series of Kuhn segments consisting of four and five consecutive PO and EO beads, respectively. The distance between consecutive beads is taken as σ. Interactions are considered by square well potentials centered on each of the beads with inner and outer radius σ and 1.62σ respectively. Only unlike intermolecular interactions between EO and PO, EO and solvent, and, PO and solvent are considered, where the energetic well depth fitted for each interaction at a temperature of 37 °C has values $\epsilon_{EO,PO} = 0.006\, kT/z$, $\epsilon_{EO,s} = 0.5\, kT/z$ and $\epsilon_{PO,s} = 2.1\, kT/z$, respectively, $z = 26$ is the coordination number. Due to the selection of two classes of beads to represent Pluronic chains together with the presence of the solvent medium, three fundamental concentration fields appear in the SCMF Hamiltonian [29],

$$\begin{aligned} H[\alpha] \approx\ & U_{intra}(\alpha) + (N-1)\epsilon_{EO,PO} \int d\vec{r}\,(\Phi_{EO}(\alpha,\vec{r})\langle c_{PO}(\vec{r})\rangle + \Phi_{PO}(\alpha,\vec{r})\langle c_{EO}(\vec{r})\rangle) \\ & + \epsilon_{EO,s} \int d\vec{r}\,\Phi_{EO}(\alpha,\vec{r}) c_s(\vec{r}) + \epsilon_{PO,s} \int d\vec{r}\,\Phi_{PO}(\alpha,\vec{r}) c_s(\vec{r}) \\ & - kT \int d\vec{r}\,\frac{\log \phi_s(\vec{r})}{v_s}\,(\phi_{EO}(\alpha,\vec{r}) + \phi_{PO}(\alpha,\vec{r})) \end{aligned} \tag{6.5}$$

The first term corresponds to the internal energy of configuration α which is taken as $\epsilon_{EO,PO}$ times the number of nonconsecutive and nonrepeating EO and PO beads belonging to the chain found within a distance lesser than 1.62σ. The second, third and fourth terms relate the intermolecular interactions of the chain with the surrounding external fields of the $N-1$ chains and solvent by interaction of the available space for units EO, $\int d\vec{r}\Phi_{EO}(\alpha,\vec{r})$, and PO, $\int d\vec{r}\Phi_{PO}(\alpha,\vec{r})$, with the mean-field concentration fields of PO, $\langle c_{PO}(\vec{r})\rangle$, EO, $\langle c_{EO}(\vec{r})\rangle$, and solvent, $c_s(r)$ species and their corresponding interaction parameters. At the same time, these fields can be calculated from the SCMF averages $\langle c_{PO}(\vec{r})\rangle = \int d\alpha P[\alpha] c_{PO}(\alpha,\vec{r})$ and $\langle c_{EO}(\vec{r})\rangle = \int d\alpha P[\alpha] c_{EO}(\alpha,\vec{r})$ where the arguments inside the integrals are the individual concentrations of each conformation α for the different moieties. Finally, the fifth term is interpreted as the intermolecular repulsive interactions arising from the inclusion of the incompressibility condition in Eq. 6.2 by means of the incorporation of a set of Lagrange multipliers in the free energy minimization, for more details see ref 29. In this scheme the incompressibility condition includes the individual EO and PO mean volume fractions $\langle \phi_{EO}(\vec{r})\rangle = \int d\alpha P[\alpha]\phi_{EO}(\alpha,\vec{r})$, and, $\langle \phi_{PO}(\vec{r})\rangle = \int d\alpha P[\alpha]\phi_{PO}(\alpha,\vec{r})$, respectively. Basically, Eq. 6.2 is now

$$\phi_s(\vec{r}) + N\,(\langle \phi_{EO}(\vec{r})\rangle + \langle \phi_{PO}(\vec{r})\rangle) = 1 \tag{6.6}$$

Once the SCMF Hamiltonian and the incompressibility condition have been identified, we proceed to perform, with aid of Eq. 6.4, a series of independent MC moves over the configurational set of sampling chains $\{\alpha\}$, recalculating the mean fields by solution the SCMF equations 6.3, 6.5 and 6.6 at every MC cycle according to the procedure introduced in the preceding section. To ensure a Rouse-like motion of the surfactants [33], the moves to displace the chains are taken to be end-bond rotation or crankshaft depending on whether the chosen segment is an end segment or not [35].

As already mentioned, this simulation scheme provides an opportunity to study the dynamic behavior of Pluronic chains at a fixed temperature. In this chapter we concentrate on the study of the kinetic exchange of monomers in micellar aggregates in the equilibrium regime. The simulation box is divided into concentric spherical shells of fixed width between 1.9σ and 2.1σ in the case of short and long Pluronics, respectively, and in consequence Eqs. 6.5 and 6.6 are reduced to a one dimensional radial coordinate according to the discretization scheme. The

exchange of monomer chains between the bulk solution and the micellar aggregate can be explicitly studied by formulation of a series of autocorrelation functions based on the direct monitoring of the evolution of the chains that initially reside in the micelle. Explicitly, we define the following autocorrelation function to follow the initially aggregated sampling chains,

$$F(t) = \frac{f(t) - f(\infty)}{f(0) - f(\infty)} \tag{6.7}$$

where $f(t)$ is the fraction of labeled chains at simulation time t that were identified as forming part of the micelle at time $t = 0$. Initially, all chains in the interior of the micelle are marked, subsequently, when a labeled chain leaves the interior of the micellar core it stops contributing to the temporal fraction $f(t)$. However, if the chain returns to the core of the micelle, it will contribute once more to the overall fraction. This autocorrelation function is close to the one used in TR-SANS experiments for n-alkyl-PEO [11] and poly(ethylene-*alt*-propylene)-poly(ethylene oxide) [10] systems where exchange kinetics in equilibrium is investigated by monitoring the behavior of deuterated and nondeuterated copolymers in micelles on mixing. This is similar to our simulation scheme where no physicochemical alterations to the system are induced.

It is important to observe that in the dynamic SCMF simulations any time dependent property will be given in terms of the MC cycles, which is the natural simulation time step. To connect these cycles with physical time units we perform a series of simulations for free chains moving in the bulk solution. This can be done by taking $N = 1$ in Eqs. 6.5 and 6.6 and following the evolution of the independent set of free moving chains by Eq. 6.4. This analysis leads to a diffusive behavior of the sampling chains and we can determine the average displacement, $\langle \Delta \vec{r}(t)^2 \rangle$, of the center of mass of the chains with respect to their original positions with time in order to obtain the diffusion coefficient in the dynamic SCMF scheme

$$D_{SCFM} = \lim_{t \to \infty} \frac{\langle \Delta \vec{r}(t)^2 \rangle}{6t} \tag{6.8}$$

where the square displacement is taken as $\sum_{i=1}^{N_{\{\alpha\}}} \left(\vec{r}_i(t)^2 - \vec{r}_i(0)^2 \right) / N_{\{\alpha\}}$ being $N_{\{\alpha\}}$ the number of sampling chains $\{\alpha\}$ used in our simulations. It is important to note, on the one hand, that all the lengths in the SCMF simulations are given in terms of the bead size diameter σ, so any position vector and in consequence the displacement term in Eq. 6.8 is given in units of σ^2. On the other hand, the temporal variable in the above equation is in cycle units in the same way as in the case of the autocorrelation function in Eq. 6.7. The diffusion constant calculated from the above equation is thus given in units of σ^2/cycles. A relation between the time involved in the experiments and the simulation time in the SCMF simulations can be established when considering that displacement of the chain monomers can be related to a diffusion coefficient, D, and a time variable, t_{exp}, comparable to the timescales in experiments in the same way as in Eq. 6.8. This means that if we consider the mean displacement, $\langle \Delta \vec{r}(t)^2 \rangle$, measured in our simulations to be close to the expected in experiments we can relate the two diffusion equations by this common quantity giving as a result a relation between the time measured in the simulations with the timescale of the experiments by relation of both diffusion coefficients, $t_{exp} = t\, D_{SCMF}/D$. To obtain the diffusion coefficient we consider the Stokes-Einstein expression for spherical particles, $D = kT/(6\pi\eta a)$ where $kT \approx 4.28 \times 10^{-21} \mathrm{kg\,m^2 s^{-2}}$ at a temperature of 37°C, the viscosity of the solvent $\eta = 6.91 \times 10^{-4} \mathrm{kg\,m^{-1} s^{-1}}$ that in this case is water, and, the size of the diffusive particle, a, given in units of σ which is taken as the average hydrodynamic radius of the chains in the free regime. The values of D, evaluated directly from the Stokes-Einstein, are found to be close to available experimental data. For

instance, we find for Pluronic P85 ($EO_{13}PO_{40}EO_{13}$) a diffusion coefficient of 9.9×10^{-11} m^{2}s^{-1} which is close to the reported value of 3.7×10^{-11} m^{2}s^{-1} in ref 36, in the case of P104 ($EO_{27}PO_{61}EO_{27}$) we obtained a value of 9.1×10^{-11} m^{2}s^{-1} which is similar to the interval $3.7 - 4.5 \times 10^{-11}$ ms^{-1} reported in ref 37 for temperatures between 35 and 40 °C, and, a value of 9.8×10^{-11} m^{2}s^{-1} was calculated for P123 ($EO_{19}PO_{69}EO_{19}$) being comparable to the value in the interval $2.8 - 3.3 \times 10^{-11}$ ms^{-1} reported from ref 38 at a temperature of 25 °C. In this chapter we have adopted the value $\sigma = 0.5$ nm from the literature [39] which is similar to the one employed in recent MD simulations for a series of Pluronics in a coarse-grained model [40].

In both cases, corresponding to independent sampling chains in a spherical concentration field of an aggregate ($N >> 1$) and in a homogeneous field for a bulk solution ($N = 1$), simulations were performed in simulation boxes with volumes between $(70\sigma)^3$ and $(95\sigma)^3$ where periodic boundary conditions were included. A total of 500 sampling chains, $N_{\{\alpha\}}$, were used for every Pluronic surfactant. Simulations were performed on 12-core Intel machines and 24-core AMD machines with RAM memories of 64 and 32 GB, respectively.

6.3 Results and Discussion

Evaluation of the autocorrelation function given in Eq. 6.7 for Pluronics, EOnPOmEOn, reveals in general a relaxation behavior coming from the expulsion process of monomers in equilibrium micelles. In all cases, the function $F(t)$ was found to follow a decreasing trend that in a logarithmic scale reveals the presence of more than one relaxation mechanism as can be observed in Fig. 6.1 for Pluronic $EO_{13}PO_{30}EO_{13}$. In there, conversion from the simulation cycles to the physical time scales is made by relating the diffusion coefficients obtained by our simulations $D_{SCMF}(L64) = 0.0023\sigma^2$/cycle and $D(L64) = 1.29 \times 10^{-10}$m^{2}s^{-1} as discussed in the previous section. Particularly, two fast exchange and one dominant exponential decreasing processes were identified, the

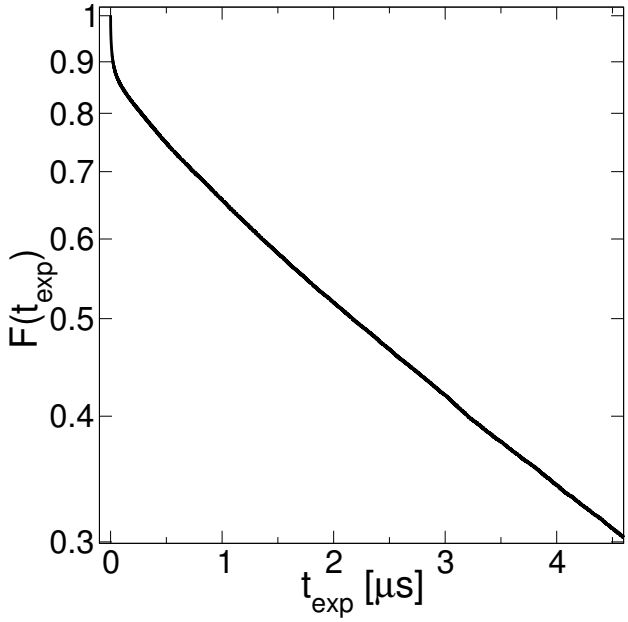

Figure 6.1: Autocorrelation function in the logarithmic scale for Pluronic L64 ($EO_{13}PO_{30}EO_{13}$) obtained from analysis of the data obtained from dynamical SCMF simulations.

latter being related to the single relaxation process, $\sim \exp(-kt)$, formulated by Halperin and Alexander [14] where k is the expulsion rate constant which is found to be independent of the micellar size N. In Table 6.1 the physical parameters of the Pluronics studied in this chapter are presented: the molecular weight MW, the total number of PO and EO units m and 2n, respectively, as well as the temperature, T, used in the experiments together with the equilibrium aggregation numbers, N, of the selected systems, and both the experimental and predicted expulsion rate constants k_{exp} and k_{SCMF}, respectively. Experimental values are taken from Ref 41 and references therein unless otherwise indicated. As can be observed, our calculations reveal a significant

Table 6.1: Physical characteristics and predictions for the Pluronic systems, EOnPOmEOn, studied in this chapter.

Pluronic	MW	m	2n	T (°C)	N	k_{exp} (s^{-1})	k_{SCMF} (s^{-1})
L44	2200	23	20		145[a]		$4.8(0.1) \times 10^5$
L64	2900	30	26	40	40	2.0×10^5	$1.9(0.9) \times 10^5$
P85	4600	40	52	37.7	40	8.4×10^4	$4.1(0.6) \times 10^4$
P84	4200	43	34	27	40	6.7×10^4	$1.3(0.5) \times 10^4$
P104	5900	61	54	24.2	50	3.8×10^3	$0.23(0.08) \times 10^3$
P123	5750	69	40	21.4	40	1.5×10^3	$0.27(0.08) \times 10^3$

[a] Taken from Ref 29 at 37 °C using SCMF simulations in equilibrium regime.

decrease in the values of the expulsion rate constants with the increase of the insoluble PO units. An increase in the hydrophobic units of all surfactants produces a growth in the energetic barrier seen by a copolymer in the interior of the micelle. The escape of the surfactant from the interior of the micelle to the bulk solution is slowed and the expulsion process is found to be not diffusion controlled as expected. In addition, changes in the number of hydrophilic units, EO, only moderately affect the values of the expulsion rates as has also been reported from experiments. This implies that an increase in the width of the soluble micellar shell does not significantly affect the height of the energetic barrier to be overcome by the copolymers.

This overall behavior is observed for all Pluronic systems in our calculations, and is supported by the experimental data in Table 6.1. In particular, the exit rate constants for the Pluronics show a progressive decrease of three orders of magnitude when the number of hydrophobic PO units is increased from 23 to 69. Although a very good quantitative agreement with the experimental data is found for L64, the experimental rate constant decreases more slowly and for the largest Pluronics, P104 and P123, that only decreases by two orders of magnitude resulting in a difference of one order of magnitude with respect to our model calculations.The nature of this discrepancy between our calculations and experimental data can be due to several factors. Firstly, in our simulations the interaction parameters in the Hamiltonian in Eq. 6.5 were fitted to predict properties at a temperature of 37 °C, however, experimental data cover in general a range of temperature below the one used in our calculations. Secondly, expulsion rate constants are usually obtained from the experimental fast relaxation times, τ_1 and the surfactant concentration, c, combined with the Aniansson and Wall [15, 16] relation of the exit rate constant, $\tau_1^{-1} = (k_{exp}/N)(N/\delta N^2 + X)$, where δN^2 is the variance of the aggregation number distribution and $X = (c - CMC)/CMC$. This means that values of k_{exp} require a precise knowledge of the aggregation numbers and the corresponding deviation in their distribution. In particular, when determining N

several discrepancies can be found in the literature: for L64 aggregation numbers between 19 and 69 have been reported [42, 43] for temperatures of 40 and 35 °C, respectively. Similarly, dynamic and static light scattering measurements reveal aggregation numbers of 53 and 30 for P104 depending on the experimental technique [38] at a temperature of 25°C. In the same way, for P123 values of 99 and 120 were reported at the same temperature.

Changes in the conformations of the surfactants entering or leaving the micelles can be followed from the ensemble averages corresponding to the temporal behavior of the independent chains as presented in Fig. 6.2 where the radius of gyration, $\langle R_g(r)\rangle$, of the chains for the different surfactants has been calculated with respect to the radial distance, r, from the center of the equilibrium micelle. Both quantities are given in units of σ. On average, the surfactants change from their original conformation in the center of the micelle as they

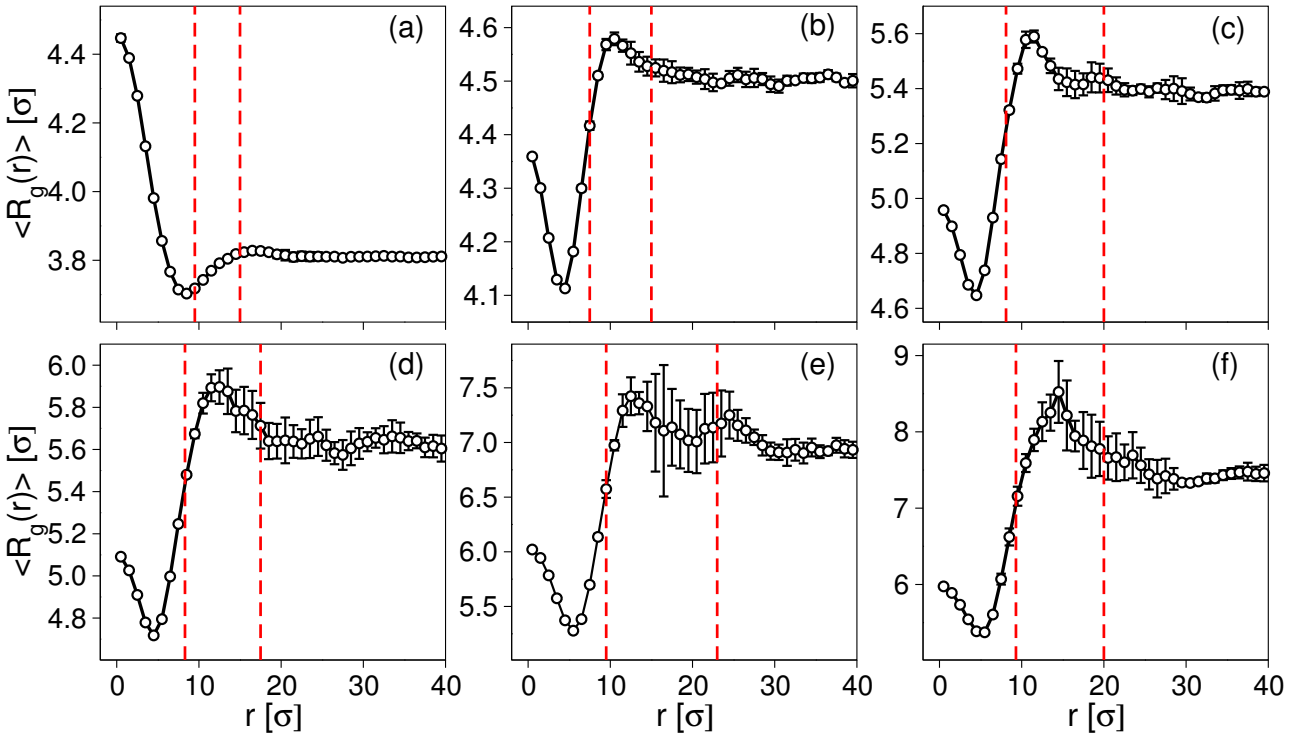

Figure 6.2: Average radius of gyration for surfactants as a function of distance from the center of the micelle for Pluronic (a) L44, (b) L64, (c) P85, (d) P84, (e) P104 and (f) P123. Vertical dashed lines represent the approximate extension of the hydrophobic micelle core and the head groups.

approach the PO-EO interface. This change is represented by a decrease in the radius of gyration of their PO blocks to later an even larger increase as the copolymers approach the EO-solvent interface where a maximum can be observed inside of the micelle corona. Once in the solvent, the chains show a constant value and is in agreement with our SCMF calculations for homogeneous fields where $N = 1$. This common behavior for all Pluronics is illustrated in Fig. 6.3 where L44 chain configurations obtained from the dynamic SCMF simulations are shown depending on their distance from the center of the micellar region. Despite this general situation, a marked difference is observed for L44, where the changes in the radius of gyration has a much larger decrease on reaching the PO-EO interface and a smaller increase towards the EO-solvent interface. This L44 case can

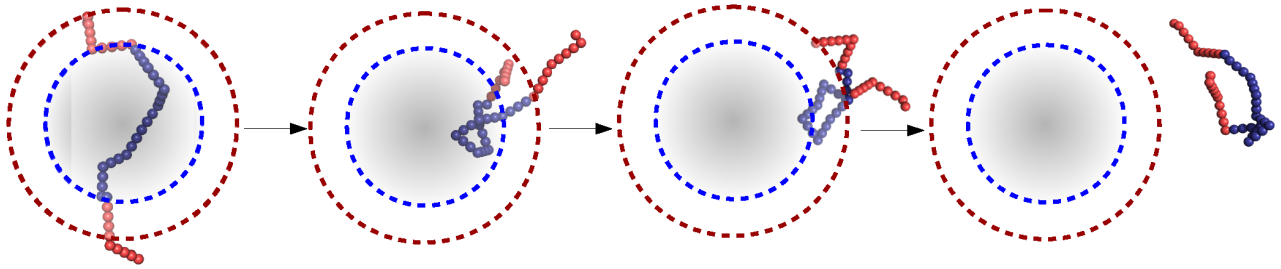

Figure 6.3: Chain conformations for Pluronic L44 when leaving the micellar region. Dashed blue and red lines represent the inner hydrophobic PO micellar core and EO hydrophilic shell boundaries, respectively. From left to right are shown representative conformations with radius of gyration 5.3σ, 2.6σ, 3.1σ and 3.5σ, respectively.

be understood by considering the relatively large diameter of the hydrophobic core, close to 19σ, being similar to the length of the fully stretched PO blocks resulting in a high stretching of the hydrophobic block inside the micelle core allowing to relax on leaving. The size of the hydrophobic core is essentially controlled by the aggregation number N that in the case of L44 is taken as 145 being more than triple the value used for other copolymers.

To compare quantitatively our results with the reported data from experiments for similar copolymer systems we consider two common scenarios where changes in the conformations of the hydrophobic blocks are obtained from fitting arbitrary parameters in the double exponential dependence of the theoretical relaxation function $R(t) = \exp -kt$, analogous to the one defined in Eq. 6.7, as a function of the expulsion rate constant $k \propto \exp(-F_a/kT)$, where F_a is the energetic barrier in the expulsion process which depends on arbitrary prefactors whose election has important consequences for the copolymer conformational information. The two main analysis come from TR-SANS and fluorescence spectroscopy experiments for diblock and triblock copolymer surfactants where collapsed [18, 10, 8] and stretched [12, 7, 13, 10] conformations have been suggested to explain the exit process of surfactants from the interior of micellar aggregates. To compare the former considerations with the results obtained from our simulations we proceed to calculate, on the one hand, the radius of the completely collapsed hydrophobic PPO block [14], $N_{PO}^{1/3}\sigma$. In the case of L44 a value of 2.8σ is found which is well below the minimum of $\langle R_g(r)\rangle$ observed in Fig. 6.2 that is close to 3.7σ. On the other hand, a calculation of the radius of gyration of PO blocks for a fully stretched L44 chains results in a value of 6.6σ being clearly higher than the values reported in our calculations either inside or outside the micellar region. This tendency between the sizes from our observations and the calculations for completely collapsed and stretched chains is also observed for all the others Pluronics considered in this chapter. In this sense, our simulations reveal, as observed in Fig. 6.2, that expulsion of a copolymer from the interior of the micelle involves a more subtle decrease in the radius of gyration but not a complete collapse or stretching of the insoluble blocks. As stated before, the results obtained by the dynamic SCMF simulations are not based on initial assumptions, and explicit information is obtained from following explicit coarse-grained chains. Contrarily, the conclusions obtained from the cited experimental analysis require the use of non-independent parameters. For example, based on the analysis of the free energy of transfer of PO groups and plots of k_{exp} versus the number of hydrophobic blocks N_{PO}

and $N_{PO}^{2/3}$ for copolymer systems Zana [44] manifested the dominance of the linear term and in consequence the preference for the stretched conformations. However, when temperature corrections are included [41] in the analysis, the fractional terms $N_{PO}^{2/3}$ become relevant and is interpreted as a preference of the system for collapsed configurations of the chains. This particular case exhibits the sensibility of the conclusions obtained when different approaches or fitting parameters are considered [18].

To evaluate in more detail the changes in conformation as the copolymers enter or leave the micelle we also calculated the angle between the center of masses of the PO blocks and the EO blocks as shown in Fig. 6.4. As

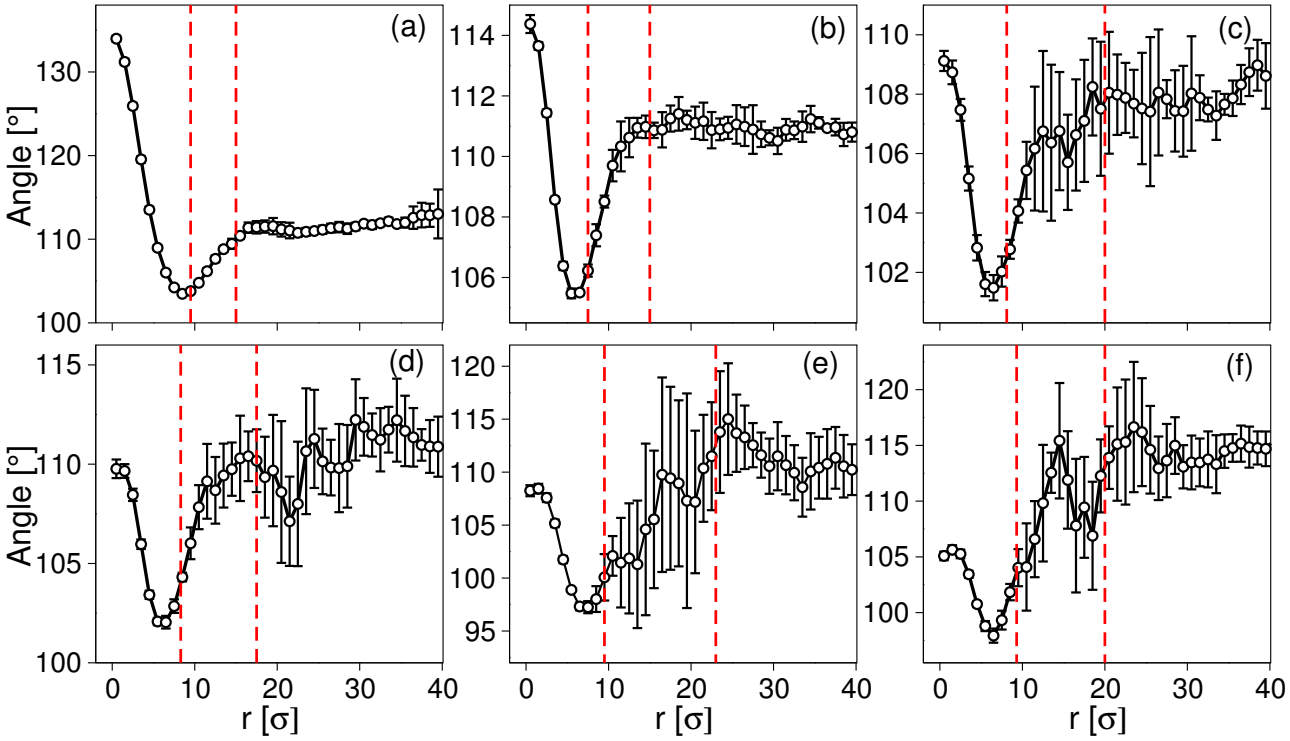

Figure 6.4: Average angle between PEO-PPO-PEO centers of mass for surfactants inside and outside a micelle for Pluronic (a) L44, (b) L64, (c) P85, (d) P84, (e) P104 and (f) P123. Vertical dashed lines represent the approximate extension of the hydrophobic micelle core and the head groups.

observed, in all cases the surfactants in the center of the micelle exhibit a decrease in the angle as they approach to the PO-EO interface to then increase when crossing the EO corona and finally relax when they completely leave the micellar aggregate. This situation is readily observed in the case of the shorter surfactants L44 and L64, but, as the number of monomers increases, the uncertainty in the predictions of the angles unfortunately becomes appreciable, but the analysis remains unaffected. As the diameter of the hydrophobic core for L44 is comparable in size with the PPO stretched block length, copolymers belonging to the micelle prefer stretched conformations near to the center of the micelle with an angle slightly above 130° to later fall until close to 105° which is consistent with the considerable decrease in its radius of gyration in the same regime as shown in Fig. 6.2 indicating a significant configurational change for L44 when leaving the micelle. This change in the average angle is less significant for the other copolymers whose hydrophobic core diameter is smaller than their stretched PPO block length. In these cases the changes are less significant given that our calculations reveal a

decrease of about 10° with respect to their original values at $r = 0$ demonstrating the quantitative impact of the micellar size as compared to the surfactant hydrophobic block size on copolymer conformational behavior.

6.4 Conclusions

In this chapter we present a systematic studio of the equilibrium expulsion kinetics for a series of surfactants at a constant temperature of 37 °C through the implementation of a dynamic version of the SCMF theory. The estimations obtained for the expulsion rate constants for the Pluronic surfactants under study show an excellent quantitative agreement with experimental available data. In particular, a significant decrease in the constants is observed when the number of hydrophobic units increases. Our simulations allow the study of the conformational changes in copolymers as they enter or leave the micellar region by means of changes in the radius of gyration of the hydrophobic blocks as a function of the radial distance from the center of the micelle revealing, in general, a slight shrinking of the hydrophobic blocks when approaching the corona region to finally relax to almost constant values in the bulk solution. This analysis was supported by also studying the changes in the angle between hydrophobic and hydrophilic blocks where a subtle decrease in the radius of gyration is detected in all cases. However, a slightly different behavior is observed if the diameter of the hydrophobic core of the micelle becomes comparable to the stretched hydrophobic block. Contrarily to the scenarios given in the literature, the surfactant chains neither fully collapse nor stretch, rather a more subtle effect is observed in our simulations where the conformation radius of gyration generally becomes slightly more compressed on leaving the hydrophobic core, before going through a maximum in the corona to finally relaxing towards the bulk value.

References

[1] A. Patist, J. R. Kanicky, P. K. Shukla, and D. O. Shah. *J. Colloid Interface Sci.*, 245(1):1–15, 2002.

[2] R. Pons. Polymeric Surfactants as Emulsion Stabilizers. In P. Alexandridis and B. Lindman, editors, *Amphiphilic Block Copolymers*, pages 409 – 422. Elsevier Science B.V., Amsterdam, 2000.

[3] E. V. Batrakova and A. V. Kabanov. *J. Controlled Release*, 130(2):98–106, 2008.

[4] Y. Matsumura and K. Kataoka. *Cancer Sci.*, 100(4):572–579, 2009.

[5] H. Nakamura, E. Koziolová, T. Etrych, P. Chytil, J. Fang, K. Ulbrich, and H. Maeda. *Eur. J. Pharm. Biopharm.*, 90:90–96, 2015.

[6] I. Goldmints, J. F. Holzwarth, K. A. Smith, and T. A. Hatton. *Langmuir*, 13(23):6130–6133, 1997.

[7] D. Schaeffel, A. Kreyes, Y. Zhao, K. Landfester, H.-J. Butt, D. Crespy, and K. Koynov. *ACS Macro Lett.*, 3(5):428–432, 2014.

[8] R. Lund, L. Willner, D. Richter, and E. E. Dormidontova. *Macromolecules*, 39(13):4566–4575, 2006.

[9] R. Lund, L. Willner, J. Stellbrink, P. Lindner, and D. Richter. *Phys. Rev. Lett.*, 96:068302, 2006.

[10] R. Lund, L. Willner, V. Pipich, I. Grillo, P. Lindner, J. Colmenero, and D. Richter. *Macromolecules*, 44 (15):6145–6154, 2011.

[11] T. Zinn, L. Willner, R. Lund, V. Pipich, and D. Richter. *Soft Matter*, 8:623–626, 2012.

[12] S.-H. Choi, T. P. Lodge, and F. S. Bates. *Phys. Rev. Lett.*, 104:047802, 2010.

[13] J. Lu, F. S. Bates, and T. P. Lodge. *Macromolecules*, 48(8):2667–2676, 2015.

[14] A. Halperin and S. Alexander. *Macromolecules*, 22(5):2403–2412, 1989.

[15] E. A. G. Aniansson and S. N. Wall. *J. Phys. Chem.*, 78(10):1024–1030, 1974.

[16] E. A. G. Aniansson and S. N. Wall. *J. Phys. Chem.*, 79(8):857–858, 1975.

[17] Y. Rharbi. *Macromolecules*, 45(24):9823–9826, 2012.

[18] R. Lund, L. Willner, J. Stellbrink, P. Lindner, and D. Richter. *Phys. Rev. Lett.*, 104(4):049902(E), 2010.

[19] T. Haliloğlu, I. Bahar, B. Erman, and W. L. Mattice. *Macromolecules*, 29(13):4764–4771, 1996.

[20] M. P. Pépin and M. D. Whitmore. *Macromolecules*, 33(23):8644–8653, 2000.

[21] M.-J. Hafezi and F. Sharif. *Langmuir*, 28(47):16243–16253, 2012.

[22] D. N. Lebard, B. G. Levine, R. DeVane, W. Shinoda, and M. L. Klein. *Chem. Phys. Lett.*, 522:38–42, 2012.

[23] Z. Li and E. E. Dormidontova. *Soft Matter*, 7(9):4179–4188, 2011.

[24] A. Ben-Shaul, I. Szleifer, and W. M. Gelbart. *J. Chem. Phys.*, 83(7):3597–3611, 1985.

[25] V. G. de Bruijn, L. J. P. van den Broeke, F. A. M. Leermakers, and J. T. F. Keurentjes. *Langmuir*, 18(26): 10467–10474, 2002.

[26] C. B. E. Guerin and I. Szleifer. *Langmuir*, 15(23):7901–7911, 1999.

[27] A. D. Mackie, A. Z. Panagiotopoulos, and I. Szleifer. *Langmuir*, 13(19):5022–5028, 1997.

[28] Z. A. Al-Anber, J. Bonet Avalos, and A. D. Mackie. *J. Chem. Phys.*, 122(10):104910, 2005.

[29] F. A. García Daza, A. J. Colville, and A. D. Mackie. *Langmuir*, 31(12):3596–3604, 2015.

[30] A. Gezae Daful, V. A. Baulin, J. Bonet Avalos, and A. D. MacKie. *J. Phys. Chem. B*, 115(13):3434–3443, 2011.

[31] F. Fang, J. Satulovsky, and I. Szleifer. *Biophys. J.*, 89(3):1516–1533, 2005.

[32] F. Fang and I. Szleifer. *Biophys. J.*, 80(6):2568–2589, 2001.

[33] M. Müller and G. D. Smith. *J. Polym. Sci., Part B: Polym. Phys.*, 43(8):934–958, 2005.

[34] F. A. García Daza, A. J. Colville, and A. D. Mackie. *J. Chem. Phys.*, 142(11):114902, 2015.

[35] K. Binder. *Monte Carlo and Molecular Dynamics Simulations in Polymer Science*. Topics in Polymer Science. Oxford University Press, 1995.

[36] A. V. Kabanov, I. R. Nazarova, I. V. Astafieva, E. V. Batrakova, V. Y. Alakhov, A. A. Yaroslavov, and V. A. Kabanov. *Macromolecules*, 28(7):2303–2314, 1995.

[37] P. Alexandridis, T. Nivaggioli, and T. A. Hatton. *Langmuir*, 11(5):1468–1476, 1995.

[38] S. L. Nolan, R. J. Phillips, P. M. Cotts, and S. R. Dungan. *J. Colloid Interface Sci.*, 191(2):291–302, 1997.

[39] M. Rubinstein and R. H. Colby. *Polymer Physics*. Oxford University Press, Oxford, 1 edition, 2003.

[40] S. Nawaz and P. Carbone. *J. Phys. Chem. B*, 118(6):1648–1659, 2014.

[41] R. Zana, C. Marques, and A. Johner. *Adv. Colloid Interface Sci.*, 123-126:345–351, 2006.

[42] G. Wu, B. Chu, and D. K. Schneider. *J. Phys. Chem.*, 99(14):5094–5101, 1995.

[43] M. Almgren, P. Bahadur, M. Jansson, P. Li, W. Brown, and A. Bahadur. *J. Colloid Interface Sci.*, 151(1): 157–165, 1992.

[44] R. Zana. Dynamics in Micellar Solutions of Amphiphilic Block Copolymers. In R. Zana, editor, *Dynamics of Surfactant Self-Assemblies Micelles, Microemulsions, Vesicles and Lyotropic Phases*, volume 125 of *Surfactant Science*, chapter 4, pages 161–231. CRC Press, Boca Raton, FL, 2005.

Chapter 7

Copolymeric Micellar Exchange Kinetics Controlled by Chain Conformation Dynamics

To be submitted to *Physical Review Letters*.

7.1 Introduction

Surfactant micelles are of special interest in a broad range of academic and technological frameworks given their ability to spontaneously self-assemble into a very well defined set of geometric shapes when the surfactant concentration surpasses a specific concentration known as the critical micelle concentration (CMC). The kinetics of chain exchange mechanisms have been found to be of paramount relevance in diverse industries including drug transport and delivery systems in nanomedicine [1], foaming processes [2], and, nanosurface design [3]. Experimental and theoretical efforts have focused on kinetic mechanisms like fusion and fission of micellar aggregates as well as the insertion/expulsion of monomer chains into/from micelles. In particular, for block copolymer systems, the kinetics exchange phenomena has been studied through diverse experimental techniques including temperature jump [4], ultrasonic relaxation [5], fluorescence cross-correlation spectroscopy [6] and time-resolved small angle neutron scattering (TR-SANS) [7, 8, 9, 10, 11, 12] which follows the traces of deuterated and hydrogenated copolymers when they redistribute in equilibrium micelles after mixing. When equilibrium is reached near the CMC, the expulsion or insertion of single chains from or into micelles have been identified as the governing mechanisms [7]. The expulsion step is the limiting process and was thought to be represented by a single relaxation exponential decay function $R(t) = \exp(-kt)$ where k is the expulsion rate constant which is concentration independent. This scenario is supported by theoretical predictions for block copolymers [13] and coarse-grained simulations [14]. However, TR-SANS experiments revealed an unexpected non-exponential behavior of the relaxation function $R(t)$ for a series of block copolymer systems suggesting the existence of a broad distribution of relaxation times [7, 8, 9]. Although these multiple time scales have been attributed to the polydispersity of the surfactants [6, 9, 10, 11, 15], the lack of explicit information on the monomer exchange kinetics due to the nanoscale lengths involved has lead to controversy of the model dependence when including polydispersity and conformational transitions of surfactants leaving the micelle [7, 15, 9], being these two assumptions subject to the fitting procedure.
In this chapter we present dynamic coarse-grained simulations for a monodisperse triblock copolymer that show the same broad distribution of relaxation times found in experimental systems demonstrating that polydispersity is not necessary to describe this behavior. Furthermore, we put forward a simple model where the energy barrier is a function of the polymer configuration, which shows several relaxation times. The experimental results can thus be explained by the effect on the expulsion rate of the conformations of the polymer chains within the micelle.

Only a few simulation studies based on molecular dynamics (MD), Monte Carlo (MC), dissipative particle dynamics and Brownian dynamics have been used to study the kinetics of micellization and equilibrium exchange for oligomeric and polymeric systems [16, 17, 18, 19, 20, 21, 14, 22], and even fewer have studied in detail the exchange mechanisms in dynamic equilibrium through a series of autocorrelation functions defined in terms of master equations [19], or, by monitoring a collection of labeled chains in a simulation box [17, 14, 22, 20]. Furthermore, issues are recognized when studying the equilibrium exchange kinetics phenomena from molecular simulations; for example, a lack of connection with real systems due to the discretized space used in lattice simulations [19, 20] and a loss in accuracy for some coarse grained models when comparing with equilibrium

experimental properties (e.g. the CMC) to validate the corresponding force fields [16]. Indeed most simulation works are devoted to study short coarse-grained surfactants due to temporal and sampling constraints.
In light of this, alternatives to these standard simulation techniques are required. Mean-field methods are an interesting alternative for copolymer systems given their proficiency when predicting and comparing results with available experimental data. In this chapter we employ the so-called single-chain mean-field (SCMF) theory which has been shown to efficiently predict equilibrium properties for short and copolymeric surfactant systems [23, 24], and is consistent with MC and MD simulations [25, 26].

7.2 Simulation and Model Details

The SCMF considers a central chain, representing the surfactant under study, subject to the influence of its intramolecular and intermolecular interactions. The intramolecular interactions are determined explicitly while the intermolecular interactions with solvent and other polymer chains are calculated in terms of mean molecular fields of the solvent and the position dependent average chain density, respectively. Formally, the starting point in the theory is the minimization of the free energy of the system subject to an incompressibility condition stating that any region in the space is filled by either chains or solvent molecules. The input in the theory comes from the set of chains, $\{\alpha\}$, that represents the surfactant conformations, and the outputs are the probability density function, $P[\alpha]$, and the solvent concentration profile [23, 24, 25, 26]. The single chain probabilities are defined as $P[\alpha] = \exp(-H[\alpha]/kT)/Q$ where the SCMF Hamiltonian, $H[\alpha]$, contains the intramolecular, intermolecular attractive mean-field and repulsive steric interactions for conformation α, k is Boltzmann's constant, T the temperature of the system and Q the partition function which ensures the normalization of the chain probabilities. The SCMF allows for the use of nonoverlapping chains and the intramolecular steric repulsions are correctly taken into account. This differs from other self-consistent field methods [27] where Markovian chains are used to represent surfactants leading to a less accurate estimation of the free energy, particularly for short chains. In this chapter we develop an explicit dynamic version of the SCMF technique to monitor the entry/exit of surfactant chains into/from a micellar aggregate in order to produce correlation functions analogous to the ones reported in TR-SANS experiments. To do so, we chose the nonionic triblock copolymer $HO(CH_2CH_2O)_{10}(CH(CH_3)CH_2O)_{23}(CH_2CH_2O)_{10}H$ also known by the trade name Pluronic L44 ($EO_{10}PO_{23}EO_{10}$). This surfactant is ideal to study the kinetic exchange mechanisms given: (i) it belongs to the family of block copolymers which means that deviations in the correlation function can be expected as inferred from several kinetic experiments for Pluronics [28] or different triblock copolymer systems [10], and, (ii) since it is a relatively short Pluronic the simulations can be performed in a reasonable amount of computer time.

The coarse-grained model to describe the surfactant is taken from a previous work [24] where a model for Pluronic surfactants was successfully developed to predict the CMCs via equilibrium SCMF. Both hydrophilic, EO, and hydrophobic, PO, units are modeled as hard spheres of the same size σ, and individual chains are conformed by nonoverlapping beads and are separated by the same bond-length distance σ. The rigidity of the chain is included by way of rigid Kuhn segments of four beads for a PO segment and five beads for EO. Individual chain intramolecular and intermolecular interactions are modeled through square well potentials for each

bead in spherical volumes with inner and outer radii of σ and 1.62σ, respectively. Only three mixed interactions are considered through Flory-Huggins parameters, namely, EO-PO, EO-Solvent and PO-Solvent with values of 0.006, 0.5 and 2.1, respectively.

To evaluate the kinetics exchange behavior of equilibrium aggregates it is necessary to establish a dynamic version of the SCMF. In this sense, we consider that the set of sampling chains $\{\alpha\}$ evolves in time by accepting or rejecting simultaneous trial moves with individual probabilities

$$p\left(\alpha_{old\rightarrow new}\right) = \min\left(1, \exp\left(-\Delta H\left[\alpha\right]/kT\right)\right), \tag{7.1}$$

where $\Delta H\left[\alpha\right] = H\left[\alpha_{new}\right] - H\left[\alpha_{old}\right]$ is the change in energy for the sampling configuration α, belonging to $\{\alpha\}$, when a trial change in its configuration is produced. This procedure allows an individual trial move for each sampling chain in every cycle producing an artificial dynamics of the temporal evolution of each sampling chain. This technique is similar in spirit to the one proposed by Müller and Smith [29] for polymer blends. In our simulations, the moves are described by local displacements to guarantee a Rouse motion as follows: first, a rigid segment is randomly chosen, if this segment is an end segment then an end-bond rotation move is used, otherwise a trial crankshaft move is attempted [30]. If no overlaps occur between segments of the same chain, the SCMF Hamiltonian for the new configuration, $H\left[\alpha_{new}\right]$, is calculated and compared with the original conformation, $H\left[\alpha_{old}\right]$. The move is accepted according to the probability given in Eq. 7.1, otherwise the original configuration is maintained. The chains are initially distributed homogeneously in the simulation box, then moved according to the aforementioned scheme. Simulations were performed in the canonical ensemble with $N = 145$ chains, a temperature $T = 37\,^{\circ}\mathrm{C}$ in a simulation box of size $(70\sigma)^3$ with periodic boundary conditions. To determine the finite size effects we have run simulations with different sizes of the box also modifying the number of sampling chains to keep its concentration around a constant value. In the smallest box 182 sampling chains are sufficient but more are required as the size is increased. The cycle unit of time, t_{cyc}, can be compared with the time scale in experiments, t, by the relation $t = t_{cyc}D_{cyc}/D$ where D_{cyc} and D are the diffusion coefficients obtained by the SCMF simulation and the one calculated via the Stokes-Einstein relation, respectively. Given that, $D_{cyc} = \langle\Delta\vec{r}(t_{cyc})^2\rangle/(6t_{cyc})$ where $\Delta\vec{r}(t_{cyc}) = \vec{r}(t_{cyc}) - \vec{r}(0)$ is the vectorial displacement of the center of mass for a sampling chain at time t_{cyc} from its original position calculated from the dynamic SCMF simulations, the diffusion of a L44 chain can be calculated from $D = kT/\left(6\pi\eta R_1\right)$ where $\eta = 6.91\times10^{-4}\,\mathrm{kg/(ms)}$ is the viscosity of water at 37 °C, and, $R_1 = 4.5\sigma = 2.3\,\mathrm{nm}$ is the average hydrodynamic radius for a L44 surfactant in the solvent. We estimate the hydrodynamic radius from a series of dynamic SCMF simulations for chains in a homogeneous solvent medium, where $\sigma = 0.5\,\mathrm{nm}$ is taken from the literature [31]. With this, the diffusion coefficients estimated from the simulations and the Stokes-Einstein relation are $D_{cyc} \approx 3.3(0.2)\times10^{-22}\,\mathrm{m^2/cycle}$ and $D = 1.5 \approx 10^{-10}\,\mathrm{m^2/s}$, respectively, and hence, $t \approx 2.3\times10^{-12}t_{cyc}\,\mathrm{s/cycle}$.

7.3 Results and Discussion

A series of autocorrelation functions can be defined based on the exchange of chains in the micellar aggregate. At time $t = 0\,\mathrm{s}$ the chains in the interior of the aggregate are labeled, and the exchange and reorganization of

chains with time is monitored and represented through the autocorrelation function

$$F(t) = \frac{f(t) - f(\infty)}{f(0) - f(\infty)}, \tag{7.2}$$

where $f(t)$ is the fraction of labeled chains in the interior of the micelle at time t. Our simulations show that for long simulation times on average half of labeled chains stay in the micelle meaning $f(\infty) \approx 0.5$. This function is comparable to the one used in the TR-SANS experiments [11, 12] where time dependent fractions of deuterated or nondeuterated surfactants in micelles are calculated from fitting the scattering intensity and has been shown to be equivalent to the correlation functions obtained directly from the square root of experimental scattering intensities [7, 8, 9, 11, 12, 10]. In Fig. 7.1 a series of relaxation functions calculated from the dynamic SCMF simulations and Eq. 7.2 are presented for different simulation box sizes. As can be observed, the SCMF

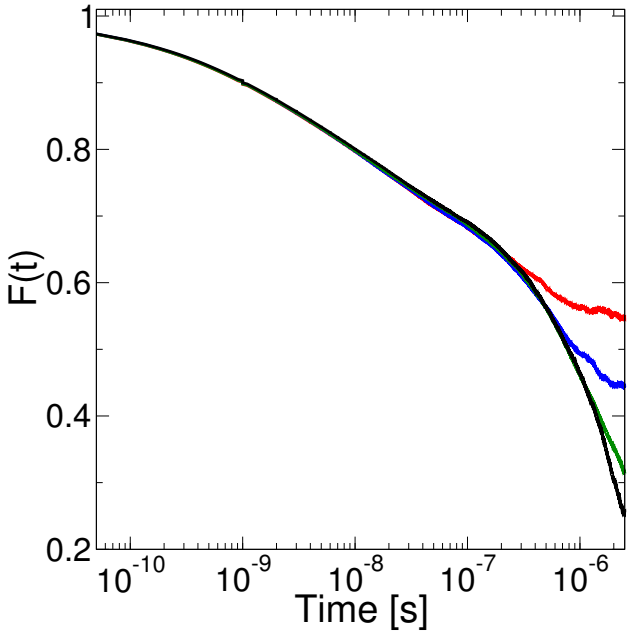

Figure 7.1: Relaxation kinetics of the L44 micellar system predicted from dynamic SCMF simulations. Red, blue, green and black lines refer to correlation functions obtained from simulation boxes with volumes (25 nm)^3, (30 nm)^3, (35 nm)^3 and (40 nm)^3, respectively from top to bottom.

simulations are able to span several orders of magnitude in time presenting three well-defined regimes. The first one extends over one order of magnitude and can be related to a fast reorganization of surfactants close to the inner core interface when the expulsion is initialised, this trend has been observed for diblock poly(ethylene-*alt*-propylene)-poly(ethylene oxide) (PEP-PEO) [11] and polystyrene-*block*-poly(oligo(ethylene glycol) methyl ether methacrylate) (PS-POEGMA) [6] surfactant systems. The second region continues over almost three orders of magnitude; this behavior corresponds to a gradual relaxation of the expulsion process coming from the reaccommodation of the surfactants near to the hydrophobic core boundary and the subsequent relaxation of this process. This linear trend has been experimentally reported for different polymeric systems as in the case of PEP-PEO [7, 8, 11], poly(styrene)-poly(ethylene-*co*-propylene) (PS-PEP) [9], PS-PEP-PS and PEP-PS-PEP [10], and, PS-POEGMA [6] systems. In this regime the autocorrelation function is independent of the size of

the simulation box. However, for longer times, $F(t)$ can be observed to deviate from this linear behavior as long as the volume of the box is large enough. A labeled chain that has been expelled from the interior of the micelle is able to encounter the periodic image of the micelle if it diffuses a large enough distance. This distance is related to the size of the simulation box, which means that for smaller boxes these finite system size effects are noted earlier in the autocorrelation function. As can be observed in Fig. 7.1, as the size of the box increases, the autocorrelation function is able to continue this deviation from the linear trend and approaches the experimental relaxation process near the CMC where the equilibrium aggregates are not close to each other. Indeed, this deviation from the linear behavior for longer times defines the third regime and has been subtly observed, but not commented on, in experimental autocorrelation functions based on master curves shifted to take into account the effects of temperature for a set of diblock [9] and triblock [9, 10] copolymer systems. In conclusion, at the very least in a qualitative sense, we can state that our results appear to contain the correct underlying physics in the kinetic exchange processes of single surfactants in the equilibrium regime.

Given that we are able to reproduce the same experimental behavior, we can now perform a microscopic analysis of the chain dynamics. Of particular interest is the possibility of the surfactants to adopt a particular configuration to facilitate their exit from the interior of the micelle. During the simulations we calculate the radius of gyration of the chains, R_g, and average this quantity with respect to time as a function of the distance from the center of the micelle, see Fig. 7.2. The statistical error is smaller than the size of the symbols and is

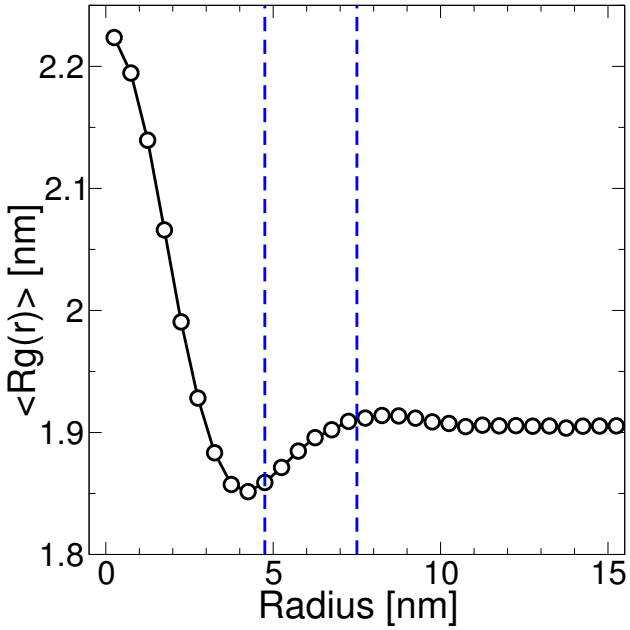

Figure 7.2: Radius of gyration for the hydrophobic block of the surfactant as a function of the distance from the center of the micelle. Vertical dashed lines represent the inner hydrophobic core and the hydrophilic shell.

not shown. As can be seen, the hydrophobic block of the surfactants tends to stretch as the chain approaches the micelle center. Contrarily, a reduction in the radius of gyration is observed as the surfactant approaches the interface between PO and EO regions (vertical dashed line, 4.75 nm). The radius of gyration then smoothly increases as the surfactant leaves the micelle and assumes a constant value on reaching the bulk solution (vertical

dashed line, 7.5 nm). It should be noted that this sequence depends on the size of the surfactant and that longer surfactants may not show this minimum for the radius of gyration on leaving the micelle, results not shown here. That is, it appears that the surfactants undergo changes to the radius of gyration as they exit the micelle revealing a series of transformations in their confirmation that aid in their escape. This suggests the existence of a wide number of relaxation mechanisms related with the chain conformation instead of only one relaxation process as suggested in the standard theoretical description [13, 14]. It should be noted that all surfactants in our calculations have the same chain length demonstrating that this behavior does not require polydispersity despite the suggestion of recent experimental works to that effect [15, 9, 6, 11, 10].

In order to better elucidate the nature or the simulation results we propose a simplistic model based on the diffusion of chain surfactants in an aggregate of size N through an energetic barrier. We impose that surfactants exist in only two states, namely: stretched (state A, populations with $R_g > 1.35$ nm) , and compressed (state B, chains with $R_g \leq 1.35$ nm). If the chains are in the compressed state then we consider that the depth of the energy well is less than in the stretched state. In addition, the surfactants have a certain probability of changing from one state to the other. All the model parameters are taken from the SCMF simulations including the transition probabilities and the energy wells calculated by way of the concentrations of surfactants in the different states as a function of distance from the micelle center. The model is solved numerically in spherical coordinates using the Einstein-Smoluchowski equation coupled with terms relating the transitions between states A and B,

$$\frac{\partial c_A}{\partial t} = -\vec{\nabla} \cdot \vec{J}_A - c_A W_{A\to B} + c_B W_{B\to A}, \tag{7.3}$$

$$\frac{\partial c_B}{\partial t} = -\vec{\nabla} \cdot \vec{J}_B + c_A W_{A\to B} - c_B W_{B\to A}, \tag{7.4}$$

where $c_{A,B}$ correspond to the concentrations of species A, B, $W_{A\to B}$ and $W_{B\to A}$ refer to the transition rates from states A to B, and, B to A, respectively. The flux $\vec{J}_{A,B} = -D\left(\partial c_{A,B}/\partial r + \left(\partial V_{A,B}/\partial r\right) c_{A,B}/kT\right)\hat{r}$ is defined for each species and is subject to the potential $V_{A,B}$. The solution of Eqs. 7.3 and 7.4 was achieved by dividing the space into concentric shells of width 0.95 nm. In every shell i we calculated from the dynamic SCMF simulations the transition rates which lie in the range 1.9×10^7 and 5.71×10^9 transitions/s for shells inside the micellar core with radius 4.75 nm and null elsewhere. The energetic barriers are calculated by taking a mean-force potential of the type $V_{A,B}(r_i) = \exp\left(-\phi^{eq}_{A,B}(r_i)/kT\right)$ where the term inside the exponential refers to the equilibrium volume fraction of each species. The minimum values of the potentials were found to be $-4.37\,kT$ and $-2.03\,kT$ for species A and B respectively whilst a common maximum value for both species was found to be $6.91\,kT$. The initial concentrations were obtained from the SCMF simulations in the equilibrium regime.

Once the diffusion equations are solved, we can follow the spatial and temporal evolution of the different surfactant concentrations A and B. In other words, we can monitor the entrance and exit of surfactant chains by evaluating the change in concentrations with respect to the initial state for the region defined as the hydrophobic core of the micelle. For simplicity, we compare in Fig. 7.3 the fraction of initial surfactants in the micellar core with the autocorrelation function $N(t) = f(t)/f(0)$ obtained directly from the dynamic SCMF simulations. As can be observed, in both schemes the exchange process has more than one relaxation process contrary to the prediction of standard theory [13]. In addition, the shape of the two autocorrelation functions is very similar

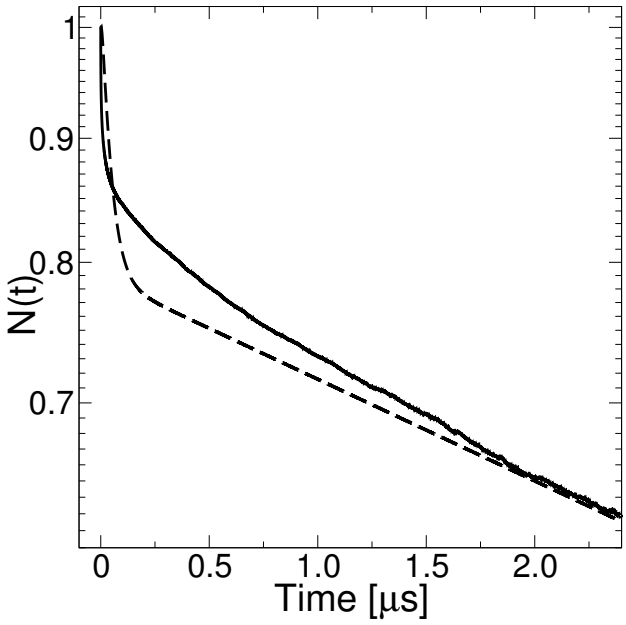

Figure 7.3: Chain-exchange kinetics analyzed from the logarithmic correlation function obtained through dynamic SCMF calculations (solid line) and solution of the diffusion equation with inclusion of mean-force potentials and transition rates between stretched and compressed surfactants (dashed line).

to the one reported in experiments for diverse copolymer systems [7, 8, 9]. In both cases a fast decrease of the autocorrelation function is detected for times below 0.3 μs, subsequently, a transition to slower processes is produced to finally relax for longer timescales. According to our observations, the initial fast decrease can be associated to a readjustment in the positions of those surfactants which are near to the interface between the core and the hydrophilic shell of the micelle at time $t = 0$ s due to the total absence of marked chains outside of the micelle, thus promoting the relatively easy exit of these chains. This corresponds to the two first regimes in Fig. 7.1 as discussed previously. After the initial accommodation of the labeled chains, the surfactants are subject to being in a mean force potential well which controls the probability to diffuse out of the micelle affecting the correlation function as shown in Fig. 7.1 in the case of the third regime. Since this potential well depends on the two model individual chain physical conformations, A and B, the loss of surfactants depends on the transition rate between the two conformations. The compressed configuration with the smaller well is able to escape much more easily than the stretched one and so the stretched surfactants are required to wait until they can become compressed before being able to leave. Our simple model is thus able to capture the mean features of the SCMF calculations being a process controlled by the ability of the surfactants to escape from the potential energy well of the micelle. In our model there are only two conformations, which leads to a more simplified dynamic response with essentially two time scales. On the other hand, the SCMF calculations have a very large number of conformations, each with its own potential well. This leads to many more time scales in the SCMF dynamics in agreement with experiments.

7.4 Summary

Our explicit dynamic SCMF coarse-grained simulations are able to model the exit exchange mechanism of a triblock copolymer surfactant from a micelle. Furthermore, the simulation relaxation exchange kinetics are qualitatively consistent with the available experimental data where an unexpected non-exponential behavior is found. Although previous works attribute this non-exponential behavior to the polydispersity of the polymeric surfactants in the experiments, our calculations use a strictly monodisperse distribution of chains. We then conclude that the polydispersity is not necessary to explain the observed non-exponential behavior. To further understand the nature of our results, we solve a simplistic two conformational state model of the diffusion equation whose parameters were extracted from the SCMF simulations. We find that this simplistic model is able to correctly reproduce the multiple time scales found in SCMF calculations, albeit with only two. The SCMF results, and hence the experimental data, can thus be fully described by the effective potential well that a particular surfactant experiences depending on its conformation. Given that the potential well essentially controls the escape dynamics, this results in multiple time scales arising from the different conformations present in the micelle and the transition rates between them.

References

[1] H. Nakamura, E. Koziolová, T. Etrych, P. Chytil, J. Fang, K. Ulbrich, and H. Maeda. *Eur. J. Pharm. Biopharm.*, 90:90–96, 2015.

[2] A. Patist, J. R. Kanicky, P. K. Shukla, and D. O. Shah. *J. Colloid Interface Sci.*, 245(1):1–15, 2002.

[3] V. K. Paruchuri, J. Nalaskowski, D. O. Shah, and J. D. Miller. *Colloids Surf., A*, 272(3):157–163, 2006.

[4] I. Goldmints, J. F. Holzwarth, K. A. Smith, and T. A. Hatton. *Langmuir*, 13(23):6130–6133, 1997.

[5] G. Waton, B. Michels, and R. Zana. *J. Colloid Interface Sci.*, 212(2):593–596, 1999.

[6] D. Schaeffel, A. Kreyes, Y. Zhao, K. Landfester, H.-J. Butt, D. Crespy, and K. Koynov. *ACS Macro Lett.*, 3(5):428–432, 2014.

[7] R. Lund, L. Willner, D. Richter, and E. E. Dormidontova. *Macromolecules*, 39(13):4566–4575, 2006.

[8] R. Lund, L. Willner, J. Stellbrink, P. Lindner, and D. Richter. *Phys. Rev. Lett.*, 96:068302, 2006.

[9] S.-H. Choi, T. P. Lodge, and F. S. Bates. *Phys. Rev. Lett.*, 104:047802, 2010.

[10] J. Lu, F. S. Bates, and T. P. Lodge. *Macromolecules*, 48(8):2667–2676, 2015.

[11] R. Lund, L. Willner, V. Pipich, I. Grillo, P. Lindner, J. Colmenero, and D. Richter. *Macromolecules*, 44 (15):6145–6154, 2011.

[12] T. Zinn, L. Willner, R. Lund, V. Pipich, and D. Richter. *Soft Matter*, 8:623–626, 2012.

[13] A. Halperin and S. Alexander. *Macromolecules*, 22(5):2403–2412, 1989.

[14] Z. Li and E. E. Dormidontova. *Soft Matter*, 7:4179–4188, 2011.

[15] R. Lund, L. Willner, J. Stellbrink, P. Lindner, and D. Richter. *Phys. Rev. Lett.*, 104(4):049902(E), 2010.

[16] G. Mohan and D. I. Kopelevich. *J. Chem. Phys.*, 128(4):044905, 2008.

[17] D. N. Lebard, B. G. Levine, R. DeVane, W. Shinoda, and M. L. Klein. *Chem. Phys. Lett.*, 522:38–42, 2012.

[18] S. J. Marrink, D. P. Tieleman, and A. E. Mark. *J. Phys. Chem. B*, 104(51):12165–12173, 2000.

[19] T. Haliloğlu, I. Bahar, B. Erman, and W. L. Mattice. *Macromolecules*, 29(13):4764–4771, 1996.

[20] M. P. Pépin and M. D. Whitmore. *Macromolecules*, 33(23):8644–8653, 2000.

[21] Z. Li and E. E. Dormidontova. *Macromolecules*, 43(7):3521–3531, 2010.

[22] M.-J. Hafezi and F. Sharif. *Langmuir*, 28(47):16243–16253, 2012.

[23] A. Gezae Daful, V. A. Baulin, J. Bonet Avalos, and A. D. Mackie. *J. Phys. Chem. B*, 115(13):3434–3443, 2011.

[24] F. A. García Daza, A. J. Colville, and A. D. Mackie. *Langmuir*, 31(12):3596–3604, 2015.

[25] A. D. Mackie, A. Z. Panagiotopoulos, and I. Szleifer. *Langmuir*, 13(19):5022–5028, 1997.

[26] C. B. E. Guerin and I. Szleifer. *Langmuir*, 15(23):7901–7911, 1999.

[27] Y. Lauw, F. A. M. Leermakers, and M. A. Cohen Stuart. *J. Phys. Chem. B*, 110(1):465–477, 2006.

[28] R. Zana, C. Marques, and A. Johner. *Adv. Colloid Interface Sci.*, 123-126:345–351, 2006.

[29] M. Müller and G. D. Smith. *J. Polym. Sci., Part B: Polym. Phys.*, 43(8):934–958, 2005.

[30] K. Binder. *Monte Carlo and Molecular Dynamics Simulations in Polymer Science*. Topics in Polymer Science. Oxford University Press, 1995.

[31] M. Rubinstein and R. H. Colby. *Polymer Physics*. Oxford University Press, Oxford, 1 edition, 2003.

Chapter 8

Concluding Remarks

8.1 Significance of the Results

In this thesis we aimed to implement a series of SCMF simulations to study a set of low weight and block copolymer surfactant systems. In particular, we sought to compare most of the results obtained in this work with available experimental data, also, we studied unexpected physical behaviors reported in experiments, and, when possible, we extracted from our simulations microscopic information difficult to reach by others simulation methods.

This thesis can be divided in two parts: (i) examination of static equilibrium properties for surfactants systems based on a series of SCMF simulations, and, (ii) study of dynamic properties in equilibrium regime for block copolymers systems from explicit dynamic SCMF simulations. Accordingly, the contributions reached in this work can be separated as follows: the first contribution of this work is a systematic analysis of diverse SCMF simulations when predicting static equilibrium properties for selected surfactants. In Chapter 3 we analyzed the aggregation properties of a series of nonionic Poly(ethylene oxide) alkyl ether surfactants with different architectures including linear (diblock and triblock), branched and gemini. We showed that properties like the CMC and aggregation number can be drastically varied by controlling the organization of the insoluble and soluble blocks in the surfactants. To understand the cause of this phenomena we evaluated the excess enthalpic and entropic contributions for all the systems under study, revealing, an increase in the solubility for triblock and branched surfactants but a decrease in their aggregation numbers. Following the model for gemini surfactants used in Chapter 3, we model a set of nonionic dimeric poly(ethylene oxide) surfactants in Chapter 4 to study the unexpected deviation from the logarithmic scale of the CMC with respect to the length of the hydrophobic units. We combined our estimations of the standard chemical potentials for free and aggregated surfactants with a micellization kinetic model to determine the possible source of the mentioned deviation. From the results we determined a series of nonequilibrium effects related with the large time scales for micelles to equilibrate, that, when are combined by an increase in the number of free surfactants and possible adsorption effects may account for the deviations of the CMC observed in experiments. In Chapter 5 we presented a coarse-grained model for poly(ethylene oxide)-poly(propylene oxide)-poly(ethylene oxide) surfactants (PEO-PPO-PEO) under the SCMF scheme. Equilibrium properties were analyzed and compared with available experimental data for a wide number of block copolymer systems. In particular, the behavior of the CMC and the aggregation numbers with the size of the hydrophobic PPO and hydrophilic PEO blocks was found to be consistent with the experimental information: the increase in PO units results in a reduction of the CMC and an increase of the aggregation number, while an increase in the PEO length subtly affects the CMC but decreases the aggregation number. Also, our simulations revealed a deviation of the CMC from experimental data in the logarithmic scale

for the most hydrophobic surfactants suggesting the existence of nonequilibrium effects similar to the studied in Chapter 4.

The second contribution of this thesis is a detailed microscopic study of block copolymer systems in a dynamic equilibrium regime. In Chapter 6 a set of Pluronic surfactants were studied by using the coarse-grained model introduced in Chapter 5 and a series of dynamic SCMF simulations. By following traced sampling chains originally placed in a micellar aggregate, a set of autocorrelation functions were defined to study the kinetic monomer exchange processes. From the fitting of the autocorrelation functions we obtained a set of exit rates constants which are compared with the data reported in experiments exhibiting a good quantitative agreement. Additionally, we observed a decrease in the radius of gyration of the PPO blocks when copolymers diffuse from the center of the micelle to the shell region. These results open the possibility of analyzing explicit conformational changes involved in the expulsion process evaluating, from a microscopic point of view, the validity of the assumptions in some theoretical and experimental works where coiled or stretched conformations have been considered. In Chapter 7 we presented an analysis of the dynamic exchange of a selected Pluronic surfactant to study a deviation reported in several experimental autocorrelation functions for similar copolymer systems. We compared the results obtained by our simulations with solutions of a diffusion model for surfactants interacting with a mean-force potential representing the micellar region. Transitions between coiled and relaxed conformations in the diffusion model are included based on the conformational changes, observed in the previous chapter, when surfactants enter or leave the micellar region. The analysis suggest the nature of the deviation to be a consequence of a diffusive process across an energetic barrier where several time scales can be reached depending on the number of the permitted size transitions for the insoluble blocks when leaving the micelle. Our results question the importance of the polydispersity of the hydrophobic blocks effects as the main cause of recently reported experimental deviations.

8.2 Future Work

The results obtained in this work present the SCMF theory as a suitable tool to study the micellization phenomena in both, static and dynamic regimes. However, it would be interesting to include the fluctuations of the system together with a more sophisticated model for the implicit solvent to consider the temperature effects which are not currently accessible from our simulations. Besides, based on the fitting procedure developed in Chapter 5, a set of different surfactants can be modeled within the equilibrium SCMF formalism to consider mixtures of surfactants. Also, it is possible to design SCMF simulations to study drug carrier systems by inclusion of a third component, representing the drug molecules, in the free energy formalism. From extension of the dynamic SCMF simulations in the final chapters of this thesis, detailed information related with the aggregates and drugs stability could be obtained, as expected, this would be of paramount interest for diverse research fields. Additionally, dynamic SCMF simulations can also be adapted to test the effects of polydispersity on the relaxation kinetics of copolymer systems by inclusion of a set of copolymers with different hydrophobic sizes, and in consequence, a test of the impact on the autocorrelation functions can be followed. Finally, by two dimensional SCMF simulations it would be also possible to study the effect of the micellar aggregates shape on the kinetic exchange mechanisms.

Appendix A

Pdf Derivation from the Free Energy Formalism

To minimize the single-chain free energy in Eq. 2.17

$$F = N\int d\alpha P[\alpha]\left(u_{intra}(\alpha)+u(\alpha)\right)+kT\left(N\int d\alpha P[\alpha]\log P[\alpha]+\int d\vec{r}c_s(\vec{r})\log\phi_s(\vec{r})\right), \tag{A.1}$$

subject to the volume-filling constraint given in Eq. 2.5

$$\phi_s(\vec{r})+N\langle\phi(\vec{r})\rangle = 1, \tag{A.2}$$

can be done by introducing the set of Lagrange multipliers $\pi(\vec{r})$ as follows

$$\begin{aligned}F =& N\int d\alpha P[\alpha]\left(u_{intra}(\alpha)+u(\alpha)\right)+kT\left(N\int d\alpha P[\alpha]\log P[\alpha]+\int d\vec{r}c_s(\vec{r})\log\phi_s(\vec{r})\right)\\ &+\int d\vec{r}\pi(\vec{r})\left(N\langle\phi(\vec{r})\rangle+\phi_s(\vec{r})-1\right).\end{aligned} \tag{A.3}$$

Before determining the set of unknowns $P[\alpha]$ and $\phi_s(\vec{r})$, we must define the analytical form of the central chain intermolecular interactions. Taking the single-chain interaction energy from Eq. 2.16

$$u(\alpha) = \frac{N-1}{2}\epsilon_{cc}\int d\vec{r}\Phi^{cc}_{int}(\alpha,\vec{r})\langle c(\vec{r})\rangle+\epsilon_{cs}\int d\vec{r}\Phi^{cs}_{int}(\alpha,\vec{r})c_s(\vec{r}), \tag{A.4}$$

the constants ϵ_{cc} and ϵ_{cs} correspond to the associated energies for chains c to interact through the volumes $d\vec{r}\Phi^{cc}_{int}(\alpha,\vec{r})$ and $d\vec{r}\Phi^{cs}_{int}(\alpha,\vec{r})$ with the concentration fields $\langle c(\vec{r})\rangle$ and $c_s(\vec{r})$ at point $\vec{r}$, respectively. The values in brackets as the found in Eqs. A.2-A.4 represent averages over the single-chain conformations, namely, $\langle\cdots\rangle = \int d\alpha P[\alpha](\cdots)$ as previously shown in Eq. 2.19. In particular

$$\begin{aligned}\langle\phi(\vec{r})\rangle &= \int d\alpha\, P[\alpha]\phi(\alpha,\vec{r}),\\ \langle c(\vec{r})\rangle &= \int d\alpha\, P[\alpha]c(\alpha,\vec{r}).\end{aligned}$$

Once the intermolecular interactions for configuration α have been established as in Eq. A.4 we proceed to calculate the probabilities $P[\alpha]$ from

$$\frac{\delta F}{\delta P[\alpha]} = 0, \tag{A.5}$$

from Eqs. A.3 and A.4

$$\begin{aligned}\frac{\delta F}{\delta P[\alpha]} =& N\Big(u_{intra}(\alpha)+\frac{N-1}{2}\epsilon_{cc}\int d\vec{r}\Big[\Phi^{cc}_{int}(\alpha,\vec{r})\langle c(\vec{r})\rangle+\langle\Phi^{cc}_{int}(\vec{r})\rangle c(\alpha,\vec{r})\Big]\\ &+\epsilon_{cs}\int d\vec{r}\Phi^{cs}_{int}(\alpha,\vec{r})c_s(\vec{r})\Big)+NkT\Big(\log P[\alpha]+1\Big)+N\int d\vec{r}\pi(\vec{r})\phi(\alpha,\vec{r})\\ =&0,\end{aligned} \tag{A.6}$$

reorganizing the terms

$$\log P[\alpha] = -\frac{1}{kT}\Bigg(u_{intra}(\alpha) + \frac{N-1}{2}\epsilon_{cc}\int d\vec{r}\Big[\Phi^{cc}_{int}(\alpha,\vec{r})\langle c(\vec{r})\rangle + \langle\Phi^{cc}_{int}(\vec{r})\rangle c(\alpha,\vec{r})\Big] + \epsilon_{cs}\int d\vec{r}\Phi^{cs}_{int}(\alpha,\vec{r})c_s(\vec{r})\Bigg) - \frac{1}{kT}\int d\vec{r}\pi(\vec{r})\phi(\alpha,\vec{r}) - 1, \tag{A.7}$$

supposing the same size for all the beads of the chains ($\Phi^{cc}_{int}(\alpha,\vec{r})\langle c(\vec{r})\rangle \approx \langle\Phi^{cc}_{int}(\vec{r})\rangle c(\alpha,\vec{r})$), additionally, taking $\beta = 1/kT$ and

$$u_{inter}(\alpha) = (N-1)\epsilon_{cc}\int d\vec{r}\Phi^{cc}_{int}(\alpha,\vec{r})\langle c(\vec{r})\rangle + \epsilon_{cs}\int d\vec{r}\Phi^{cs}_{int}(\alpha,\vec{r})c_s(\vec{r}), \tag{A.8}$$

it is easy to see that Eq. A.7 is now

$$\log P[\alpha] = -\beta\left(u_{intra}(\alpha) + u_{inter}(\alpha)\right) - \beta\int d\vec{r}\pi(\vec{r})\phi(\alpha,\vec{r}) - 1, \tag{A.9}$$

with this, the *pdf* is found to be

$$P[\alpha] = \frac{1}{q}\exp\left[-\beta\left(u_{intra}(\alpha) + u_{inter}(\alpha) + \int d\vec{r}\pi(\vec{r})\phi(\alpha,\vec{r})\right)\right], \tag{A.10}$$

where the constant in the right side of Eq. A.9 has been absorbed in q which in turn ensures the proper normalization of the probabilities ($\int d\alpha P[\alpha] = 1$). In order to find the unknown solvent volume fraction, or equivalent, the solvent concentration $c_s(r)$, it would be necessary to calculate

$$\frac{\delta F}{\delta c_s(\vec{r})} = 0, \tag{A.11}$$

which according to Eqs. A.3 and A.4, together with the relation between the solvent concentration and volume fraction, $v_s c_s(\vec{r}) = \phi_s(\vec{r})$, with v_s as the volume of a solvent monomer

$$\begin{aligned}\frac{\delta F}{\delta c_s(\vec{r})} &= N\epsilon_{cs}\int d\alpha P[\alpha]\Phi^{cs}_{int}(\alpha,\vec{r}) + kT\Big(\log\phi_s(\vec{r}) + 1\Big) + v_s\pi(\vec{r}) \\ &= 0.\end{aligned} \tag{A.12}$$

Taking the first term in the right hand side of the above equation as an average value, the solvent volume fraction will be

$$\log\phi_s(\vec{r}) = -\beta v_s\pi(\vec{r}) - \beta N\epsilon_{cs}\langle\Phi^{cs}_{int}(\vec{r})\rangle, \tag{A.13}$$

which leads to the final expression for the solvent volume fraction

$$\phi_s(\vec{r}) = v_s c_s(\vec{r}) = \exp\left[-\beta\left(v_s\pi(\vec{r}) - N\epsilon_{cs}\langle\Phi^{cs}_{int}(\vec{r})\rangle\right)\right], \tag{A.14}$$

from here, considering negligible the chain interaction volume with respect to the surrounding available volume, it is possible to determine the Lagrange multipliers based on the following approximated expression

$$\pi(\vec{r}) \approx -\frac{kT}{v_s}\log\phi_s(\vec{r}). \tag{A.15}$$

Equations A.2 A.10 and A.15 form of a set nonlinear equations and from their solutions it is possible to obtain the values of the variables $\{P[\alpha], c_s(\vec{r}), \pi(\vec{r})\}$ and in consequence any average value or thermodynamic quantities in equilibrium.

Appendix B

Numerical Solution of the SCMF Equations

Solution of the SCMF equations require certain approximations. In the first place the geometry of the system must be stated in order to the define the elementary volumes dividing the space, namely, 1D planar layers or concentrical spherical and cylindrical shells, 2D cylindrical and planar layers, and, 3D cubic volumes as illustrated in Fig. B.1. Once the discretization has taken place, we proceed to formulate the SCMF equations within this approximation. In this sense, the space integrals become in sums over the discretized N_k shells each one with volume v_k. In consequence, the chain molecular fields $c(\alpha, \vec{r})$ and $\phi(\alpha, \vec{r})$ and the corresponding interaction volume fractions $\Phi^{cc}_{int}(\alpha, \vec{r})$ and $\Phi^{cs}_{int}(\alpha, \vec{r})$, the solvent volume fraction $c_s(\alpha, \vec{r})$ and therefore the Lagrange multipliers $\pi(\vec{r})$ will contribute to the shells defined in the discretization procedure. To determine the contribution of any of the chain volumetric quantities to the corresponding layer k we proceed as follows:

1. To calculate the concentrations $c(\alpha, k)$ of chain α in layer k. We identify the number of units, composing the chain, located in the layer, then by dividing by the layer volume v_k we determine the concentration of the conformation. However, to complete the calculation we must sum over all the units belonging to the conformation depending on the moieties taken into account, i.e., there many concentration fields as species in the chain model. This consideration is also held for calculation of the chain volume fractions and interaction volumes.

2. In the case of the chain volume fractions $\phi(\alpha, k)$ we throw a random number of points N_{ran} inside the volume enclosed by every unit of the conformation, then, we calculate the number N^k_{ran} of points located in layer k to determine the volume fraction of the unit in volume v_k by calculating $v_c N^k_{ran}/(N_{ran} v_k)$ where v_c is the volume of one unit of the chain α.

3. To calculate the interaction volume fractions $\Phi^{cc}_{int}(\alpha, k)$ we proceed in a similar way as in the previous item, however, instead of generate random points in the interior of the units volumes v_c we throw them inside the interaction volume $v_{int} = 4/3\pi(r^3_{int} - \sigma^3)$ enclosed by a shell of inner and outer radius σ and r_{int}, respectively. The interaction radius, r_{int} is the maximum distance for units, of diameter σ, to interact with the surrounding fields.

Once the contributions of all the molecular fields for every sampling chain α have been calculated with the former procedure we proceed to calculate the chain probabilities $P[\alpha]$, the solvent volume fractions $c_s(k)$ and the Lagrange multipliers $\pi(k)$ from the SCMF equations stated in Chapter 2 and Appendix A. To start, the

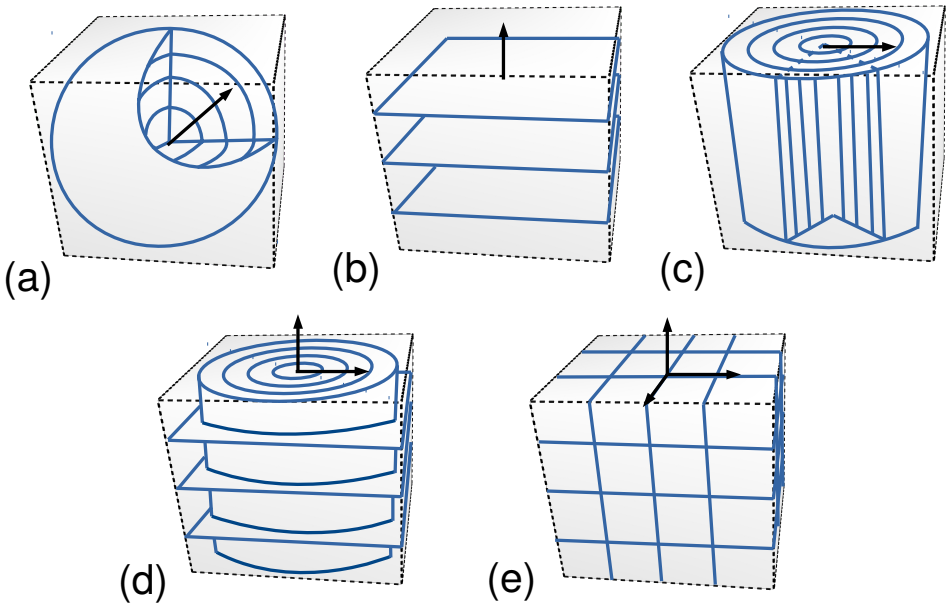

Figure B.1: Discretization of the simulation box according to the geometry imposed to the system: 1D (a) spherical shells, (b) planar slices, and, (c) cylindrical shells, 2D (d) planar layers in cylindrical shells, and, 3D (e) cubic volumes. Arrows indicate the axis of symmetry for every case.

incompressibility condition in Eq. A.2 is now

$$\phi_s(k) + N\langle\phi(k)\rangle = 1, \tag{B.1}$$

with

$$\langle\phi(k)\rangle = \sum_{\alpha=1}^{N_\alpha} P[\alpha]\phi(\alpha,k), \tag{B.2}$$

here, the integrals over all the possible chain conformations are not longer considered given the finite number, N_α, of sampling chains used in the simulations. In this approximation, from Eq. A.10, the chain probabilities can be written as

$$P[\alpha] = \frac{1}{q}\exp\left[-\beta\left(u_{intra}(\alpha) + u_{inter}(\alpha) + \sum_{k=1}^{N_k} v_k\pi(k)\phi(\alpha,k)\right)\right], \tag{B.3}$$

where the partition function is chosen to fulfill the condition $\sum_\alpha P[\alpha] = 1$. The intramolecular energies are calculated as ϵ_{cc} times the number of nonconsecutive units belonging to the same chain which are close to each other a distance below r_{int} from their centers. From Eq. A.8, the intermolecular mean-field energy for chain α is

$$u_{inter}(\alpha) = (N-1)\epsilon_{cc}\sum_{k=1}^{N_k} v_k\Phi^{cc}_{int}(\alpha,k)\langle c(k)\rangle + \epsilon_{cs}\sum_{k=1}^{N_k} v_k\Phi^{cs}_{int}(\alpha,k)c_s(k), \tag{B.4}$$

with $c_s(k) = \phi_s(k)/v_s$, and the average concentration fields calculated from the single-chain contributions in a similar way as the volume fractions in Eq. B.2

$$\langle c(k)\rangle = \sum_{\alpha=1}^{N_\alpha} P[\alpha]c(\alpha,k). \tag{B.5}$$

Finally, from Eq. A.15 the Lagrange multipliers are now

$$\pi(k) \approx -\frac{kT}{v_s} \log \phi_s(k). \tag{B.6}$$

In consequence, solution of Eqs. B.1, B.3 and B.6 with aid of Eqs. B.2, B.4 and B.5 will provide the solutions of the chains *pdf* together with the solvent concentration fields. Given the discretization scheme all the fields and probabilities are considered now in a matrix representation: solvent, $c_(k)$ and $\phi_s(k)$, and chain, $\langle\phi(k)\rangle$ and $\langle c(k)\rangle$, fields are represented by vectors with N_k components, while the chain probabilities, $P[\alpha]$, as well as the intramolecular energies are vectors with N_α elements. Terms in the vectorial intermolecular energy in Eq. B.4 come from operations between the matrices of size $N_\alpha \times N_k$ representing the interaction volume fractions $\Phi^{cc}_{int}(\alpha, k)$ and $\Phi^{cs}_{int}(\alpha, k)$ with the vectors of size N_k for chain and solvent concentrations $\langle c(k)\rangle$ and $c_s(k)$, respectively. Additionally, mean volume fractions values as in Eq. B.2 are calculated from the product between the vector of the probabilities with N_α elements and the matrix of volume fractions with $N_\alpha \times N_k$ elements resulting in a vector of size N_k representing the average $\langle\phi(k)\rangle$ values. A similar procedure is considered in the case of the mean concentration fields in Eq. B.5. From here, solution of the system equations can be addressed by several techniques including iterative or Newton-Raphson methods, in fact, we found identical solutions obtained from both methods in the case of short chains. Besides, given the solutions of the system are given in terms of matrix operations we can fast the calculations by (i) reduction of zero-valued elements, and, (ii) parallelization of the matrix-vector operations via OpenMP platform. Once the *pdf* and the solvent concentrations have been determined from solution of the above equations, any structural or thermodynamic quantity can be calculated for the system under study.